

OSLO METROPOLITAN UNIVERSITY
STORBYUNIVERSITETET

Master's Degree in
Structural Engineering and Building Technology
Department of Civil Engineering and Energy Technology

MASTER'S THESIS

THESIS TITLE	DATE
Local buckling of welded I-sections in high strength steel subjected to axial compression	25.05.2022
	NUMBER OF PAGES
	64
AUTHOR	SUPERVISORS
Vegard Mauren Richardsen	Aase Reyes Katalin Vertes
SUMMARY	
<p>Because of a continuous development in yield strength, and the lack of design codes covering the topic, this thesis investigates the local buckling behaviour of high strength steel (HSS). As the increase in strength allows for slenderer members and structures, this also makes them more prone to buckling. They are also more likely to be of class 4, where local buckling comes of topic. First, a literature review covering topics such as buckling, finite element method (FEM), and HSS is performed. A FE-model for analysing buckling behaviour of S800 welded I-sections is then validated against literature found in thee review. This model is further applied to investigate the buckling behaviour of class 4 I-sections of S960 and S1100, in addition to S800. Based on the results from the FE-analyses performed, two additional buckling curves are suggested so that the design rules in Eurocode 3 may be applied to HSS welded I-sections.</p>	

3 KEYWORDS
Buckling
High Strenght Steel
Finite Element Method

Project assignment Spring 2022

Vegard Mauren Richardsen

Local buckling of welded I-sections in high strength steel subjected to axial compression

High-strength steel is becoming increasingly interesting for the construction sector, and the FE modeling of the material behavior, welding and fracture are issues for research. Due to high strength combined with high ductility, high strength steels have been used in protective structures for many years. One issue that can be critical for beams and columns in high strength steels is local buckling. Due to the high strength, the thickness can be reduced, but this means that the slenderness will decrease, and the cross sections can be more prone to local buckling. As of now, higher strengths are not included in Eurocode 3. This topic will be studied further in the present project.

The project can consist of some (not all) of the following activities:

1. Theory and literature study about the modeling of high-strength steel and buckling analyses.
2. State-of-the-art on local buckling of high-strength steel structures.
3. Construction of buckling curves for high strength steel by means of FE analyses
 - a. Validate a numerical model by comparison of experimental results in the literature.
 - b. Parameter study: variation of different cross sections and different strengths.

The candidate can focus the work on specific parts of the assignment, or assess other aspects in consultation with the supervisors.

The form of the report will be as a scientific research report where emphasis is placed on a clear and well-arranged presentation.

Supervisors: Katalin Vertes & Aase Reyes, Oslo Metropolitan University

The report is due at the Department of Civil Engineering and Energy Technology at May 25 2022.

OsloMet, January 19 2022

Katalin Vertes & Aase Reyes
Supervisors


Preface

This thesis is written and delivered as my final work for the master's degree *Structural Engineering and Building Technology*, with specialisation in *Structural Engineering*, at the Department of Civil Engineering and Energy Technology, Oslo Metropolitan University (OsloMet) during the spring of 2022.

I must first and foremost thank my supervisors at OsloMet Professor Aase Reyes and Associate Professor Katalin Vertes. They have been of great help through the work with this thesis. Initially, with establishing the topic and objective of the thesis, and throughout the work with regular meetings where they provided me with good feedback and guided me in the direction this thesis has taken.

I would also like to thank my employer who has allowed for me to prioritize finishing my degree, as well as my colleagues who have been understanding of my occasionally absence from the office during this semester.

Lastly, it is important for me to thank my partner and my family who have been supporting throughout my degree, but especially now in the last semester when working with this thesis.



Vegard Mauren Richardsen

Oslo, May 25th, 2022

Abstract

As a result of the continuous development in steel production there are at the time several grades of high strength steels (HSS). Due to this increase in strength, structures are potentially designed slenderer than before. A problem which then comes of relevance is the buckling problem, as slender structures are more prone to buckling. The use of existing design codes is also limited to steel grades well below what is available.

This thesis aims to answer the research question: *“Is it possible to define additional buckling curves, so that Eurocode 3 may also cover design against local buckling in cross-section class 4 of HSS beyond S800?”*. Through a literature study, theory on HSS, relevant design codes, and buckling is reviewed. The finite element method (FEM) is thereafter applied to investigate buckling behaviour of HSS of cross sections in class 4.

During the theory review, which covered necessary and central topics, it was also implied that Eurocode 3 and other design codes does not cover HSS to a sufficient degree. A FE-model is validated against literature that reported results from physical tests on welded S800 I-sections in class 4, subjected to compressional load.

This validated FE-model is further applied to investigate the local buckling behaviour in welded I-sections of class 4 and steel grades S800, S960 and S1100. In total, 114 analyses are performed, 34 for each steel grade, plus 12 for validation of the model.

It is observed that most of the results from the FE-analysis scatters around the existing buckling curves in Eurocode 3. However, there is also a number of results that deviates from this, for which the buckling curves in Eurocode 3 would overestimate the buckling capacity of the investigated specimens.

Based on the results from the analyses performed, two new buckling curves are suggested for designing class 4 I-sections. One modified version of curve d in Eurocode 3, and one new curve that covers local buckling of I-section where both flange and web are classified as class 4 sections.

Content

Preface	ii
Abstract	iii
Content.....	v
List of Figures.....	vii
List of Tables	ix
Notations.....	x
1. Introduction	1
1.1. <i>Objective and Scope</i>	3
1.2. <i>Method.....</i>	4
2. Theory	6
2.1. <i>High Strength Steel.....</i>	6
2.1.1. <i>Material Properties</i>	7
2.1.2. <i>Metallurgy and Manufacturing</i>	9
2.1.3. <i>Availability</i>	10
2.1.4. <i>Environmental Impact</i>	10
2.2. <i>Relevant Standards for Design of Steel Structures</i>	11
2.2.1. <i>Buckling in Eurocode 3 vs ANSI/AISC 360.....</i>	12
2.2.2. <i>Design Against Buckling in Eurocode 3.....</i>	14
2.2.3. <i>Cross Section Class</i>	15
2.3. <i>Buckling.....</i>	16
2.3.1. <i>Euler Buckling Theory</i>	17
2.3.2. <i>Slenderness</i>	19
2.3.3. <i>Buckling of HSS</i>	21
2.3.4. <i>Plate Buckling</i>	21
2.4. <i>Numerical Solution Methods to Nonlinear Problems.....</i>	24
2.4.1. <i>Buckling in FEM</i>	25
2.5. <i>Material Models for Steel.....</i>	27
2.5.1. <i>Ramberg-Osgood and Offset Method</i>	29

2.5.2.	Work Hardening Models in ABAQUS/CAE	30
3.	Finite Element Analyses	32
3.1.	<i>Verification of FE-Model for HSS I-sections Under Axial Compression</i>	<i>32</i>
3.1.1.	Test Setup.....	33
3.1.2.	Defining the FEA	35
3.1.3.	Evaluation of the Results	39
3.2.	<i>S800.....</i>	<i>42</i>
3.2.1.	Results	44
3.3.	<i>S960.....</i>	<i>47</i>
3.3.1.	Material Data.....	47
3.3.2.	Results	48
3.4.	<i>S1100.....</i>	<i>51</i>
3.4.1.	Material Data.....	51
3.4.2.	Results	52
4.	Evaluation of Results and Buckling Curves.....	55
4.1.	<i>Evaluation of the Model.....</i>	<i>58</i>
4.2.	<i>Proposal for Buckling Curves.....</i>	<i>59</i>
5.	Conclusion.....	63
5.1.	<i>Further Work.....</i>	<i>64</i>
	Bibliography	65
	Appendices	70

List of Figures

Figure 1: Historical development of steel grades [4].....	2
Figure 2: Global formability diagram [22].....	7
Figure 3: Stress-strain curves of various steel grades[29].	8
Figure 4: Buckling curves from ANSI/AISC-36 and Eurocode 3 [41].	13
Figure 5: Comparison of capacity calculations from EC3, E.C.P. and AISC [42].....	14
Figure 6: Buckling curves from EC 3-1-1 (fig. 6.4) [9].....	15
Figure 7: Illustration of global and local buckling [45].....	17
Figure 8: Buckling curve from Euler theory, slenderness vs. critical load [47].....	18
Figure 9: Illustration of divergence actual buckling load vs slenderness [47].....	19
Figure 10: Type of buckling, based on slenderness [50].....	20
Figure 11: Illustration of plate under compressional loads [43].	22
Figure 12: Buckling shapes of plates with two free edges (a) and one free edge (b) [43].....	22
Figure 13: Out-of-plane displacement vs load curves for buckling of columns (a) and plates (b) [43].....	24
Figure 14: First and second iteration in Newton’s method, as applied in ABAQUS/CAE [56].	25
Figure 15: Load-displacement case with unstable static response [62].....	26
Figure 16: Illustration of limitation of Newton’s method after limit point [63].....	27
Figure 17: Illustration of iterations using Arc-Length method [63].....	27
Figure 18: Elastic and plastic strain on stress-strain curve [65]	28
Figure 19: Stress-strain curves without (a), and with (b) Luder’s strain [67].....	30
Figure 20: Multilinear kinematic hardening model[73].....	31
Figure 21: Illustration of test setup [18].	33
Figure 22: Illustration of dimensions on I-section [51].....	34
Figure 23: Average stress-strain relation from tensile tests, and illustration of multi-linear model [18].....	36
Figure 24: Meshing of cross section (H-A1).	38
Figure 25: Buckling shapes of I-sections in ABAQUS/CAE. H-A1 (top left), H-B1 (top right), H-C1 (bottom left) and H-D1 (bottom right).	40
Figure 26: Results from analysis of S800 I-sections. Critical load vs relative slenderness.	46

Figure 27: Reduction factor vs relative slenderness (S800), with buckling curves from EC3.	46
Figure 28: Calculated stress-strain curve for S960.	48
Figure 29: Results from analysis of S960 I-sections. Critical load vs relative slenderness.	50
Figure 30: Reduction factor vs relative slenderness (S960), with buckling curves from EC3..	50
Figure 31: True and engineering stress-strain curves for S1100.	52
Figure 32: Results from analysis of S1100 I-sections. Critical load vs relative slenderness. ...	54
Figure 33: Reduction factor vs relative slenderness (S1100), with buckling curves from EC3.	54
Figure 34: Results from analysis of S800, S960 and S1100 I-sections. Critical load vs. relative slenderness.	55
Figure 35: Reduction factor vs. relative slenderness for all test, with buckling curves from EC3.	56
Figure 36: Buckling shapes of specimen S12F9W9 (a), S1F5W8 (b), S5F10W10 (c) and S16F9W10 (d).....	58
Figure 37: Suggestions for new buckling curves, curve e (orange) and curve f (blue).....	60

List of Tables

Table 1: Discrepancy in results from the reference articles	32
Table 2: Dimensions of tested cross sections unit mm [18].	34
Table 3: Average results from tensile tests [18].	37
Table 4: Discrepancy between developed FE-model, and FE-analysis and test performed by Cao, et al. [18].	41
Table 5: Dimensions of analysed cross section [18].	43
Table 6: Results from analyses of buckling capacity of S800 I-sections.	45
Table 7: Results of tensile test of S960, performed by Ban, et al. [51]	47
Table 8: Results from analyses of buckling capacity of S960 I-sections.	49
Table 9: Material data from tensile test of S1100 [76].	51
Table 10: Results from analyses of buckling capacity of S1100 I-sections.	53
Table 11: Calculation of buckling capacity with suggested curves.	62

Notations

A	-	Cross sectional area
A _{eff}	-	Effective area
B	-	Width of cross section
b	-	Width of plate
b _{eff}	-	Effective width of plate
CMS	-	Conventional mild steel
E	-	Modulus of Elasticity/Youngs modulus
EC3	-	Eurocode 3/NS-EN 1993
f _{cr}	-	Critical stress
FE	-	Finite Element (Method/Model/Analysis)
f _u	-	Ultimate stress
f _y	-	Yield stress
H	-	Height of cross section
HSS	-	High Strength Steel
i	-	Ratio of inertia
I	-	2 nd moment of inertia
ISF	-	Imperfection scale factor
L	-	Length
L ₀	-	Initial length
L _k	-	Buckling length
LPF	-	Load proportionality factor
n	-	Ramberg-Osgood coefficient
N _{b,Rd}	-	Design buckling resistance
N _{cr}	-	Critical axial load/buckling load
t	-	Thickness of plate
t _f	-	Thickness of flange
t _w	-	Thickness of web
χ	-	Reduction factor (buckling)
ε	-	Strain

ϵ_y	-	Yield strain
ϵ_u	-	Ultimate strain
ϵ_e	-	Engineering strain
ϵ_t	-	True strain
ϵ_{pl}	-	Plastic strain
γ_M	-	Material factor
λ	-	Slenderness
λ_{rel}	-	Relative slenderness
ν	-	Poisson's ratio
ρ	-	Density
σ	-	Stress
σ_e	-	Engineering stress
σ_t	-	True stress

1. Introduction

Steel is a material that has been applied in buildings and constructions for over 2000 years [1], and is one of the most used materials in today's construction and building industry. Some of the benefits steel has as a construction material is high strength compared to self-weight, as well as recyclability. However, production of steel requires a lot of energy. In the Global Status Report for Buildings and Construction (2020) by the United environment programme [2], it is stated that the building sector is accountable for 38% of global energy-related CO₂-emissions, approximately 11% of this is from building materials and construction. They also state that direct emissions from buildings should be reduced by 50% within 2030 [3]. In other words, the use of steel should be limited to help achieve a global reduction in CO₂-emissions.

Over the years, the steel industry has had continuous and rapid development in production technology which has resulted in higher and higher graded steels, without affecting the weight considerably [4]. The illustration in Figure 1, which was made by Maraveas, et al. [4] who based it on an illustration by Schröter [5], shows the rapid development of steel grades with regards to yield strength. This increase in strength has not provided any considerable increase in emissions [6, 7]. As a result of the increase in strength-to-weight ratio, slenderer structures are often achieved. Slender structures and members subjected to compressional loads are potentially prone to buckling.

Even though the design codes cover the most used steel grades at the time (S355-S460 [8]), there are steel grades available beyond what they cover. For example, the European design code for steel structures, NS-EN 1993/Eurocode 3 (EC3) [9], is only applicable up to S460 graded steel, with some additional rules for grades up to 700. And the American design code ANSI/AISC 360 [10] is only valid up to S690.

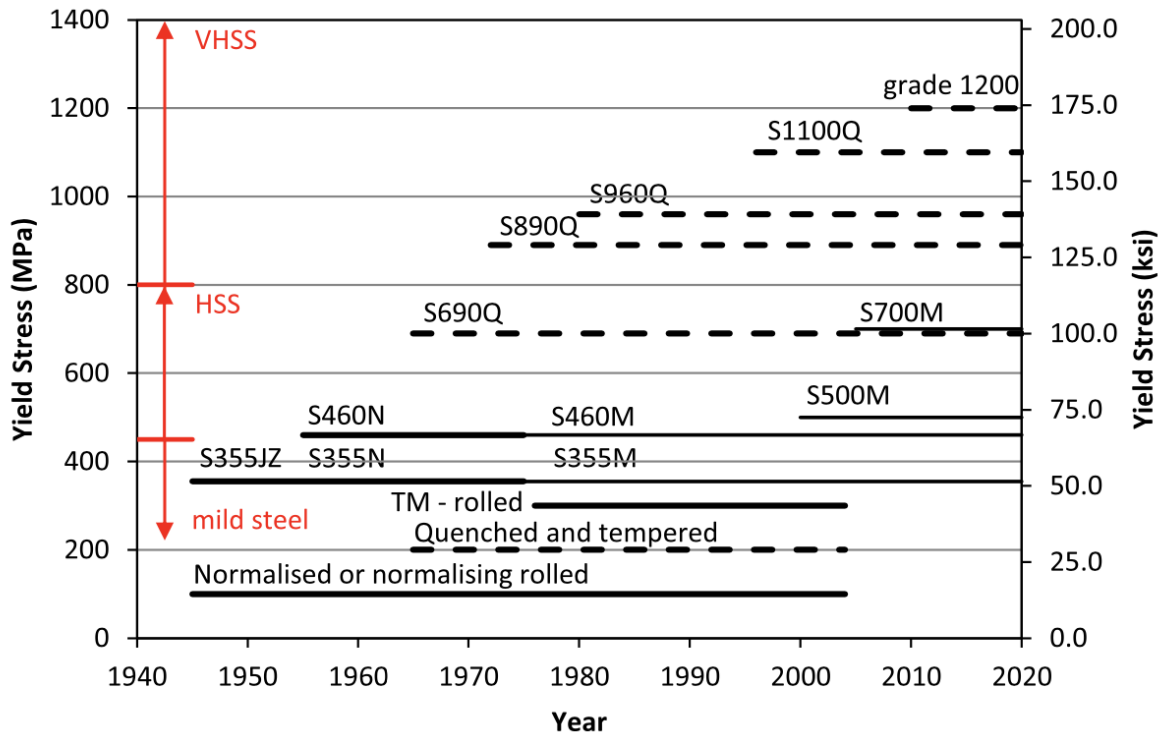


Figure 1: Historical development of steel grades [4].

Many studies have investigated different topics regarding design of structures with high strength steel (HSS). Especially within the topic of buckling and stability, a lot of research has been performed.

On behalf of the European Commission, Schillo, et al. [11] performed a project named “Rules on high strength steel (RUOSTE)”, where they investigated the applicability of Eurocode 3 on steel grades S500-S960. With regards to buckling, they had indications of conservatism for global buckling, and too optimistic capacities in the case of local buckling.

Wang, et al. [12] studied local buckling behaviour of hollow sections of various steel grades up to S960, both hot-rolled and cold-rolled sections. The conclusions from their study were mainly on the ductility and slenderness limits given in Eurocode 3, and not directly related to the buckling curves. Indications of the need of a higher safety factor (γ_M) for HSS than for conventional mild steel (CMS) was also found, and therefore it was suggested to use a value of 1.1 for γ_M for slender HSS sections of cross section class 4.

Alongside these, many other studies has been performed on topics related to buckling of HSS. Chen, et al. [13] looked at local buckling in I-sections of steel grades up to S700. Wang, et al. [14] investigated how elevated temperatures affected the local buckling behaviour of S960 graded welded H-sections. Shuchang, et al. [15], and Wang and Qiu [16] both investigated global buckling of S690 columns, respectively of H- and tube-sections. While Cao, et. al [17-19] and Li, et al. [20] examined the local buckling behaviour of S800 welded T-, I-, H- and box-sections with regards to Chinese, American and European design codes.

To summarize what can be found in existing literature; a large portion of it focuses on buckling of HSS, which is a rather central topic as higher material strength potentially results in slenderer structures. Few of them focus on development of buckling curves applicable for HSS, but more on material factors, and general behaviour under certain conditions. Some have also developed additional steps that for example calculates a “magnifying slenderness-factor” [17-20], which is meant as an addition to design codes in EC3.

It can then be highlighted that there is the lack of studies on steel grades above S960, and it mostly focuses on grades below S800. In addition, few focus directly on the buckling curves used in several design codes, especially curves for local buckling and cross-section class 4.

1.1. Objective and Scope

Based on the topics and gaps in the literature presented above, the following research question is formulated:

“Is it possible to define additional buckling curves, so that Eurocode 3 may also cover design against local buckling in cross-section class 4 of HSS beyond S800?”

In this thesis the goal is to answer the research question, through a theoretical study and numerical simulations, where the objective is to establish buckling curves that can be used to design against local buckling for HSS. Within the research question there is also a wish for simplicity, therefore new curves are desired, rather than additional rules and calculation steps. The focus is within the area of structural systems, and structural engineering.

Regarding time, the work is limited to the period from January to May 2022. Due to this, the study is limited with regards to steel grades, section types, as well as the general extent in number of analyses performed.

The evaluation of buckling capacity and behaviour is limited to calculations and simulations in finite element (FE) software, no physical tests are to be performed. Neither tensile tests, nor buckling tests of full sections. Licensing and access to relevant software is limited to those that are accessible through the university, OsloMet.

Exact steel grades are chosen based on available literature containing the relevant results from tensile tests, aiming for grades above S800. The same applies for the section type, where the analysis will be dependent on validation against tests performed by others.

HSS is available in many different grades and qualities, with a variation in several material properties. Through what was found in the literature study it was decided that this thesis is limited to focus on the steel grades S800, S960 and S1100 steel, and mainly applied on welded I-sections.

1.2. Method

In general, the method consisted of four steps:

First, a literature review was performed on relevant theory. Topics at focus were HSS, buckling and finite element analysis (FEA), separately and in combination. Especially the combined topic of buckling and FEA was attained attention.

Relevant literature was found through academic search engines such as; Engineering Village (<http://www.engineeringvillage.com>), Scopus (www.scopus.com), ScienceDirect (www.sciencedirect.com), and Google Scholar (<https://scholar.google.com>). Access to the three first was granted using student-licensing from OsloMet, while Google Scholar is freely accessed. Other literature, such as books, theory manuals from ABAQUS/CAE, standards (Eurocodes) and lecture notes, were also reviewed.

Through the literature review, the second step was in mind: establishing a validated finite element model for analysing local buckling in HSS. From the literature review, reports covering experimental tests and verification of a finite element (FE)-model for S800 I-, H, T-

and box-sections were found. The report for S800 I-sections was further used as basis for creating a validated FE-model. OsloMet has student-licences to ABAQUS/CAE, thus this FE-software was used.

Thirdly, with a verified FE-model, the analysis was applied to additional steel grades (S960 and S1100), as well as an extended review of S800. New material models were established based on results from tensile test on said steel grades found in the literature review.

Finally, the results were used to analyse the behaviour of HSS-members prone to local buckling. From these results, new buckling curves that will allow for the use of EC3 in design against local buckling for I-sections of the evaluated grades of HSS was defined.

2. Theory

In this section relevant literature and theory is reviewed. This extends to theory on HSS, relevant standards, buckling theory, solution methods for nonlinear problems and material models for describing the behaviour of steel.

During the fall semester of 2021, in the course MABY5010 at OsloMet, the author of this thesis carried out a project that focused on HSS and FE-modelling of buckling. The report from this project covered theory on said topics. Some of the theory covered there, is also relevant for this thesis, and therefore parts of the theory section hereunder is from the report written in MABY5010 [21].

2.1. High Strength Steel

There are many terms for steel with high strength and advanced properties in use. Advanced high strength steel (AHSS), ultra-high strength steel (UHSS) and high-performance steel (HPS) are some of them. The term “high strength” simply indicates that the steel is stronger than what is commonly used at the time. For instance, in 2006 Schröter [5] defined HSS as steel with higher yield strength than 355 MPa. S355 was before this again called HSS since it had a greater yield strength than the steel grade most commonly used at the time. Now the most regularly used steels are S355, S420 and S460 [8], which implies that S355 is no longer a HSS.

According to World Steel Association AISBL [22], AHSS/HSS can be defined as steel with a yield strength above 440 MPa, while others choose to use “ultra” as in UHSS, for steels with yield strength above 960 MPa. However, some define UHSS as steel with yield strength greater than 700 MPa [23]. It can also be noted that the Norwegian Steel Association defines HSS as steel with yield strength above 420 MPa [24]. This indicates a lack of clear definitions concerning HSS. Further in this thesis the definition of the Norwegian Steel Association is used; all steel grades above S420 are referred to as HSS.

The continuous development in steel production has led to several generations of HSS. In Figure 2 different types of steel are shown in what is called a Global formability diagram (GFD). The diagram illustrates the relation between tensile strength and elongation (ductility) for different steel grades. The green steels are conventional mild steels (CMS), the lower orange ones (MS, PHS, CP etc.) are considered as the 1st generation of HSS, TWIP goes under the 2nd

generation, and the grey area represents the 3rd generation of HSS which is under development [22].

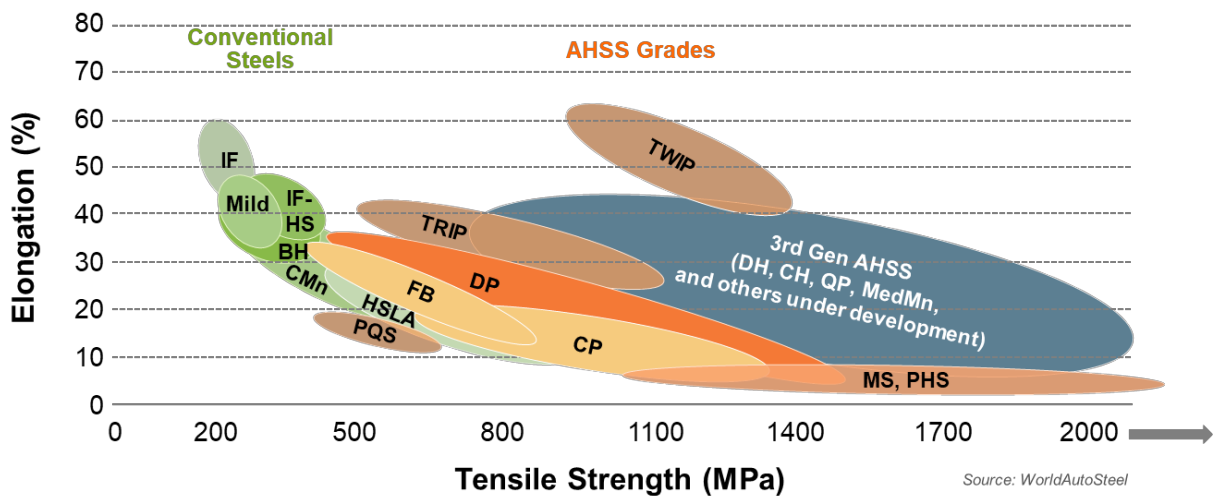


Figure 2: Global formability diagram [22].

In the GFD, it is illustrated that traditionally for steel high ductility is equal to lower tensile strength (CMS and 1st gen. HSS). The 2nd generation of HSS differs from this trend with high ductility and strength. The 3rd generation, under development, aims to fill a gap between the 1st and 2nd generation of HSS with regards to increased ductility-properties.

2.1.1. Material Properties

Among all the different definitions, the most central property is that HSS is a steel alloy that is stronger than the more commonly used steel types at the time. However, the yield strength is not the only factor that varies for different alloys. As seen in Figure 2, elongation/ductility is another material property that varies. There are also several other properties, some of the most important ones for describing steel are [25]:

- Weldability, which describes how easy it is to weld the material.
- Formability, ability to be formed by plastic deformation (hot or cold).
- Resistance against corrosion.
- Tensile strength, resistance against fracture under tension.
- Hardness, resistance against dents, plastic deformation, scratches etc.
- Toughness against brittle fracture.
- Ductility, ability to elongate.

HSS is naturally identified by high strength. Typically, HSS has reduced weldability [26] and ductility [27] compared to CMS. Ductility is defined as a materials ability to deform without fracture [28]. From Figure 3, stress-strain curves are plotted for multiple steel grades varying from S235-S960. As seen the maximum strain reduces for higher graded steels, this highlights the fact that higher graded steels have lower ductility since ultimate strain is reached at a much lower strain than for CMS.

The main advantage of HSS is increase in strength, without any significant changes in self-weight of the structure. In weight, HSS is costlier than CMS, but the total cost might be reduced since less steel is needed for the same structural performance. The cost-benefit of HSS compared to CMS is highly case-dependent. Schillo, et al. [11] concluded that 10-20% cost-savings can be achieved using HSS in some cases but emphasizes that this is dependent on the specific case.

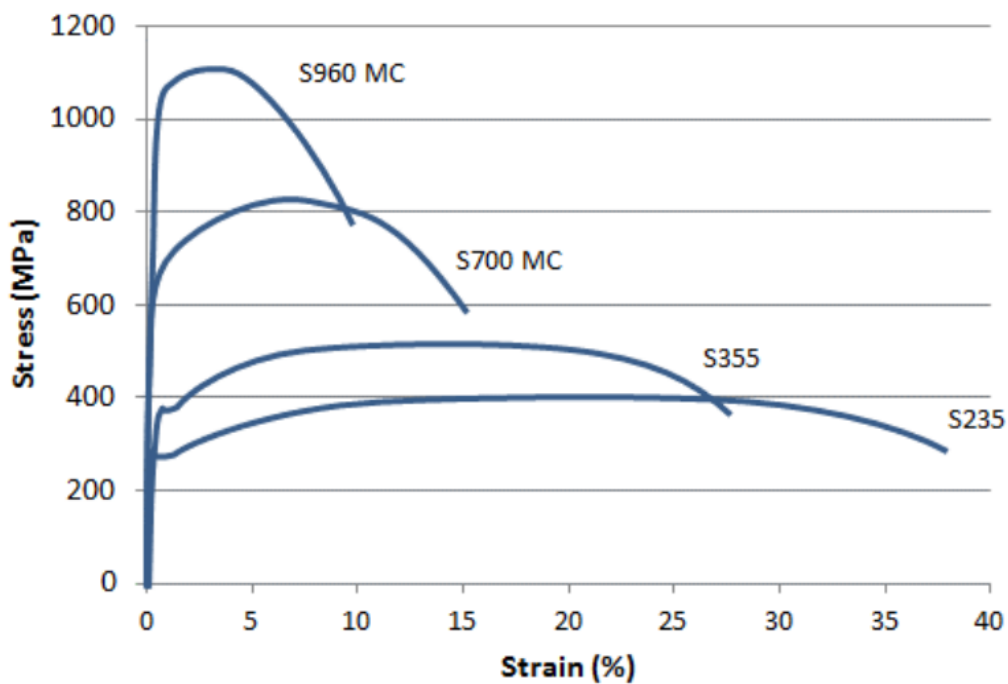


Figure 3: Stress-strain curves of various steel grades[29].

2.1.2. Metallurgy and Manufacturing

There are many types of steel with variation in material properties apart from strength (formability, ductility, weldability, etc.). These variations in material properties are due to differences in the production method and alloy [30].

Steel is mainly manufactured by mixing liquid pig iron with a variation in alloying elements. Pig iron is a product of iron ore [30] and Iron stands for almost all the material 98-99 % (in weight), while the rest is alloying elements. Some common alloying elements, and how it affects the steel alloy is listed below [1, 30]:

- Carbon: Up to 2% of the weight. Increases hardness and strength. Reduces ductility and toughness.
- Manganese: Increases strength and toughness.
- Nickel: Increases hardening and ductility.
- Silicone: Reduces pores in the steel.
- Copper: Reduces risk of corrosion.

In addition to the above-mentioned alloying elements aluminium, chrome, molybdenum, vanadium, wolfram, niobium, titanium and boron are other elements that are used in different steel alloys [30]. For HSS with yield strength above 780 MPa, carbon and manganese are the most used alloying elements. In addition are all of the following elements also often used in HSS: boron, vanadium, titanium, molybdenum, niobium, aluminium, chromium and silicone [31].

Along with alloying material, there are multiple production methods for steel that also affects the steel properties. For HSS, quenching and tempering (Q&T), and direct quenching (DQ) are the two most common production methods [32]. DQ is a process where the temperature of steel is quickly reduced by bathing it in water or oil [33]. For Q&T, the steel is after the quenching, tempered (heat treated) [34]. The strength of the steel is mostly from the quenching process, and the tempering provides the ductility and toughness. For grades S355-S700 rolling procedures at low temperatures has proven to provide high toughness[4].

2.1.3. Availability

In Norway, Norsk Stål AS is one of the largest producers of steel. According to their websites the highest yield strength for pre-made beams is grade S355 [35]. S355 and S235 are the qualities that occur the most on their products. But they do deliver hot rolled steel-plates of grades up to S700. This indicates that the availability of Norwegian high strength steel products in Norway depends on import.

The reason for there not being any pre-made sections available of HSS is found in NS-EN10025-6 [36]. This standard defines delivery conditions for hot rolled flat products of HSS. It is valid for different steel grades from S460 up to S960, and only for flat products. This is in accordance with the assortment of Norsk Stål. In other words, HSS is only available in the form of plates, which then must be assembled into preferred sections, either by welding or by cold forming. This allows for different graded plates to be combined within the same sections.

2.1.4. Environmental Impact

The Global Efficiency Intelligence has performed studies aiming to benchmark the climate impact from steel [37]. In their study it is stated that steel production has doubled from 2000 to 2020, and that the iron and steel industry accounts for 11% of the global CO₂-emissions.

With the use of HSS, naturally, the capacity of structures might be higher or the same, with the use of less steel. Stroetmann [38] investigated the environmental impact for various grades of steel in the range of S355 to S690, compared them to S235. In his report it was indicated that the higher the steel grade, the higher the weight savings should be to justify the use of HSS. For example, the use of S690 requires a weight reduction of at least 17.1%, compared to S235, to acquire lower environmental impact. This due to higher graded steel, having somewhat higher emissions from production. 17.1% weight reduction is relatively small with regards to the 293,6% increase in yield strength. However, there is not a direct correlation between the weight reduction and increase in strength in all cases. For this to be the case, the structural component may not be prone to buckling, the design significantly affected by dynamic effects or deflection being the design criteria. It is also pointed out that for structures where weight is a large part of the loading, the weight reduction will have a

double effect. The reduction in weight will reduce the load, thus again possibly reducing the weight and dimensions even further.

Sperle and Hallberg [6], [7] has also performed a case-study on the use of HSS compared to CMS. The study mainly focused on automotive constructions, but it still gives a picture of the potential in HSS. Just as the studies mentioned above, his studies stated that the increase in environmental impact (per weight unit) from CMS to HSS is relatively small, compared to the reduction in weight. According to the study, a 25% weight reduction was achievable for structures where CMS was changed with HSS, and that the weight-saving-potential was even higher in some cases. Thus, there are indications of a high potential with regards to reducing the environmental impact with the use of HSS compared to CMS.

2.2. Relevant Standards for Design of Steel Structures

There are multiple sets of design rules for steel structures, dependent on the location of the structure. In Europe, the European standards apply (Eurocodes). United States has their own code, ANSI/AISC 360 [10]. In other parts of the world, such as in other parts of America, China, Japan, etc. other codes apply. In this thesis, the main focus is on the European design rules, but key differences between European and the American codes are pointed out below.

The European standardisation organization, CEN, has developed the European standards for constructions. There are mainly ten standards, also called Eurocodes for the construction industry in Europe [39].

These standards are approved in Norway by Norsk Standard. Design of steel structures are covered in NS-EN 1993, or Eurocode 3 (EC3). EC3 is again divided into general rules and application rules. There are 12 general codes which covers topics such as fire design, joints, fatigue, etc. for steel structures. These are numbered NS-EN 1993-1-1 to NS-EN 1993-1-12.

EC 3-1-1 [9] covers the general rules for steel design [9]. According to EC 3-1-1 3.1(2) this part of EC 3 only covers steel grades up to S460. EC 3-1-12 [40], is a part of EC 3 that adds design rules for steel grades between S460-S700 (EC 3-1-12 1.1(1)). These are the two most relevant of the Eurocodes with regards to the design of HSS structures.

EC 3-1-1 [9] only covers design rules for steel grades up to S460. As well as EC 3-1-12 that contains some additional rules for grades up to S700. But there are no design rules for grades above this. In 2016 European Commission's Research Fund for Coal and Steel (RFCS) evaluated the material requirements for HSS for use in construction [11]. The focus of this study was on steel grades S500-S960 with regards to existing rules on CMS in EC3.

NS-EN 10025-6 [36] is another relevant standard for steel design. This was mentioned earlier, and states requirements for delivery conditions for flat products of HSS.

In the United States, ANSI/AISC 360 [10] is the standard that covers design rules for steel structures. It is developed by the American Institute of Steel Construction (AISC) and approved by American National Standards Institute (ANSI).

2.2.1. Buckling in Eurocode 3 vs ANSI/AISC 360

Multiple studies can be found that compare specific parts and topics of different design codes. Topkaya and Sahin [41] and Khaled, et al. [42] are two studies that have performed a general comparison of EC3 and ANSI/AISC 360 with regards to design of steel structures.

For this thesis, the rules on design against buckling are the most relevant ones. The concept of buckling is described later in section 2.3, and design rules in section 2.2.2. Some of the key findings from these two articles, that are of relevance for this thesis, are summarized below:

- EC 3 classifies cross sections as class 1-4, while AISC uses only three classes: compact, non-compact, slender. Where compact, roughly covers class 1 and 2, while non-compact equals class 3, and slender equals class 4. There is also a small difference in the limits between the different classes. [41, 42].
- In calculation of width to thickness ratios of flanges, AISC divides the width of the flange by two, while EC 3 also subtracts thickness of web, and welds [41, 42].
- Both design codes use a relative slenderness (λ_{rel}) as basis of calculation of compressional capacity, with the use of a reduction factor (χ) [42].
- EC3 does not state any limitations of maximum slenderness, while AISC sets it to maximum 180 for members subjected to compression [42].

- In EC3, five different buckling curves are given (a0, a, b, c, d), depending on cross sectional criteria, whereas AISC only states one curve [41]. In Figure 4 the different curves are shown. Curve *a* from EC3 is the one that is the most similar to the curve in AISC.

Khaled, et al. [42] also investigated the difference in buckling capacity according to EC3, AISC and the Egyptian steel code (E.C.P.) for a column of a HE-B 200 section, with varying lengths. The results are illustrated in Figure 5, and show that AISC yielded highest capacity, E.C.P. the lowest capacity, while EC3 yielded slightly lower capacity than AISC.

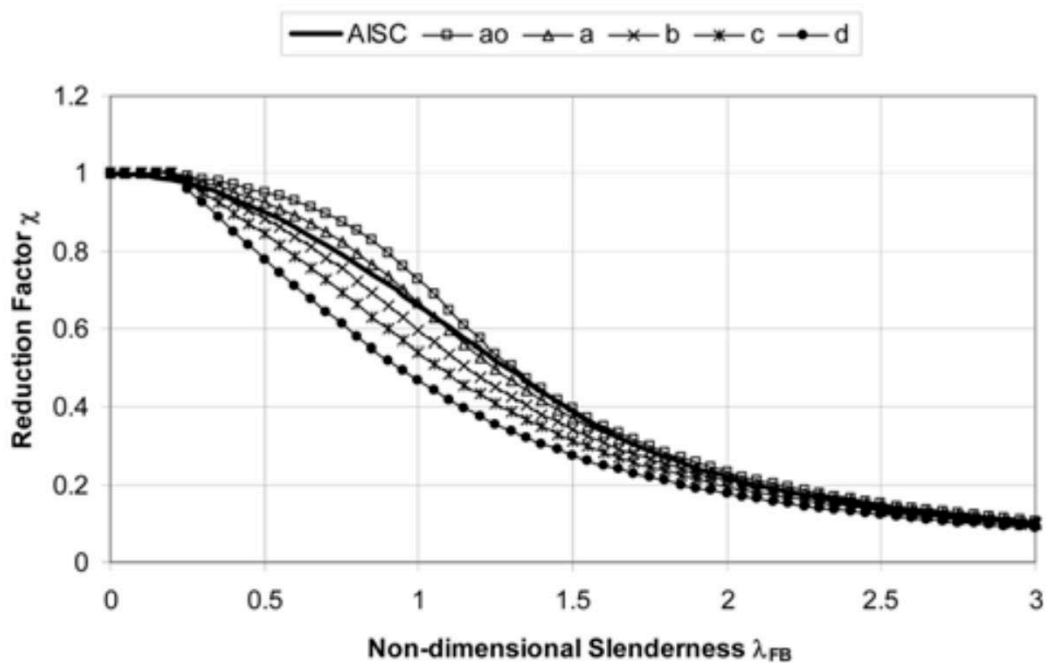


Figure 4: Buckling curves from ANSI/AISC-36 and Eurocode 3 [41].

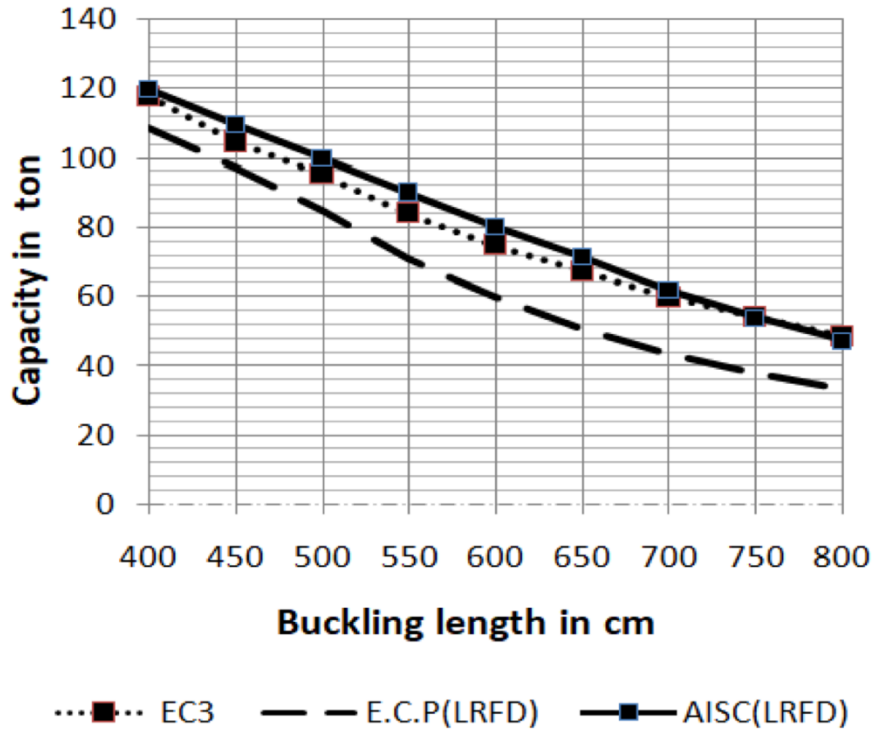


Figure 5: Comparison of capacity calculations from EC3, E.C.P. and AISC [42].

2.2.2. Design Against Buckling in Eurocode 3

EC 3-1-1-6.3 [9] covers design rules for stability control of steel structures. The following steps describe the procedure for designing against buckling:

1. Relevant buckling curve (Figure 6) is decided based on table 6.2 in EC 3-1-1, which considers for web/flange/plate thickness and yield strength.
2. Calculate λ_1 then λ_{rel} according to equation (6.50) and (6.51) in EC 3-1-1.
3. Find reduction factor, χ , based on λ_{rel} and buckling curve in Figure 6.
4. Designing buckling capacity, $N_{b,Rd}$, is calculated as Eqn. 1. Where γ_M is the material safety factor.
5. Control against design load $N_{Ed} \leq N_{b,Rd}$

$$N_{b,Rd} = \frac{\chi * A * f_y}{\gamma_M} \quad \text{Eqn. 1}$$

According to EC 3-1-1 2.2(1), these simplified calculations are verified to have sufficient ductility through experiments [9]. Both the partial safety factor method is applied, as well as conservative calculations. In EC 3-1-12 there are no additional design rules so that this method can be applied to steel grades greater than S460. The buckling curves are determined based

on experiments and simulations, where factors such as variation of yield strength, cross-section, deviation from cross-sectional measures, shape-deviations and residual stresses are incorporated [39].

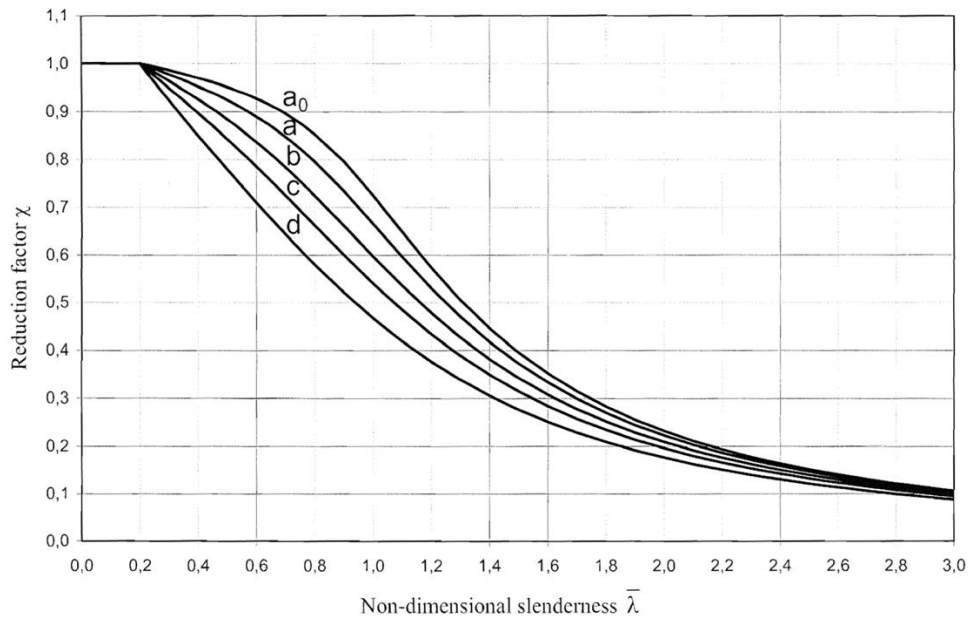


Figure 6: Buckling curves from EC 3-1-1 (fig. 6.4) [9].

Alternatively, the reduction factor can also be calculated according to equations given in EC 3-1-1 6.3.2.1 if the column is prone to centric loading. An imperfection factor, α , is applied. This imperfection factor is chosen based on the buckling curve corresponding to the cross section.

2.2.3. Cross Section Class

The behaviour of web/flange in a section is highly determined by the geometry and yield strength of the material [39]. Four cross section classes are defined in EC3, and can briefly be described as [43]:

- Class 1: May develop plastic hinges.
- Class 2: May develop plastic moment resistance, but not hinges.
- Class 3: Reaches yield strength.
- Class 4: Local buckling will occur before yield strength is reached.

The class of a given section is determined based on the slenderness of plates (width-to-thickness-ratio of flange and web for I-sections) and the yield strength of the material. As seen earlier, these classes vary somewhat between different design codes, both with regards to name and to limit criteria [41, 42]. If a section under compression does not fulfill class section 3 limits, it is defined as class 4.

For cross sections in class 4, EC3 states that in Eqn. 1, A should be set equal to the effective area of the cross-section, A_{eff} . The reason for this is described further in section 2.3.4.

2.3. Buckling

Buckling is a stability problem that occurs in slender structures/members under compressive forces. The subjected stress is lower than that of the material strength, but a small increase in load will, if buckling occurs, result in a large deformation. Cook, et al. [44] defines buckling as loss of stability, prior to or without fracture of the material. In other words, buckling is a problem that occurs somewhat independently from yield strength.

For columns under axial compression, buckling mainly occur in two ways: local buckling or global buckling. Global buckling is when the whole column deforms in the longitudinal direction. Local buckling is another form of buckling where for example only the flanges in I/H-beams buckle. Figure 7 illustrates the differences between global (named “general” in the figure) and local buckling.

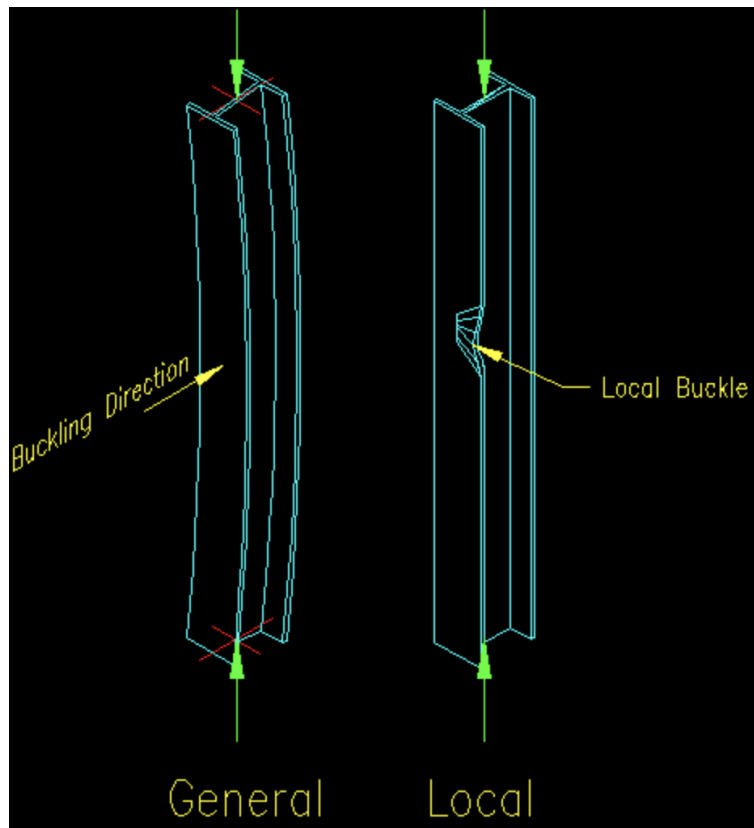


Figure 7: Illustration of global and local buckling [45].

For a perfectly straight and elastic element, N_{cr} is the value of the axial load that makes the element appear in an indifferent equilibrium (buckle). This problem is defined as an eigenvalue-problem [39].

2.3.1. Euler Buckling Theory

In 1759 the Swiss mathematician Leonhard Euler published his description on the elastic buckling behaviour of columns [46], this has later been known as Euler buckling theory or classical buckling theory. Buckling was described in different forms by multiple persons before him, but the one from Euler is the one that has been used in modern times [47]. Euler's theory is based on the assumptions of:

- Isotropic and perfectly elastic material.
- Straight column, without any eccentricity of loading.
- No imperfections.
- Hinged ends.

With these assumptions, the following formula for critical buckling load for columns was established by Euler:

$$N_{cr} = \frac{\pi^2 * EI}{L^2} \quad \text{Eqn. 2}$$

Later, the buckling length (L_k) of a member under compression has been defined so that the force needed for buckling to occur is equal to that which is needed to buckle a simply supported beam with length L [39]. To apply the same formula for columns that have other boundary conditions than hinged ends, L is multiplied by a correction factor based on the actual boundary conditions, and L is simply replaced with L_k in the equation.

With the definition of slenderness, which is discussed further below, one can plot curves for critical load vs. slenderness, also called buckling curves, as seen in Figure 8. For infinite elasticity, the curve for Eulers theory (called Euler curve) would continue upwards, but the steel will in reality behave inelastically for stress above yield stress. Therefore, the new path marked “plastic yield” in the figure, is applied to account for inelastic buckling and not allow for stress greater than yield stress.

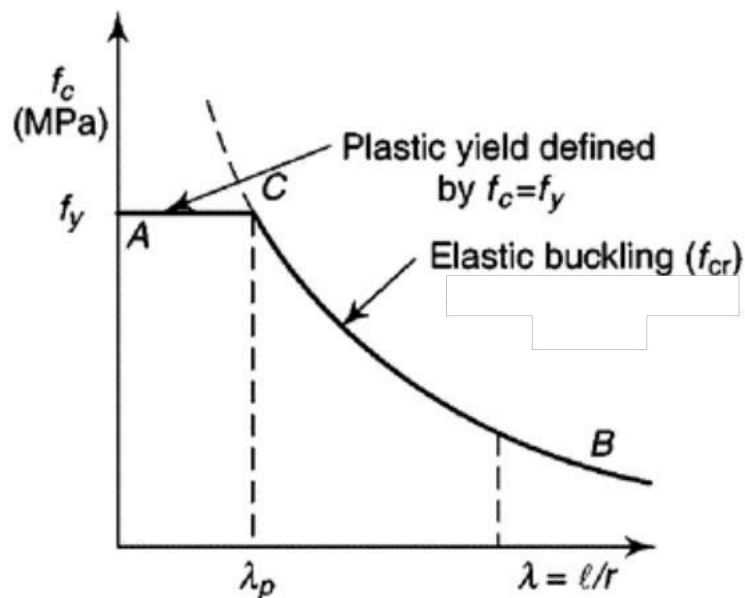


Figure 8: Buckling curve from Euler theory, slenderness vs. critical load [47]

However, Euler’s buckling theory proves to overestimate the buckling capacity when compared to tests, thus it is not directly applied in structural design. The reason for this was

that the assumptions taken in the theory does not represent reality, as imperfections, residual stress, different buckling forms (local, global and lateral) not perfectly hinged end-constraints, etc. are some additional factors that affect the actual buckling capacity of a column [47].

In Figure 9 the typical range of actual buckling resistance is illustrated with the grey area. As illustrated the results may vary more for lower slenderness, while for higher slenderness the results correlate better with the elastic buckling load. The divergence also indicates that for slender columns that buckles elastically, the Euler theory provides reasonably accurate results. While in the inelastic zone the Euler curve will potentially highly overestimate the capacity of the column [48].

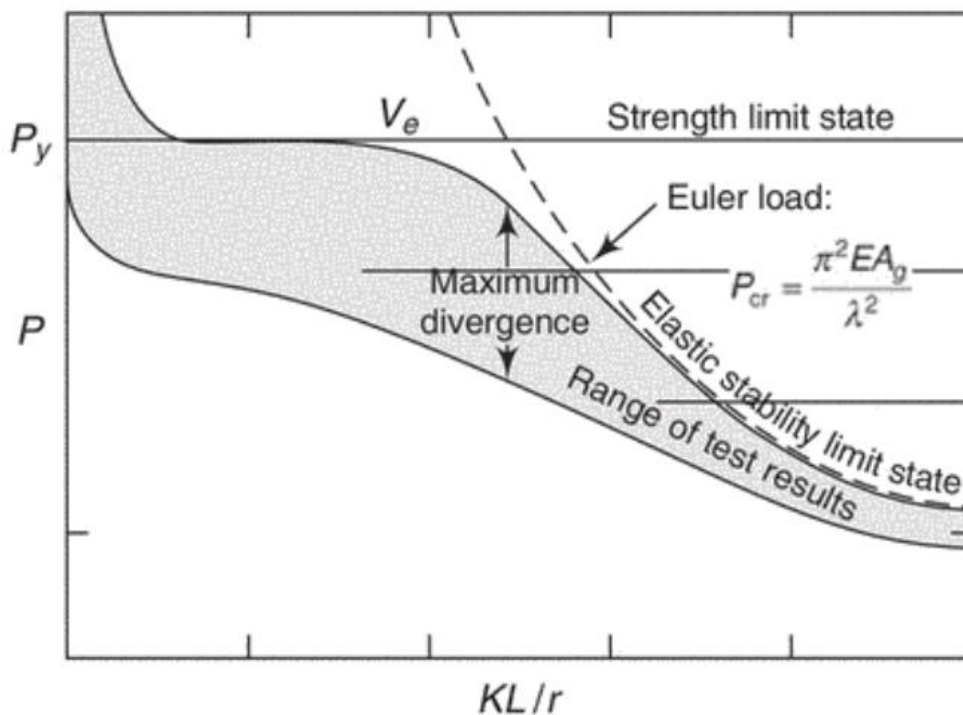


Figure 9: Illustration of divergence actual buckling load vs slenderness [47].

For this reason, the buckling curves in EC3, as seen in Figure 6, have through experience and extensive testing been determined including imperfections, residual stress etc. Through this, the limit point for the plastic yield-path, λ_p , has also been determined to 0.2 [49].

2.3.2. Slenderness

In metals, the buckling-stress is highly determined by the slenderness (λ), where the slenderness will vary for each steel grade. To avoid this problem, relative slenderness (λ_{rel}) is

often used instead [39]. λ_{rel} is calculated as defined in Eqn. 3. λ_1 is the slenderness where critical stress (f_{cr}), equals the yield stress (f_y), and can be calculated as given in Eqn. 4.

$$\lambda_{rel} = \frac{\lambda}{\lambda_1} \quad \text{Eqn. 3}$$

$$\lambda_1 = \pi \sqrt{\frac{E}{f_y}} \quad \text{Eqn. 4}$$

And λ can be calculated as the following, where L_k is the buckling length of the member and i is the radius of inertia for the section:

$$\lambda = \frac{L_k}{i} \quad \text{Eqn. 5}$$

The formulas above describe the slenderness of columns. For plates, the slenderness is generally defined as the width to thickness ratio (b/t) [39].

As seen from the buckling curves in Figure 6, the lower the slenderness λ , the closer to the yield strength of the material the critical load will be. Typically, $\lambda < 20$ yields material failure, $20 < \lambda < 108$ yields plastic buckling and $\lambda > 108$ yields elastic buckling [50], the different types of buckling are illustrated in Figure 10.

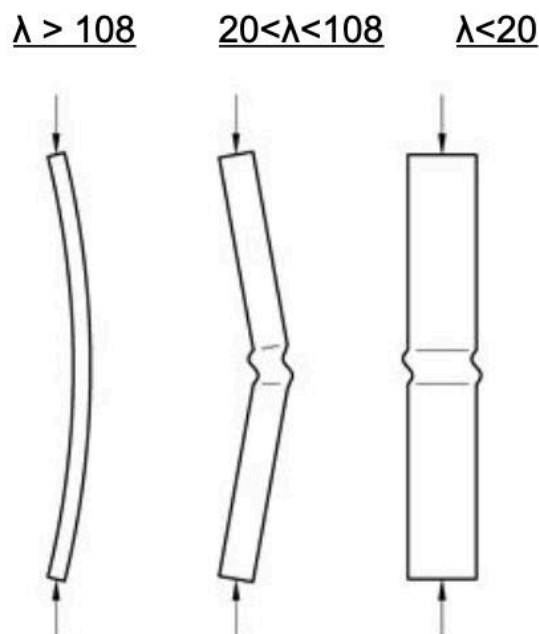


Figure 10: Type of buckling, based on slenderness [50].

2.3.3. Buckling of HSS

In EC3, there are no design rules for designing against buckling of HSS above S700. EC 3-1-12 only adds rules up for steel grades up to S700 and does not provide any additional rules for buckling design. As mentioned before, Schillo, et al. [11], investigated the applicability of EC3 on steel grades S500-S960. With regards to buckling, the conclusion was a suggestion of a higher buckling curve for HSS. It also concluded that curve *b* could be used for all welded box sections and cold-formed structural hollow sections with qualities S500-S960, when designing against global buckling. For local buckling a large scatter was seen in the results. There were also indications that suggested that the material factor γ_M , should be set to 1.1. However, there was no final conclusion on this.

Several studies have been performed on the stability of HSS, with regards to relevant design rules in EC3. Ban, et al. [51] experimented with the buckling behaviour of welded I- and box sections of S960. They proposed new buckling curves that need further confirmation, and also concluded that buckling curve *a* in EC3 can be used conservatively for global buckling. Somodi and Kövesdi [52] investigated the buckling resistance of cold-formed hollow sections, with steel grade S235-S960. They performed both laboratory, and numerical tests. For S960, they concluded with a buckling curve that was higher than buckling curve *a* in EC3. Su, et al. [53] looked at welded I-sections of S960 under compression and a minor bending moment. They investigated the applicability of proposed design rules for S700 in EC 3-1-12. They concluded with the high conservatism and low accuracy of failure loads. Wang, et al. [54] looked at the flexural buckling of pin-ended press-braked S960 channel sections. Just as the above-mentioned research, they also concluded with a high conservatism in EC3.

2.3.4. Plate Buckling

Often, structures are built up of slender plate-components that classifies as cross-section class 4, which implies that the buckling occurs locally [39]. In structural engineering, instability is generally change in geometry, resulting in loss of bearing capacity. For local buckling change in geometry occurs in the flange, web or both parts of the cross section [43].

Local buckling is best studied by looking at plates with large length and width compared to thickness, subjected to compressional loads, such as the one illustrated in Figure 11.

Timoshenko and Gere [55] defined the critical stress for such a plate to Eqn. 6, where k is the buckling coefficient which is dependent on the constraints along non-loaded edges, for example flange/web in I-sections.

$$f_{cr} = \frac{\pi^2 k E}{12(1 - \nu^2) \left(\frac{b}{t}\right)^2} \quad \text{Eqn. 6}$$

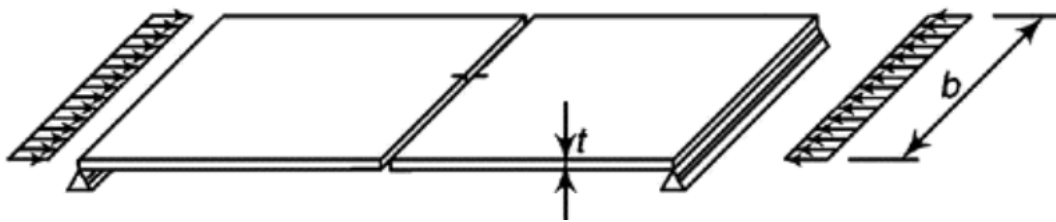


Figure 11: Illustration of plate under compressional loads [43].

In Figure 12 the buckling shape of plates with free edges (a) and one constrained edge (b) are illustrated. For many types of sections, the local buckling may be assumed as plates where free edges are unsupported, and connected edges are simply supported [43].

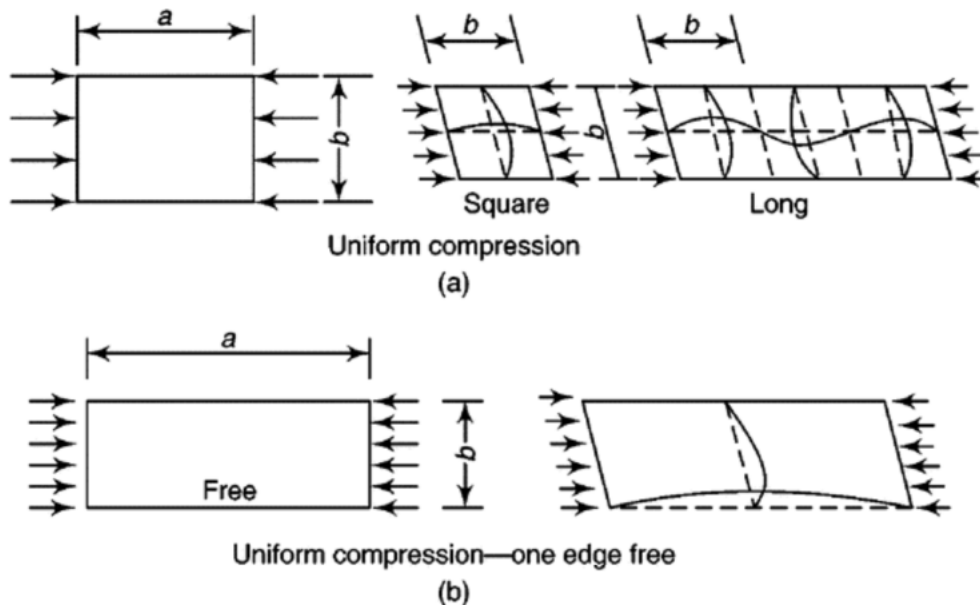


Figure 12: Buckling shapes of plates with two free edges (a) and one free edge (b) [43].

To determine whether the plates will buckle elastically or inelastically, cross section class is determined based on the slenderness of the plate.

For class 4 sections, typically a reduced area should be used when calculating, named effective area (A_{eff}), which is based on effective widths of the plates (b_{eff}). Plates, unlike columns, have a post-buckling capacity [43]. This difference in column and plate buckling can be illustrated as seen in Figure 13a and b.

It is illustrated (Figure 13a) that theoretically, the column yields zero deformation, up until the point where the load critical loading and buckling of the column, which is the Euler load as described in section 2.3.1. This path is called the fundamental path. At this point the curve bifurcates, and will deform infinitely along the secondary path, due to buckling and loss of strength [43]. In reality the transition to a stable path will follow a smoother curve due to imperfections etc.

For plates (Figure 13b) the fundamental path is identical, following the y-axis, but the secondary path will follow a secondary path illustrating a higher capacity than the Euler load/critical load. In other words, plate buckling is not necessarily synonymous with collapse, but this post-buckling capacity differentiates based on boundary conditions of the plates, for example plates with one constrained edge (as shown in Figure 12 b) does not have any significant post-buckling strength.

This post-buckling capacity is due to local buckling causing a loss of stiffness, and thus a redistribution of stresses occurs. This redistribution then again causes a non-linear distribution of the stresses, and for plates with supports along the longitudinal direction, this results in an increase in critical loading [43]. This redistribution is accounted for in EC3 by implementing A_{eff} .

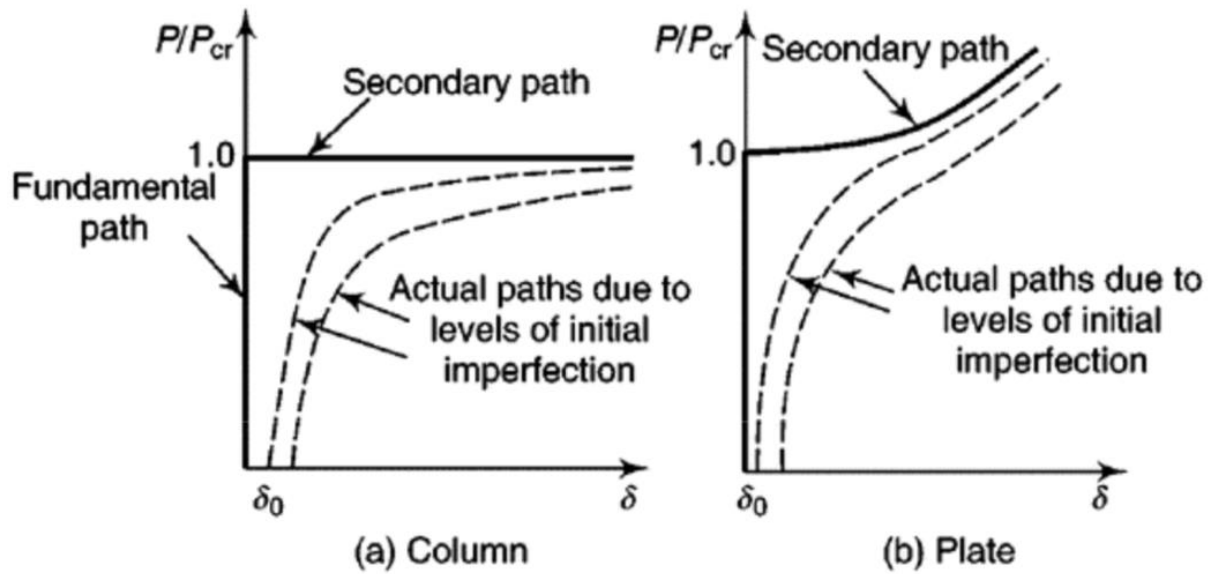


Figure 13: Out-of-plane displacement vs load curves for buckling of columns (a) and plates (b) [43].

2.4. Numerical Solution Methods to Nonlinear Problems

With regards to modelling and analysing nonlinear problems, there are three types of nonlinearities within structural engineering: material, geometric and contact. Material nonlinearity is when material has nonlinear description of material properties (stress/strain). Plasticity is an example of this. Geometric nonlinearity covers large deformations, so large that equilibrium must be considered with regards to deformed geometry. And when contact areas change with the contact force, or frictional forces are defined as contact nonlinearities [44].

Newton's method, also called Newton-Raphson (N-R), is an iterative method used in FEM to generate the force (P), vs. displacement (u), curve. This is performed using the initial tangent stiffness to adjust according to equilibrium [44]. Figure 14 shows an illustration of the first and second iteration, with correction to equilibrium [56]. The method is used as a solution method for nonlinear problems, and in ABAQUS/CAE, this is the solution method that is generally used [57]. There also exist other solution methods for such problems: modified Newton-Raphson, direct substitution-, initial stiffness, and Arc-Length method are some [44].

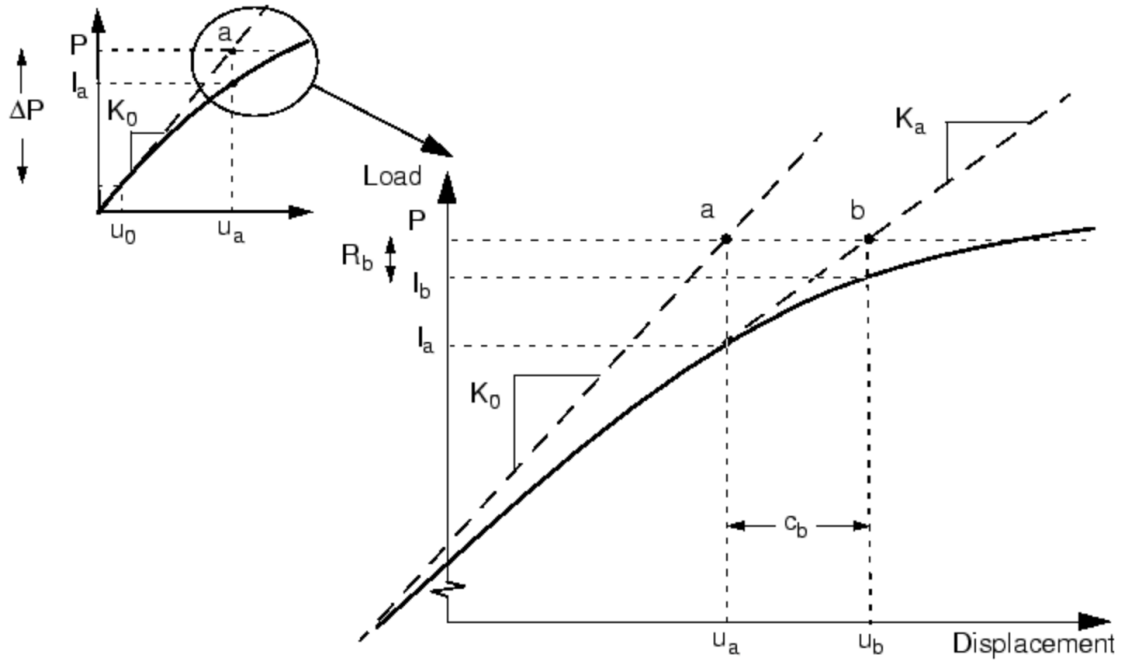


Figure 14: First and second iteration in Newton's method, as applied in ABAQUS/CAE [56].

When it comes to describing material plasticity, which is highly relevant for steel materials, material models are needed. Often these are based on approximations based on a few known parameters. These are further discussed in section 2.5.

2.4.1. Buckling in FEM

The buckling problem of steel structures is a problem where both geometric and material nonlinearities can be implemented. When performing a FEA with regards to stability, there are mainly two types of analysis of interest: linear and nonlinear. In the linear analysis, the eigenvalue problem is solved. Here a set of buckling factors with their corresponding mode shapes are calculated. For the nonlinear analysis, stiffness and response are incrementally evaluated [58]. When comparing the two methods, the nonlinear more accurately describes the behaviour and the linear solutions tends to over-predict the buckling load [59].

In a FEA on buckling, the problem is similar to the eigenvalue problem solved in vibration/dynamic problems. The difference is that the mass matrix $[M]$ in dynamic problems, is substituted with the stiffness matrix $[K_\sigma]$, which is an increased stiffness matrix $[K]$, due to considering the effect of membrane stresses [44].

The ABAQUS Analysis User's Guide states that the eigenvalue buckling prediction is to be used when the critical load of a structure is to be estimated, for linear cases [60]. When the material include nonlinearities, or one wants to predict instability for geometric nonlinearities of a structure, the Riks method should be used [61]. Load-Displacement cases such as that shown in Figure 15, where the response is unstable and a nonlinear static equilibrium, requires a nonlinear solution method such as the Riks algorithm[62].

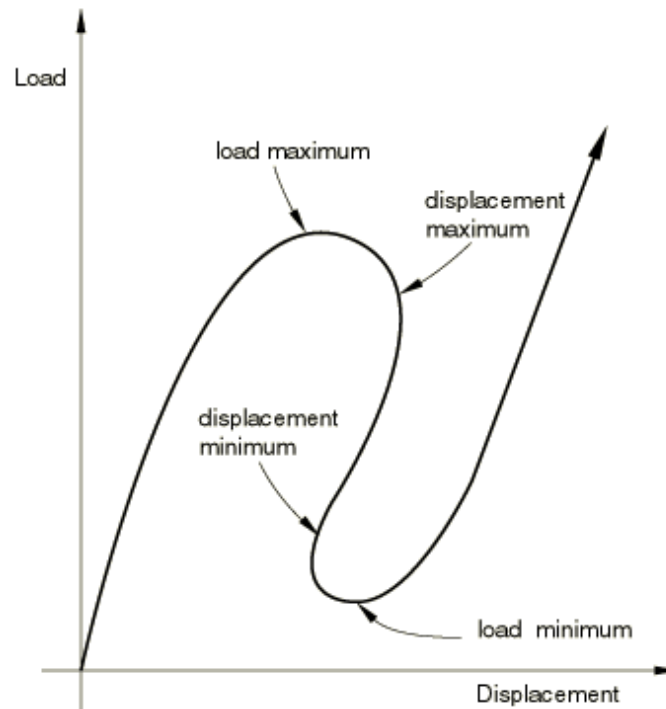


Figure 15: Load-displacement case with unstable static response [62].

According to Vasios [63] the Riks algorithm in ABAQUS/CAE is named after the Riks method developed by E. Riks [64]. The Riks algorithm use the Arc-Length method. Newton's method is a good method for solving nonlinear problems, however the solution method has problems predicting solutions after a limit point, such as the load-displacement case shown in Figure 16. Buckling analysis is a problem were such cases occur [63].

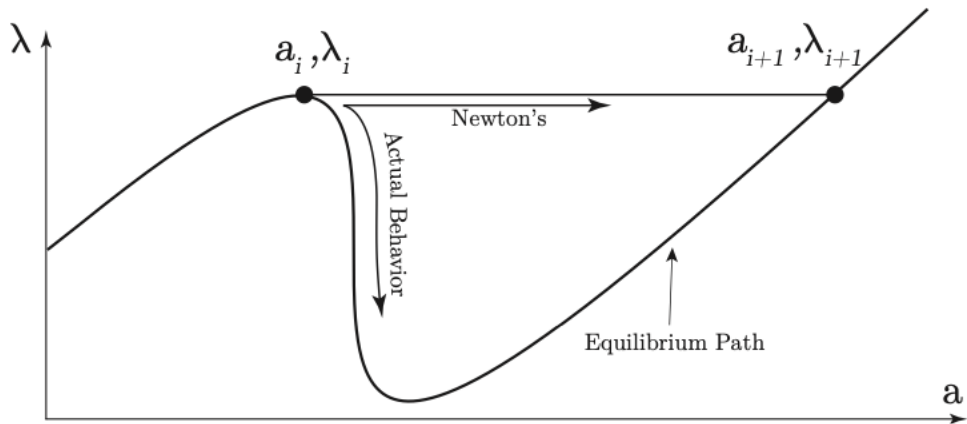


Figure 16: Illustration of limitation of Newton's method after limit point [63].

With the Arc-Length method, this problem is avoided. This method is a form of Newton-Raphson iteration where the iterations lie on a curve with radius Δl as seen in Figure 17 (left) [44]. In Figure 17 (right) it is illustrated how this method avoids the problem of Newton's method at limit points.

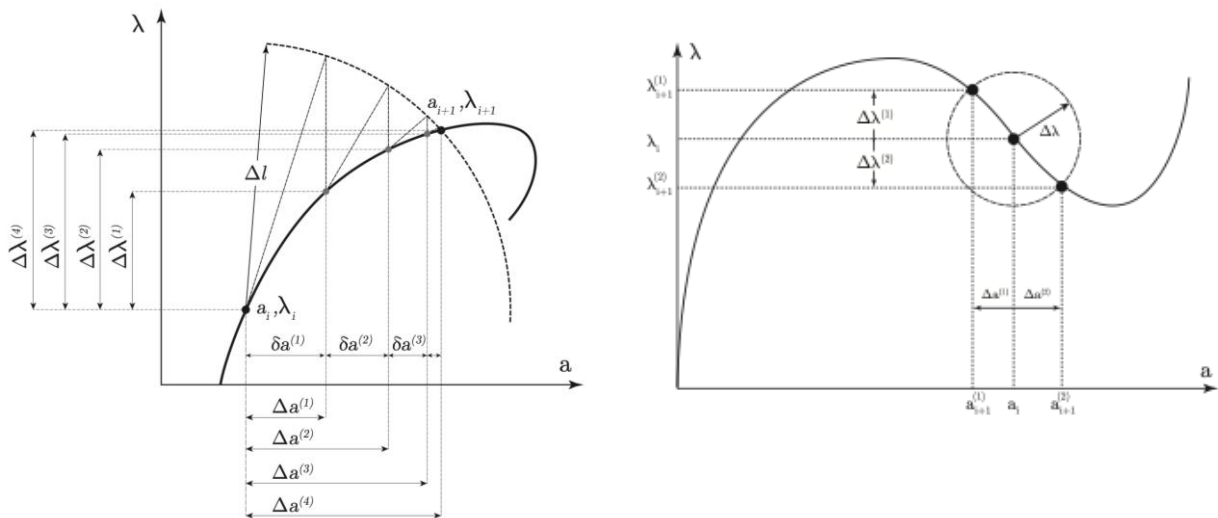


Figure 17: Illustration of iterations using Arc-Length method [63].

2.5. Material Models for Steel

Typically, the behaviour of steel can be split between two types. The first being elastic behaviour, where the material will undeform to its original state after unloading. And the second, plastic behaviour, where deformations are permanent. Figure 18 shows the different zones. In the elastic zone, the linear behaviour is described by Young's modulus (E), which is

the relation between the stress and strain. The plastic behaviour on the other hand is described nonlinearly.

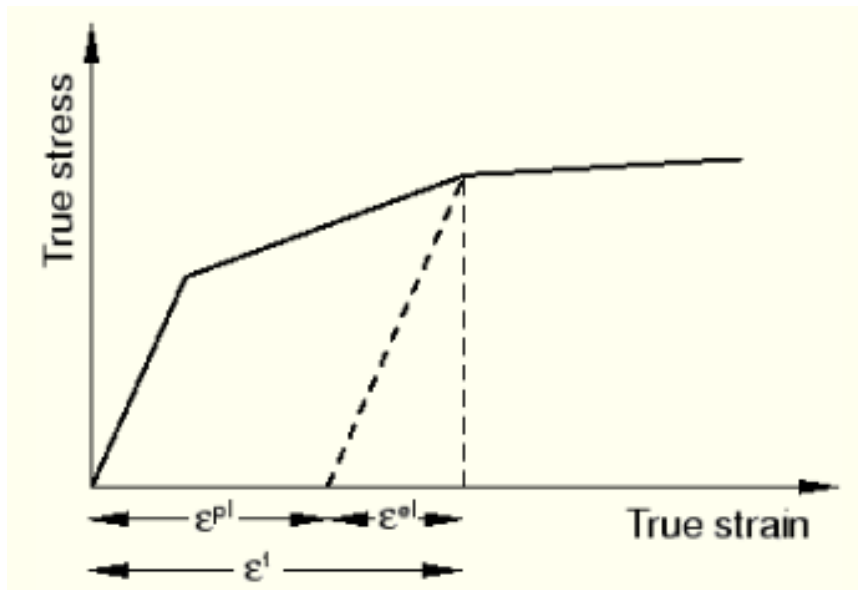


Figure 18: Elastic and plastic strain on stress-strain curve [65]

The most common way of defining the plastic behaviour is through tensile tests of the material. Applied stress, and resulting strain are then measured/calculated in terms of engineering stress-strain (σ_e / ϵ_e). In ABAQUS/CAE, the plastic behaviour of a material should be defined in terms of true stress (σ_t) and plastic strain (ϵ_{pl}). Eqn. 7- Eqn. 11 describes these relations, where F is applied force, A_0 is the initial cross section, L_0 is initial length, L is length after deformation, ϵ_{el} is the elastic part of the total true strain [65].

$$\sigma_e = \frac{F}{A_0} \quad \text{Eqn. 7}$$

$$\epsilon_e = \frac{L - L_0}{L_0} \quad \text{Eqn. 8}$$

$$\sigma_t = \frac{F}{A} = \sigma_e(1 + \epsilon_e) \quad \text{Eqn. 9}$$

$$\epsilon_t = \ln(1 + \epsilon_e) \quad \text{Eqn. 10}$$

$$\epsilon_{pl} = \epsilon_t - \epsilon_{el} = \epsilon_t - \frac{\sigma_t}{E} \quad \text{Eqn. 11}$$

2.5.1. Ramberg-Osgood and Offset Method

In some cases, there is a lack of detailed data for establishing a stress-strain curve of the nonlinear behaviour of metals. In 1943 Walter Ramberg and William R. Osgood developed a method, known as Ramberg-Osgood method, for approximating the nonlinear stress-strain relation in terms of only 3 parameters [66]. The method has proven highly applicable to metals, where the three parameters are Young's modulus (E), yield strength (f_y) and ultimate strength (f_u). Eqn. 12 gives this relation.

$$\varepsilon_e = \frac{\sigma_e}{E} + K * \left(\frac{\sigma_e}{f_y}\right)^n \quad \text{Eqn. 12}$$

Here ε_e , is the engineering strain, σ_e is the engineering stress, K is the constant for plastic offset, and n is the Ramberg-Osgood coefficient. n is calculated as given in Eqn. 13.

$$n = \frac{\ln\left(\frac{\varepsilon_u}{0.2}\right)}{\ln\left(\frac{f_u}{f_y}\right)} \quad \text{Eqn. 13}$$

ε_u is the strain at rupture in percentage %.

Patwardhan, et al. [67] concluded that for materials without Luder's strain the plastic offset strain can be set to 0.2%. Luder's strain is a strain plateau at yield strength, as shown in Figure 19b, and without Luder's in Figure 19a. As seen earlier, in Figure 3, higher graded steels, with less ductility, tends to not have this strain plateau.

If plastic offset strain is assumed to 0.2%, Eqn. 14 can be derived. This assumption of the yield strain is called the offset method, and is a method that is used with good results for metals [68].

$$\varepsilon_e = \frac{\sigma_e}{E} + 0.002 * \left(\frac{\sigma_e}{f_y}\right)^n \quad \text{Eqn. 14}$$

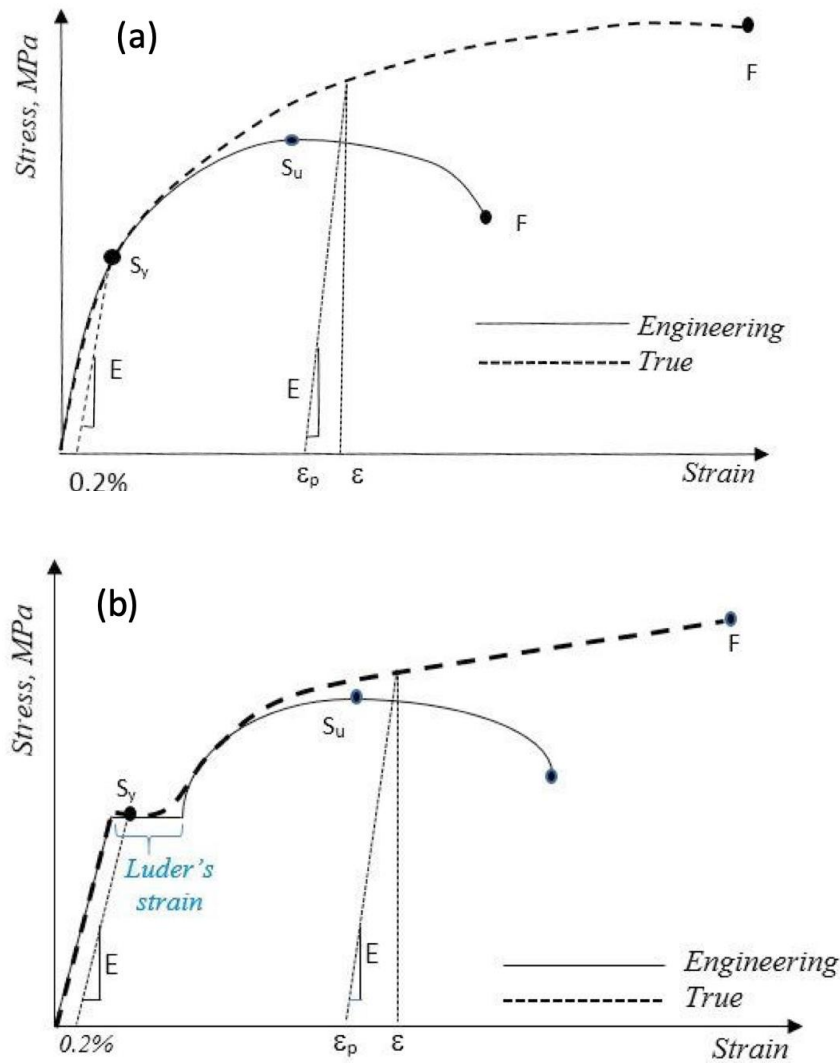


Figure 19: Stress-strain curves without (a), and with (b) Luder's strain [67].

2.5.2. Work Hardening Models in ABAQUS/CAE

When metals are subjected to plastic deformation, the material will strengthen due to dislocations in the crystal structure when subjected to plastic deformation. This process is called work hardening or strain hardening. As a result of this, the material becomes less ductile and more brittle [69]. This effect might be both desirable and undesirable, depending on the specific case and use of the material.

When defining material plasticity in ABAQUS/CAE, one must define the model to be used to describe the hardening. Several options are available:

- Isotropic hardening: Suitable for dynamic problems or problems with large plastic strains [70].
- Kinematic hardening: Intended to describe the plastic behaviour under with cyclic loading, with a constant hardening modulus [71].
- Multilinear kinematic hardening: The same as kinematic hardening, but with multiple constant hardening modules (H_i) as seen in Figure 20.
- Combined hardening: a combination of isotropic and kinematic hardening.
- Johnson-Cook: A type of isotropic hardening, mostly used for adiabatic transient dynamic analyses[72].

In the case of buckling Cao, et al. [17-19] and Li, et al. [20] successfully applied the Multilinear-Kinematic model in the investigation of buckling in S800 steel sections.

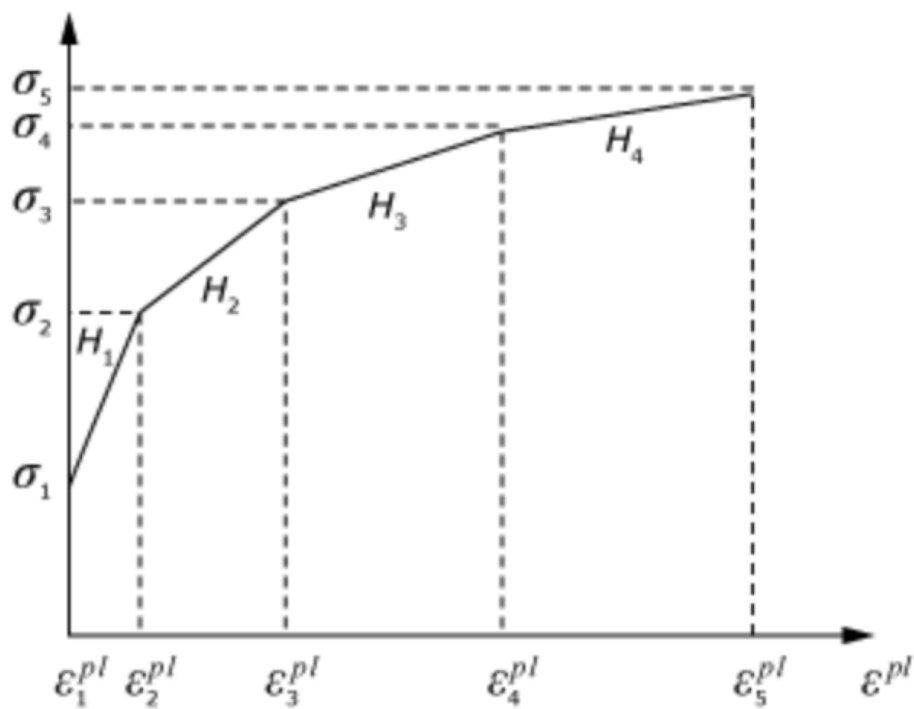


Figure 20: Multilinear kinematic hardening model[73].

3. Finite Element Analyses

When analysing multiple similar analyses, an established and verified procedure for the FE-model is important. A reliable procedure for modelling and analysing specific cases also eliminates the need for multiple physical tests. However, some physical tests are often valuable to verify the underlying methods and definitions used in a numerical method. In other words, physical test often provides verification and reliability to an FE-model. Hereunder, a FE-model is developed and validated against tests, and further applied to calculate the critical buckling load for I-sections of S800, S960 and S1100 graded steel.

3.1. Verification of FE-Model for HSS I-sections Under Axial Compression

Cao, et al. [17-19] and Li, et al. [20] performed tests on multiple I-, H-, T- and box-sections made of welded 800 MPa steel plates (S800) and developed a FE-model which was validated against the tests in each of the reports. In total 42 tests were performed, where 12 of them were on I-sections. The FE-models in these studies were generally accurate compared to the results from the test. In Table 1 the discrepancy in the results from the FE-analysis are represented in terms of average discrepancy and standard deviation. All the articles concluded with a FE-model accurate enough to estimate ultimate loads of S800 welded sections under compression.

Table 1: Discrepancy in results from the reference articles

Section type	Average	Standard deviation	Reference
I	5.14 %	5.30 %	[18]
T	1.60 %	7.77 %	[17]
H	4.11 %	6.47 %	[19]
Box	2.19 %	3.32 %	[20]

Since these articles concluded with accurate FE-models, the model in this thesis is to be based on the same properties and modelling approach, and the goal in this section is to verify the model against the results from the article covering I-sections[18], both the tests and the FE-analyses. However, Cao, et al. [17-19] and Li, et al. [20] used the FE-software ANSYS, and due to using ABAQUS/CAE in this thesis, some adjustments and modifications to the described

methods must be performed. There is also a lack of detailed information about the FE-analysis in the articles, which causes the need for some assumptions and trial-and-error when developing a new FE-model in ABAQUS/CAE. Both of these might cause some small discrepancies from the reported results.

3.1.1. Test Setup

A 12 mm thick steel plate was welded to both top and bottom of the test-specimens. The specimen was then placed in a compressional unit, where the bottom was a “double-knife-edge”-support, which allows some rotation of the endplates and correction of eccentricity, thus the specimen is constrained as hinged. Figure 21 shows the test setup for I-sections.

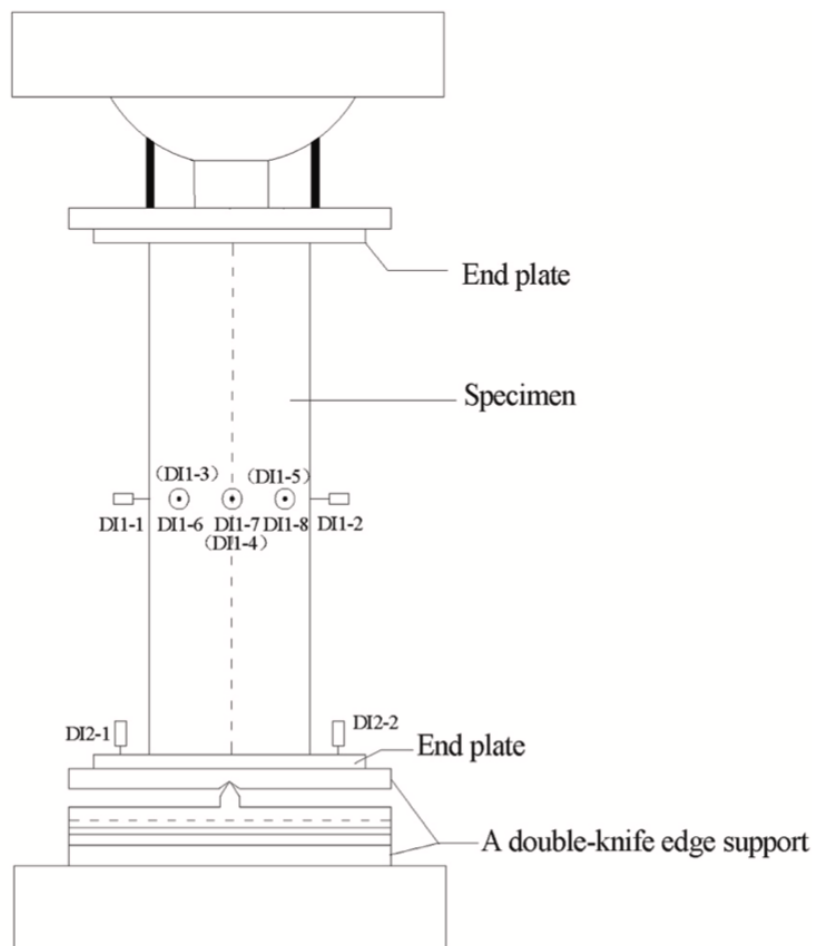


Figure 21: Illustration of test setup [18].

Figure 22 illustrates a generic I-section, and names the different dimensions in the cross section. In Table 2 the dimensions of the cross sections used in the 12 tests are given. These are the dimensions used in this study to validate of the FE-model.

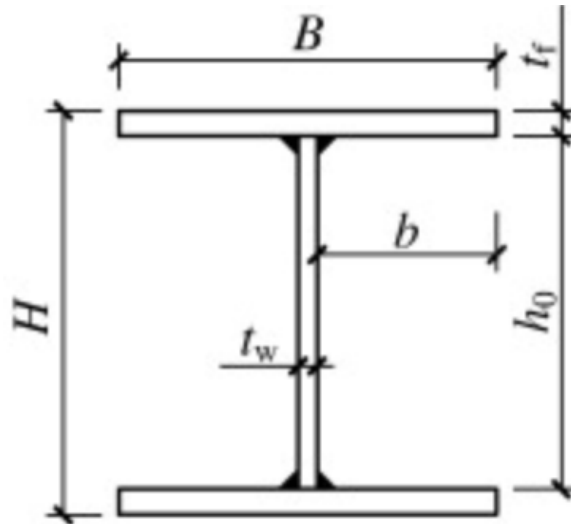


Figure 22: Illustration of dimensions on I-section [51].

Table 2: Dimensions of tested cross sections unit mm [18].

ID	Length, L [mm]	H [mm]	B [mm]	t_f [mm]	t_w [mm]
H-A1	549.0	160.7	198.8	7.36	7.36
H-A2	696.3	202.5	254.2	7.29	7.29
H-A3	845.2	244.0	309.3	7.35	7.31
H-B1	450.8	309.7	198.0	7.26	7.25
H-B2	598.2	394.2	253.2	7.26	7.45
H-C1	196.8	301.7	100.2	7.13	7.21
H-C2	243.5	397.7	130.2	7.16	7.12
H-C3	295.8	477.5	153.7	7.13	7.19
H-D1	549.3	308.5	100.3	7.34	7.26
H-D2	749.2	309.7	98.7	7.53	7.45
H-D3	1149.5	161.0	196.2	7.23	7.15
H-D4	1898.0	158.8	197.7	7.25	7.27

3.1.2. Defining the FEA

Just as for ANSYS, the nonlinear buckling analysis in ABAQUS/CAE generally consists of two steps: first a linear buckling analysis to find eigenmodes, and its corresponding eigenvalue with the application of a unit load and the. This step is called “Buckling” in ABAQUS/CAE and it estimates the bifurcation load. Lastly, a nonlinear analysis using the Riks method, is performed. In this step, the load is set equal to the eigenvalue for the first eigenmode from the linear analysis, and an initial imperfection in the shape of the eigenmode is applied. From this analysis, the maximum Load Proportionality Factor (LPF) can be found in ABAQUS, which is multiplied with the applied load for the nonlinear analysis to find the critical loading, N_{cr} .

Since a high number of analyses are to be made within a limited time period, the simplicity of the modelling is important. This is so that modelling time per analysis is kept at a minimum, but without affecting the validity and accuracy of the model.

Hereunder, the parameters and method, that further define the FE-model are described. These consist of what is described in the four reference studies [17-20]:

Geometry

The geometry consists of I-sections as defined in the article for I-sections [18]. Two 12mm thick steel plates are tied at the top and bottom to simulate the welded plates and plates of the compressional unit. To define the sections in ABAQUS/CAE, the “Solid, Extrusion” function is used. The cross section can there be drawn, before it is extruded in length.

The sections consist of welded plates, where the flange is welded to the web-plates using 6mm fillet welds. Plates and welds can be seen illustrated in Figure 22. These welds do in fact increase the cross-sectional area and thus, to some extent, provide additional capacity in the cross section. However, this effect is so small, that they are neglected for the sake of reducing modelling time.

Boundary conditions and loads

To simulate the boundary conditions of the test setup, the bottom plate is restrained in x-, y- and z-direction, while the top plate is restrained in x- and y-direction.

The compressional load (z-direction) is applied through a Reaction Point placed at the centre of the top plate. As mentioned above, the magnitude of the load is set to 1 for the linear analysis, and equal to the eigenvalue of the first eigenmode for the nonlinear analysis.

In the article that investigated I-sections [18], they investigated the influence of residual stress, from the production process, on the buckling capacity of the sections. For the examined cases, it only caused a reduction in capacity between 1 and 5% and concluded that it had little influence on the buckling load. With regards to this, and the significant increase in modelling time per analysis required, the residual stresses are not included in the analysis performed in this thesis.

Material properties

Tensile tests were performed for S800 in the reference studies in each of the articles, the material data for the steel was defined according to the average of the tests in each of the articles. In Figure 23 (left), the average stress-strain curve from the tensile test in relation to the I-section tests is plotted.

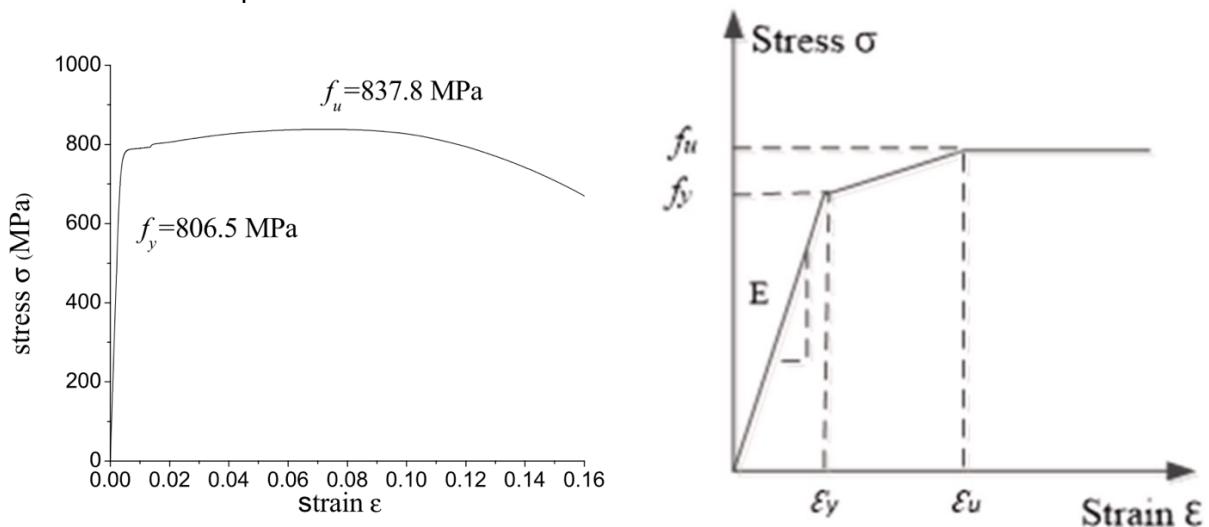


Figure 23: Average stress-strain relation from tensile tests, and illustration of multi-linear model [18]

In the analysis of I-sections, a multi-linear kinematic hardening model was applied, such as the one illustrated in Figure 23 (right). They used a rather coarse model with only two points to describe the non-linear material behaviour (yield and ultimate point), which results in a tri-linear-model. The average results from the tests for these values are given in Table 3. The table also states the average Youngs-modulus.

Table 3: Average results from tensile tests [18].

Yield strength, f_y [MPa]	Ultimate strength, f_u [MPa]	Youngs modulus, E [GPa]	Strain, ϵ_y [mm]	Strain, ϵ_u [mm]
806.5	837.8	215.6	0.012	0.068

These data are presented in engineering stress and strain and must accordingly be converted to true stress and plastic strain to be used as input in ABAQUS/CAE. The relations described in section 2.5 are thus applied.

Poisson's ratio and density are not mentioned in the reference articles, but are determined based on traditional values for steel as they do not vary much by different steel alloys [9]:

- Density, $\rho = 7850 \text{ kg/m}^3$
- Poisson's ratio, $\nu = 0.3$

Element and mesh

In [19, 20] the SHELL181 element was applied, while in [17, 18] the SOLID95 element was applied. Both element-types (shell and cube) proved to be reliable according to the studies. In [18, 19] the mesh size was set to approximately 10mm, and [17, 20] used approximately 20mm mesh.

For this thesis, the C3D20-element was chosen, since it is ABAQUS/CAE's-equivalent to the ANSYS SOLID95-element (brick with 20 nodes, each with 3 degrees of freedom) [74]. Further a mesh size of approximately 10 mm was used, as this was used in the analysis of I-sections by Cao, et al. [19]. Figure 24 shows the mesh on specimen H-A1 and illustrates how the meshing in general distributes over the cross section.

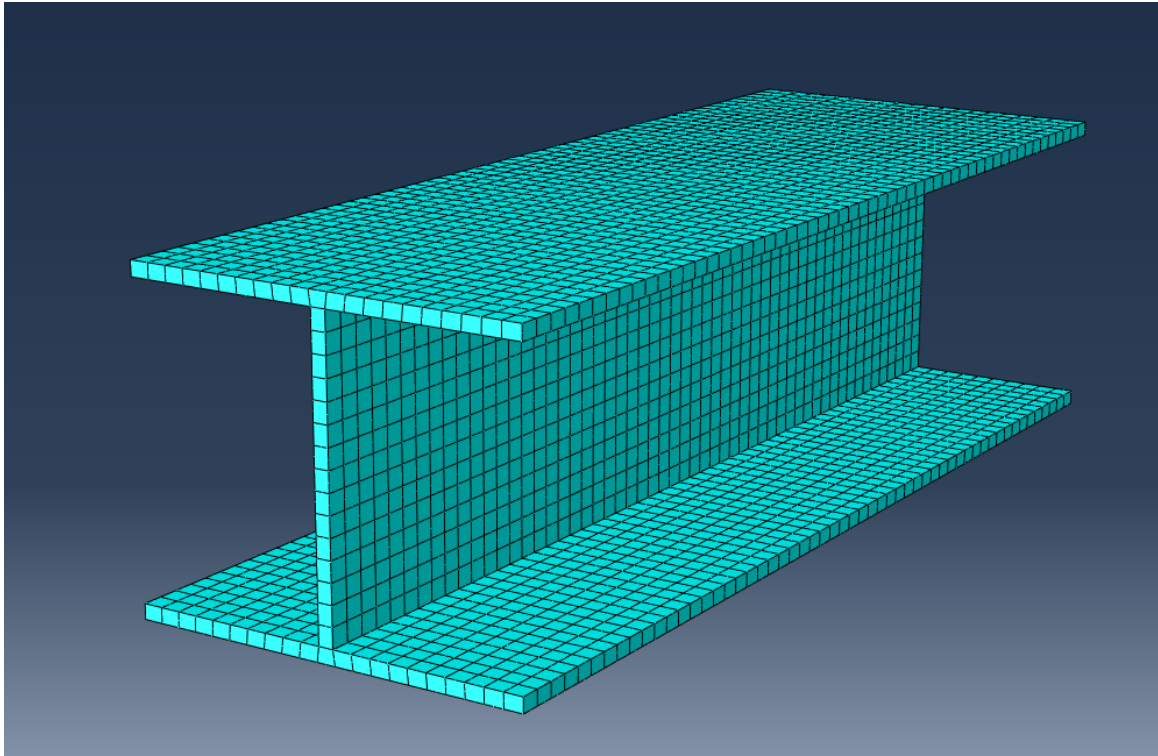


Figure 24: Meshing of cross section (H-A1).

Imperfections

The shape of the first eigenmode is used to apply imperfections to the nonlinear analysis. To perform this in ABAQUS/CAE, the following lines must first be inserted at the end of the keyword-file of the linear analysis:

```
*NODE FILE  
U
```

This ensures that the deformed node-locations are printed in the job-file. The deformation can then be applied in the nonlinear analysis by insert the following lines before the “Step”-section in the keyword-file:

```
*IMPERFECTION, FILE="Name-of-Linear-Job-FILE", STEP=1  
1, "ISF"
```

Here the name of the linear job is inserted. The number “1” in line two refers to the eigenmode number, which is mode number 1 in this case, and “ISF” is the imperfection scale factor. This applies a deformation where the maximum deformation of the first eigenmode is set equal to the value ISF, and the rest of the deformations are scaled in reference to this.

According to Kwon and Hancock [75] the shape of the imperfection has a larger effect on the capacity and behaviour, rather than the size of the imperfection. In the reference articles the scaling factor for the imperfection is set equal to length of the specimen divided by 1000. This is in accordance with the out-of-straightness that should be considered according to ANSI/AISC 360 [10]. The same ISF-values are therefore also used here. In ABAQUS/CAE, the desired imperfection must be multiplied with the thickness of the element (here: equal to plate thickness). Thus Eqn. 15 is used to determine the ISF for the FE-models.

$$\text{ISF} = t * \frac{L}{1000} \quad \text{Eqn. 15}$$

3.1.3. Evaluation of the Results

To validate that the FE-model described above provides reliable results, it is compared against the results from both the FE-analysis and the experimental tests performed on I-sections by Cao, et al. [18]. In appendix A, results from each test are presented with more details.

First, the buckling shapes can be evaluated. In Figure 25 the buckling shapes for some of the specimens are shown, these correspond well with what was seen in images presented in [18], both from the ANSYS analysis, and photos of the physical test. In addition, the location of the buckling also coincides, where the H-A specimens buckle at webs, H-B at flange and web, H-C at flange and H-D specimens are prone to global buckling.

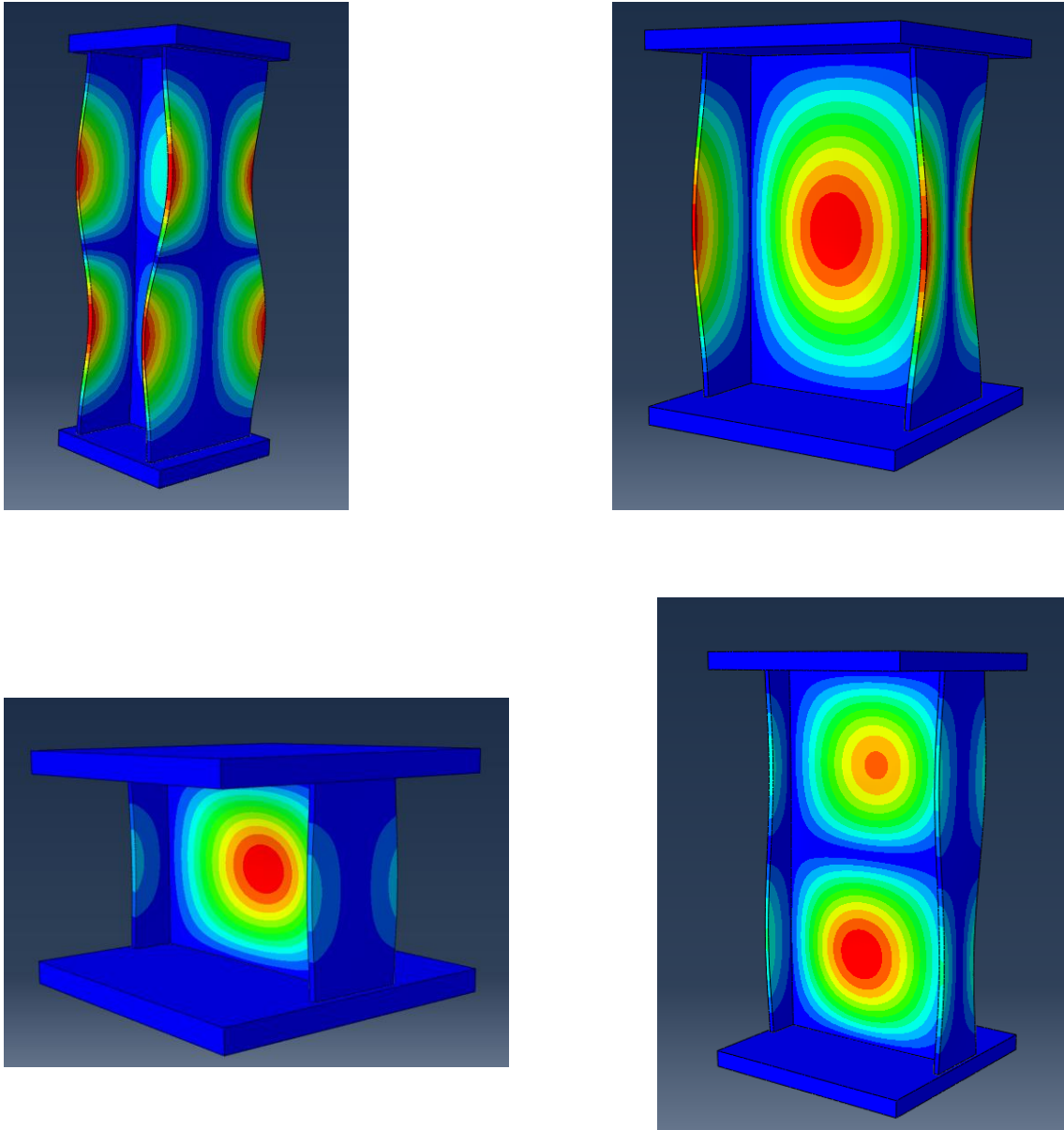


Figure 25: Buckling shapes of I-sections in ABAQUS/CAE. H-A1 (top left), H-B1 (top right), H-C1 (bottom left) and H-D1 (bottom right).

In Table 4 the calculated buckling loads are presented. As seen, the results correlate well with those both from the tests, and the FE-analysis performed by Cao, et al. [18] (without residual stress). The exception is the test H-C3, but as noted in the report, a crack was observed on the specimen, which quite likely caused a significant reduction in capacity. Apart from this, the rest of the calculations provide a discrepancy in the range of $\pm 0.1-6.2\%$, compared to both the ANSYS-tests and the physical tests. Based on these results, the FE-model is considered to yield reliable results for analysing buckling in S800 I-sections.

Table 4: Discrepancy between developed FE-model, and FE-analysis and test performed by Cao, et al. [18].

ID	N_{cr} ABAQUS/CAE [kN]	N_{cr} from [18] [kN]	Discrepancy (FEA)	N_{cr} - Test [kN]	Discrepancy (Test)
H-A1	2500	2503	-0.1%	2380	5.0%
H-A2	2574	2621	-1.8%	2558	0.6%
H-A3	2903	2809	3.3%	2884	0.7%
H-B1	2450	2378	3.0%	2490	-1.6%
H-B2	2670	2567	4.0%	2690	-0.7%
H-C1	2415	2428	-0.6%	2390	1.0%
H-C2	2537	2561	-0.9%	2460	3.1%
H-C3	2776	2671	3.9%	2164*	28.3%*
H-D1	1921	1887	1.8%	1928	-0.3%
H-D2	1819	1757	3.5%	1742	4.4%
H-D3	2553	2564	-0.4%	2404	6.2%
H-D4	2470	2551	-3.2%	2408	2.6%

*Crack observed in test-specimen

3.2. S800

Since the model is verified against the test results of S800 I-sections, it is first used to perform multiple analysis of that. In [18], 72 analyses of S800 I-sections were performed, where the tests varies in slenderness, and in which parts are cross section class 4 (flange, web or both). A selection of these which represents the different degrees of slenderness and cross-sectional classes, are analysed again. The specimens are either classified as class 4 by the slenderness of the web, flange or both. Selected specimens with dimensions are given in Table 5.

Method of defining the FE-model is just as described in the validation process, and the geometry is as defined in the report by Cao, et al. [18]. The main difference from this part to the validation part, is that the validation process was trial-and-error based where the goal was to come as close to the existing results, especially the test results. While these analyses are performed independently, and the results here are the ones that are analysed further.

The ID of the different analyses are the same as used in [18], where the ID is of the form “SxFyWz”, which refers to slenderness x, flange dimension y, and web dimension z. The numbers are not dimensions in mm or slenderness, but only types that are the same. So S1F1W1 and S2F1W1 have the same dimensions of flanges and web, but vary in length, so that they differ in slenderness.

In Table 5 it is also given which part of the section that is classified as class 4 section. They might in theory vary for the different steel grades further analysed, but they turned out to be the same for all steel grades.

Table 5: Dimensions of analysed cross section [18].

ID	Length, L [mm]	H [mm]	B [mm]	t_f [mm]	t_w [mm]	Cross section class 4 (S800)
S1F1W4	616.9	210	100	7	7	Web
S1F5W8	983.6	160	140			Flange
S2F1W7	1486.7	300	100			Web
S2F5W8	2622.9	160	140			Flange
S3F9W9	988.6	160	200			Flange
S4F9W9	1482.8	160	200			Flange
S5F9W9	1977.1	160	200			Flange
S6F9W9	2471.4	160	200			Flange
S7F9W9	2965.7	160	200			Flange
S8F9W9	3459.9	160	200			Flange
S10F9W9	4448.5	160	200			Flange
S11F9W9	4942.8	160	200			Flange
S12F9W9	5931.3	160	200			Flange
S13F9W9	6919.9	160	200			Flange
S14F9W9	7908.4	160	200			Flange
S3F10W10	371.7	300	100			Web
S4F10W10	557.5	300	100			Web
S5F10W10	743.3	300	100			Web
S6F10W10	929.2	300	100			Web
S7F10W10	1115.0	300	100			Web
S8F10W10	1300.8	300	100			Web
S9F10W10	1486.7	300	100			Web
S10F10W10	1672.5	300	100			Web
S11F10W10	1858.3	300	100			Web
S12F10W10	2230.0	300	100			Web
S13F10W10	2601.7	300	100			Web
S14F10W10	2973.3	300	100			Web
S15F9W10	441.1	300	200			Both
S16F9W10	661.6	300	200			Both
S17F9W10	1102.6	300	200			Both
S18F9W10	1543.7	300	200			Both
S19F9W10	1984.8	300	200			Both
S21F9W10	2866.9	300	200	Both		
S22F9W10	3307.9	300	200	Both		

3.2.1. Results

In appendix B, results from each analysis are presented with more details.

As seen in Table 6, where the results are presented, discrepancy from the test performed by Cao, et al. [18] are approximately within the same range as what was seen for the validation process performed above. Some of the difference might be assigned to the inclusion of residual stresses in the analysis performed in the article referred to, as well as small numerical differences between the software ANSYS and ABAQUS/CAE.

The results are also plotted in relation to relative slenderness, in Figure 26, and in Figure 27 the necessary reduction factor (χ) to the cross-sectional capacity is plotted against the relative slenderness, which is the same units as the buckling curves in EC3. The reduction factor is found by solving Eqn. 1 for χ , which gives Eqn. 16.

$$\chi = \frac{N_{cr,FEA}}{f_y * A} \quad \text{Eqn. 16}$$

In the plot of Figure 26, the results show a good distribution of results, where higher slenderness yields lower capacity against buckling. In Figure 27 indications of a relation with regards do relative slenderness is also observed. And to a certain degree they seem to correlate well with the curves form EC3, however for some cases the curves given in EC3 will yield overestimated capacities.

It may also be pointed out that due to restrictions in number of nodes in the ABAQUS/CAE-licensing, the meshing of the S13F9W9 and S14F9W9 had to be increased from 10mm to approximate size of 15mm.

Table 6: Results from analyses of buckling capacity of S800 I-sections.

ID	Slenderness, λ	Relative slenderness	N_{cr} FEA [kN]	N_{cr} from [18] [kN]	Discrepancy
S1F1W4	30	0.58	1758	1645	6.9 %
S1F5W8	30	0.58	1911	1880	1.7 %
S2F1W7	80	1.55	1342	1381	-2.8 %
S2F5W8	80	1.55	1144	1226	-6.7 %
S3F9W9	20	0.39	2262	2405	-5.9 %
S4F9W9	30	0.58	2136	2145	-0.4 %
S5F9W9	40	0.78	1915	1845	3.8 %
S6F9W9	50	0.97	1638	1575	4.0 %
S7F9W9	60	1.16	1368	1321	3.6 %
S8F9W9	70	1.36	1104	1125	-1.9 %
S10F9W9	90	1.75	873	816	7.0 %
S11F9W9	100	1.94	702	680	3.2 %
S12F9W9	120	2.33	615	574	7.1 %
S13F9W9*	140	2.71	420	410	2.5 %
S14F9W9*	160	3.10	360	349	3.2 %
S3F10W10	20	0.39	2086	2142	-2.6 %
S4F10W10	30	0.58	1880	1923	-2.2 %
S5F10W10	40	0.78	1757	1682	4.5 %
S6F10W10	50	0.97	1537	1444	6.5 %
S7F10W10	60	1.16	1195	1230	-2.8 %
S8F10W10	70	1.36	1068	1048	1.9 %
S9F10W10	80	1.55	894	897	-0.4 %
S10F10W10	90	1.75	829	773	7.2 %
S11F10W10	100	1.94	722	672	7.4 %
S12F10W10	120	2.33	587	566	3.8 %
S13F10W10	140	2.71	463	439	5.5 %
S14F10W10	160	3.10	393	383	2.7 %
S15F9W10	10	0.19	2469	2296	7.6 %
S16F9W10	15	0.29	2081	2005	3.8 %
S17F9W10	25	0.48	1867	1823	2.4 %
S18F9W10	35	0.68	1694	1631	3.8 %
S19F9W10	45	0.87	1472	1406	4.7 %
S21F9W10	65	1.26	1076	1027	4.8 %
S22F9W10	75	1.45	851	826	3.1 %

*Mesh reduced to approximate size 15mm.

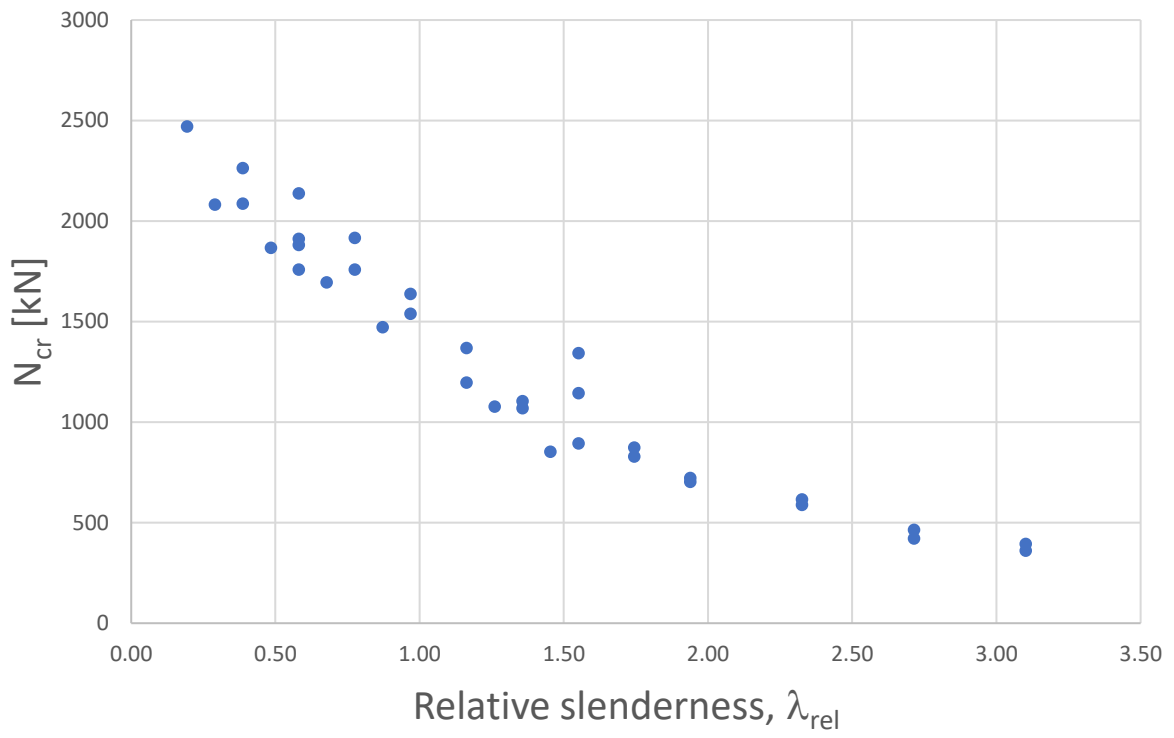


Figure 26: Results from analysis of S800 I-sections. Critical load vs relative slenderness.

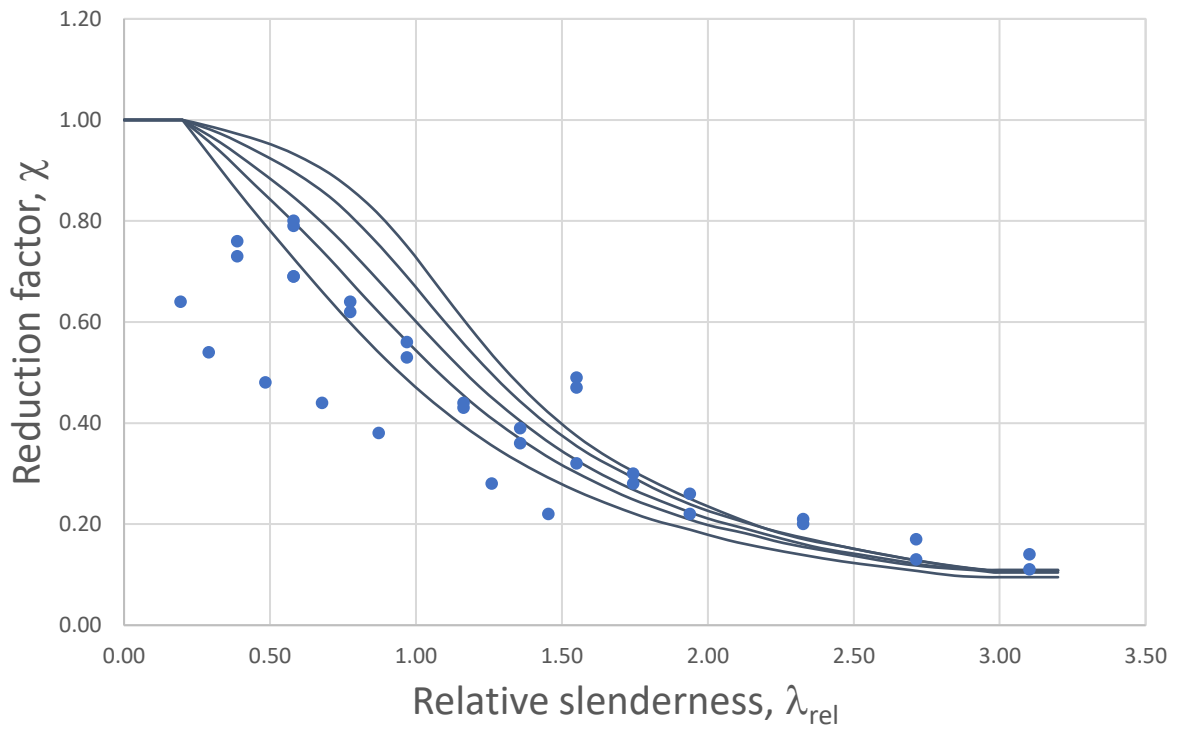


Figure 27: Reduction factor vs relative slenderness (S800), with buckling curves from EC3.

3.3. S960

With a verified FE-model for welded I-sections of S800, the same model is further applied to analyse the stability of S960 welded I-sections. Only material data is changed, all other parameters, such as mesh, loading-method, element, solver, are unchanged further in the analyses. For this to be possible, a material model for S960 must first be established.

3.3.1. Material Data

Ban, et al. [51] performed tensile tests on three specimens of S960. Results of the tests are given in Table 7. From these three tests, the E-modulus of S960 was averaged to $2.08 \cdot 10^5$ MPa. Density was assumed to 7850 kg/m^3 and Poisson's ratio, ν , set to 0.3, which are the same as what was used for S800.

Table 7: Results of tensile test of S960, performed by Ban, et al. [51]

Tension coupon no.	E-modulus [MPa]	Yield strength, f_y [MPa]	Ultimate tensile stress, f_u [MPa]	Strain at peak stress, ϵ_u
1	2.11 E+05	963.5	1042.9	0.016
2	2.03 E+05	983.5	1054.0	0.015
3	2.11 E+05	972.7	1059.1	0.025
Average	2.08 E+05	973.2	1052.0	0.019

For the nonlinear part, plasticity data for S960 must be calculated based on the data given above. This was performed using the Ramberg-Osgood method (section 2.5.1), and data from the tensile tests given in Table 7. Engineering stress and strain was then used to calculate true stress and plastic strain, which were used as material plasticity data in ABAQUS/CAE. Figure 28 shows the stress-strain curve from the calculations, both engineering, and true stress/strain.

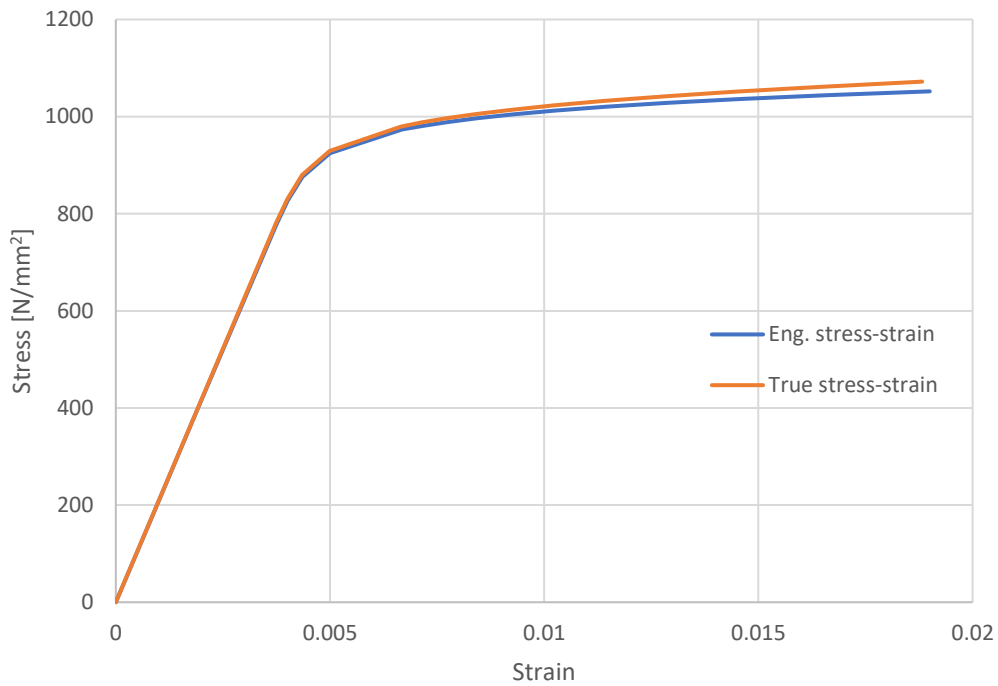


Figure 28: Calculated stress-strain curve for S960.

3.3.2. Results

With the material data set, the exact same procedure as what was applied for S800, is applied to analyse the same specimens, but with S960. Results are presented in Table 8. The results are also compared to the results from the S800 results. In appendix B, results from each test are presented with more detail.

In Figure 29 and Figure 30 the same plots as for the S800 results are provided; N_{cr} vs relative slenderness, and reduction factor vs relative slenderness.

A wide variety of increase is seen, ranging from approximately 0-20%. Especially the ones with high relative slenderness, tends to not have any significant increase. While the ones with low relative slenderness generally has an increase around 20%, which corresponds well with the general increase in yield strength ($960/800 = 20\%$ increase). Two cases with a reduction in capacity are also observed, but these are of rather small size (-0.6 and -0.8%), and thus assumed to only be the cause of numerical differences in the FE-software.

Table 8: Results from analyses of buckling capacity of S960 I-sections.

ID	Slenderness, λ	Relative slenderness	N_{cr} FEA [kN]	Increase from S800
S1F1W4	30	0.65	2028	15.4 %
S1F5W8	30	0.65	2228	16.5 %
S2F1W7	80	1.73	1383	3.0 %
S2F5W8	80	1.73	1221	6.8 %
S3F9W9	20	0.43	2673	18.2 %
S4F9W9	30	0.65	2616	22.5 %
S5F9W9	40	0.86	2267	18.4 %
S6F9W9	50	1.08	1782	8.8 %
S7F9W9	60	1.30	1358	-0.8 %
S8F9W9	70	1.51	1258	14.0 %
S10F9W9	90	1.95	912	4.4 %
S11F9W9	100	2.16	721	2.7 %
S12F9W9	120	2.59	628	2.1 %
S13F9W9*	140	3.03	427	1.5 %
S14F9W9*	160	3.46	362	0.6 %
S3F10W10	20	0.43	2369	13.6 %
S4F10W10	30	0.65	2179	15.9 %
S5F10W10	40	0.86	1989	13.2 %
S6F10W10	50	1.08	1737	13.0 %
S7F10W10	60	1.30	1343	12.4 %
S8F10W10	70	1.51	1159	8.5 %
S9F10W10	80	1.73	959	7.3 %
S10F10W10	90	1.95	876	5.7 %
S11F10W10	100	2.16	753	4.3 %
S12F10W10	120	2.59	606	3.2 %
S13F10W10	140	3.03	473	2.1 %
S14F10W10	160	3.46	399	1.6 %
S15F9W10	10	0.22	2780	12.6 %
S16F9W10	15	0.32	2385	14.6 %
S17F9W10	25	0.54	2161	15.8 %
S18F9W10	35	0.76	1986	17.3 %
S19F9W10	45	0.97	1492	1.4 %
S21F9W10	65	1.41	1130	5.0 %
S22F9W10	75	1.62	846	-0.6 %

*Mesh reduced to approximate size 15mm.

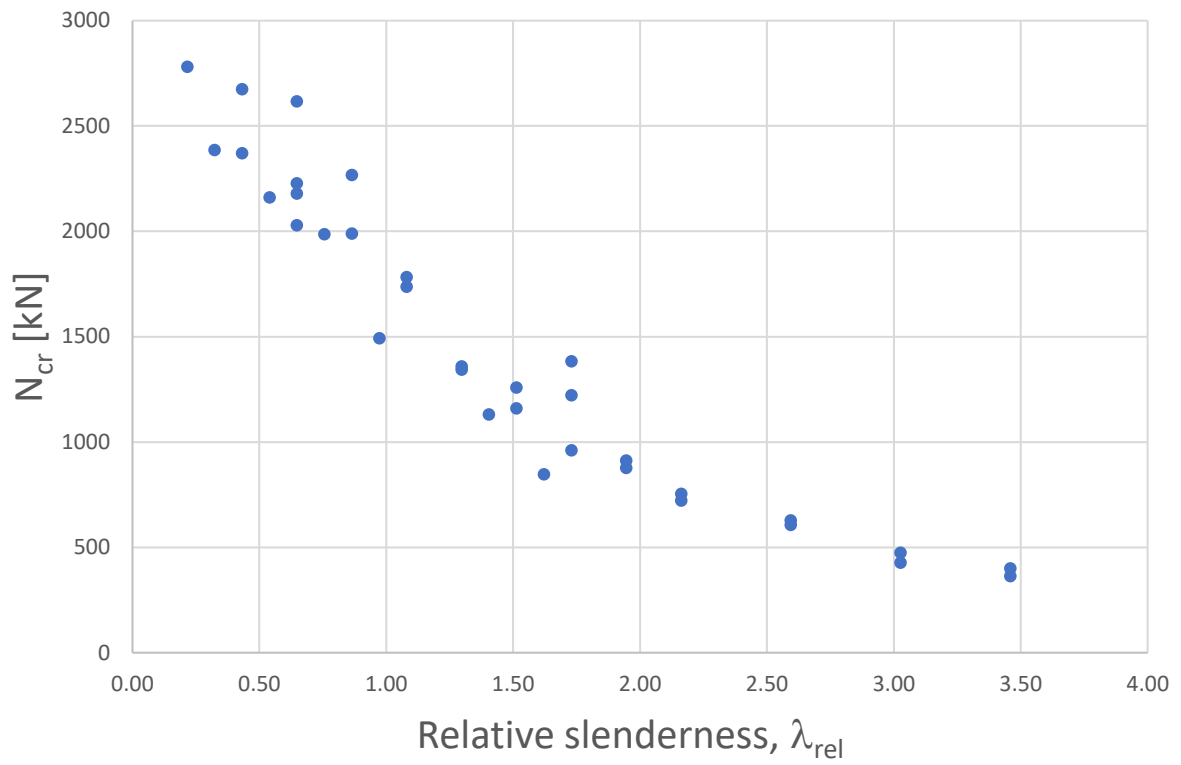


Figure 29: Results from analysis of S960 I-sections. Critical load vs relative slenderness.

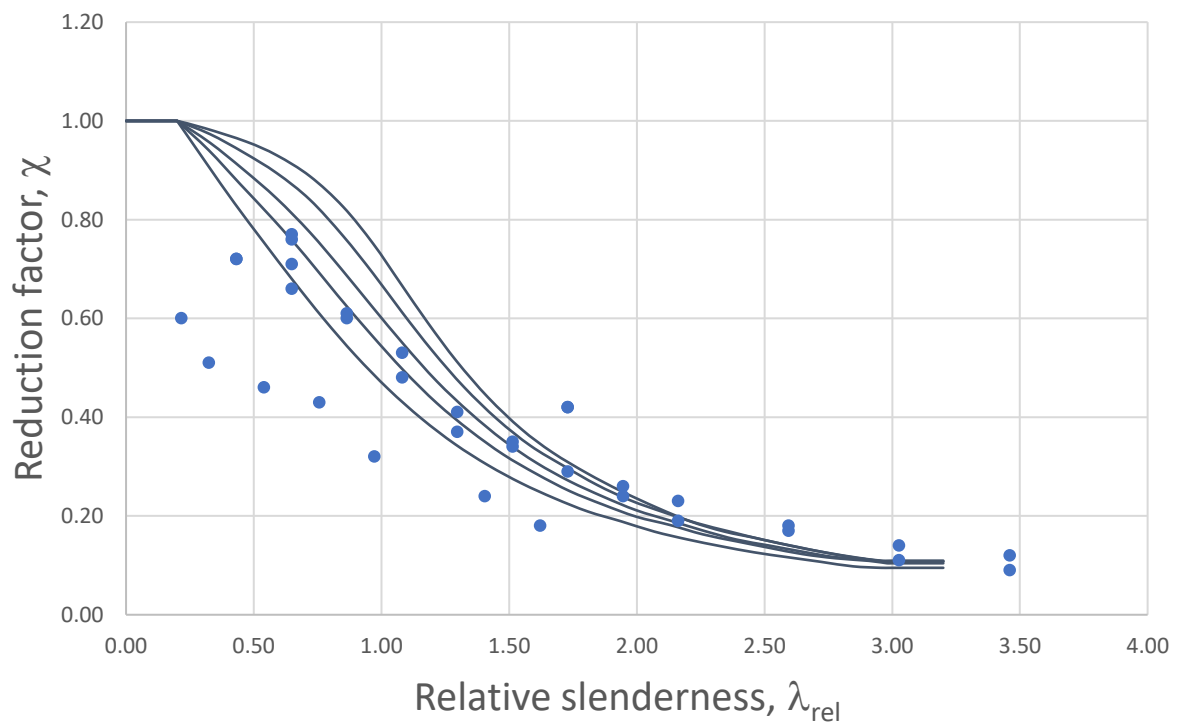


Figure 30: Reduction factor vs relative slenderness (S960), with buckling curves from EC3.

3.4. S1100

With results from analysis of buckling behaviour in class 4 I-sections of both S800 and S960, the same procedure is further applied to analyse even higher graded steel; S1100.

3.4.1. Material Data

Just as for S960, a material model to describe the plastic behaviour of S1100 is needed. For this, data from a tensile test is once again preferably the basis of the material model. Ma, et al. [76] performed such tests on, among others, S1100-graded steel. In Table 9 the relevant results for S1100 are summarised.

Table 9: Material data from tensile test of S1100 [76]

E-modulus [MPa]	Yield strength, f_y [MPa]	Ultimate tensile stress, f_u [MPa]	Strain at peak stress, ϵ_u
2.07 * 10 ⁵	1152	1317	0.022

Again, the Ramberg-Osgood method is applied to calculate true stress and plastic strain, thus having the necessary material input to describe the plastic behaviour of the material in ABAQUS/CAE. In Figure 31 the calculated true and engineering stress-strain curves are presented.

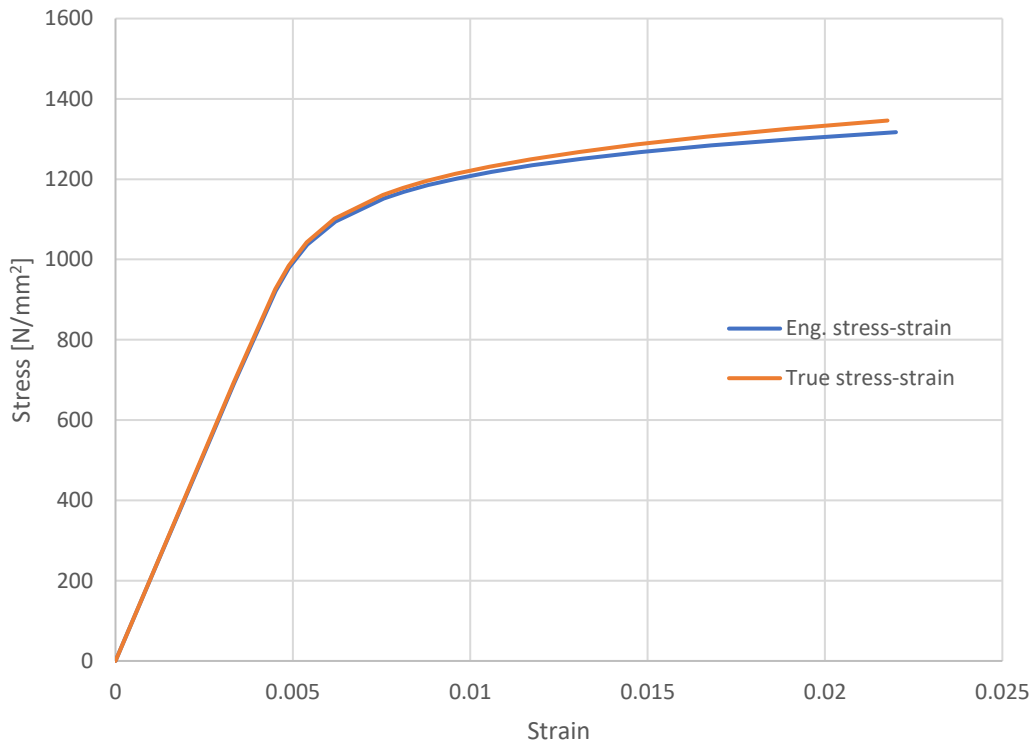


Figure 31: True and engineering stress-strain curves for S1100.

3.4.2. Results

The verified FE-model is applied in the same way as earlier, but with the new material model, to analyse the critical buckling load for the same I-sections as before. Results are given in Table 10 and the same plots are given in Figure 32 and Figure 33. More detailed results are given in appendix B.

The same tendencies can be seen here. The increase in buckling load, to some degree, varies with the relative slenderness, and is generally around 35% for the slenderest columns, which just as for S900, corresponds well with the increase in yield strength ($1100/800=37,5\%$ increase). It was also for S1100 one case of small reduction of -0.3% compared to S800 is seen for S7F9W9.

Table 10: Results from analyses of buckling capacity of S1100 I-sections.

ID	Slenderness, λ	Relative slenderness	N_{cr} FEA [kN]	Increase from S800
S1F1W4	30	0.70	2322	32.1 %
S1F5W8	30	0.70	2569	34.4 %
S2F1W7	80	1.86	1462	9.0 %
S2F5W8	80	1.86	1320	15.3 %
S3F9W9	20	0.46	3108	37.4 %
S4F9W9	30	0.70	3004	40.6 %
S5F9W9	40	0.93	2565	34.0 %
S6F9W9	50	1.16	1886	15.2 %
S7F9W9	60	1.39	1364	-0.3 %
S8F9W9	70	1.62	1392	26.2 %
S10F9W9	90	2.09	953	9.1 %
S11F9W9	100	2.32	757	7.8 %
S12F9W9	120	2.78	652	6.1 %
S13F9W9*	140	3.25	441	4.8 %
S14F9W9*	160	3.71	373	3.6 %
S3F10W10	20	0.46	2721	30.5 %
S4F10W10	30	0.70	2486	32.2 %
S5F10W10	40	0.93	2255	28.3 %
S6F10W10	50	1.16	1989	29.4 %
S7F10W10	60	1.39	1512	26.5 %
S8F10W10	70	1.62	1266	18.5 %
S9F10W10	80	1.86	1035	15.8 %
S10F10W10	90	2.09	934	12.7 %
S11F10W10	100	2.32	805	11.6 %
S12F10W10	120	2.78	638	8.6 %
S13F10W10	140	3.25	495	6.8 %
S14F10W10	160	3.71	415	5.6 %
S15F9W10	10	0.23	3192	29.2 %
S16F9W10	15	0.35	2726	31.0 %
S17F9W10	25	0.58	2488	33.3 %
S18F9W10	35	0.81	2302	35.9 %
S19F9W10	45	1.04	1556	5.7 %
S21F9W10	65	1.51	1171	8.8 %
S22F9W10	75	1.74	855	0.4 %

*Mesh reduced to approximate size 15mm.

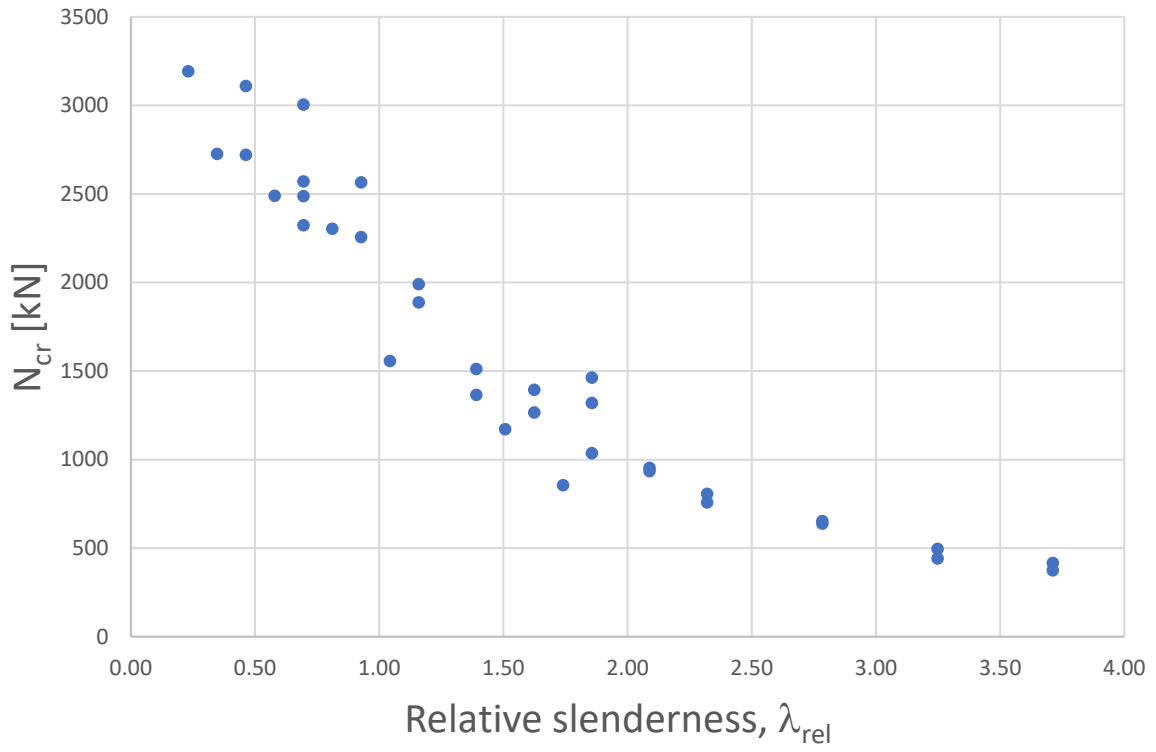


Figure 32: Results from analysis of S1100 I-sections. Critical load vs relative slenderness.

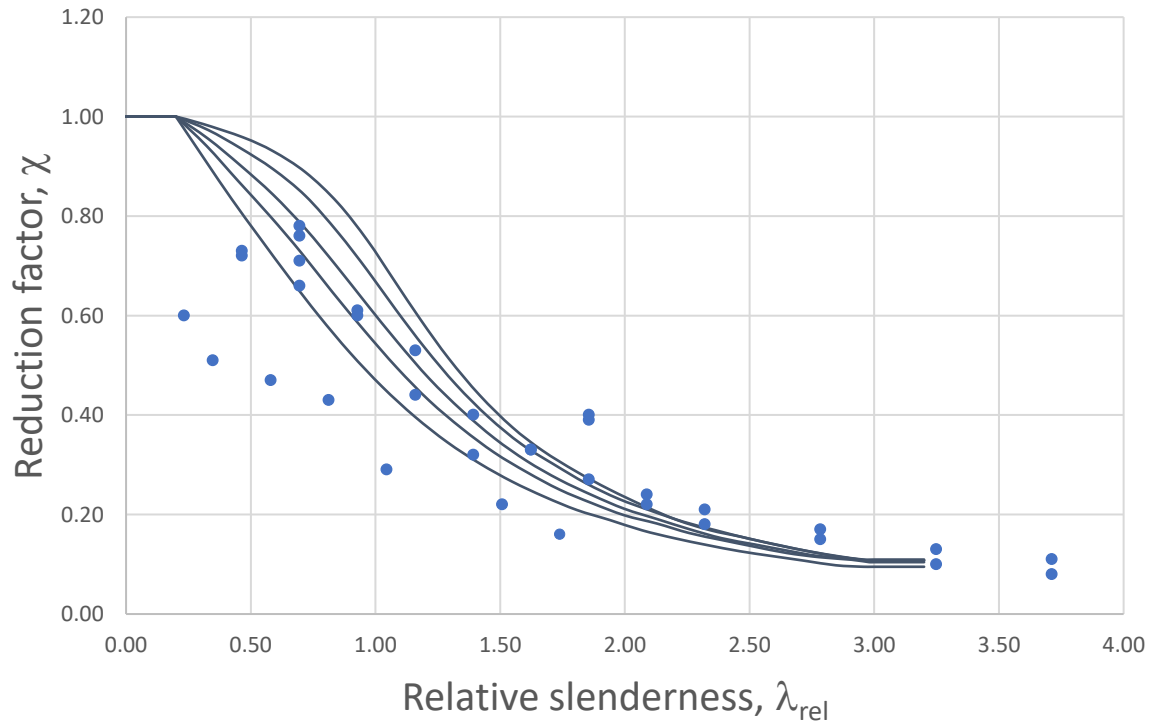


Figure 33: Reduction factor vs relative slenderness (S1100), with buckling curves from EC3.

4. Evaluation of Results and Buckling Curves

In total 114 FE-analysis have been executed, 34 analyses per steel grade, plus 12 analyses in the validation process. The analyses represent a wide variety of specimens with regards to slenderness, and the results forms a good foundation for further evaluating buckling of HSS I-sections.

In both the case of S960 and S1100, the increase in buckling capacity (compared to S800) seems to be highly related to the relative slenderness. In Figure 34, where the buckling load is plotted against the relative slenderness for all three steel grades, it can be observed that for high relative slenderness, the difference between the buckling capacity is rather small, while on the left side, where the relative slenderness is low, the yield strength of the material seems to have a greater impact on the buckling capacity.

It may also be noted that there are cases where S800/S960 has greater capacity against buckling than S960/S1100 for approximately the same slenderness. This indicates that also other parameters are affecting the results, and not only the relative slenderness.

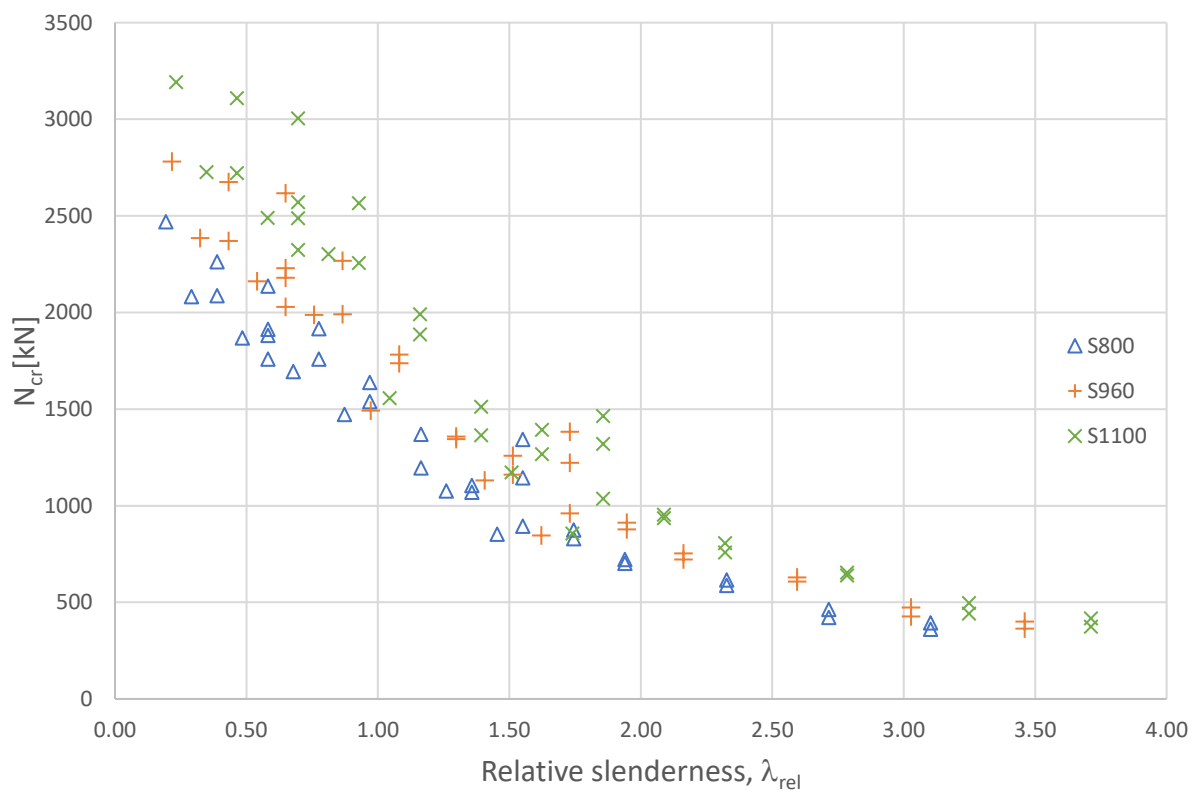


Figure 34: Results from analysis of S800, S960 and S1100 I-sections. Critical load vs. relative slenderness.

Reduction factor vs. relative slenderness for all three steel grades is plotted in Figure 35, alongside the buckling curves from EC3. The reduction factor plotted is the necessary reduction factor to yield results equal to the actual capacity according to the FE-analysis. This means that when designing by buckling curves, the value of the reduction factor should be on the conservative side. Therefore, a buckling curve should be below the plotted results, so that when designing according to the methods in EC3, conservative results are yielded.

It may then be seen that for most of the results, the lowest curve from EC3 (curve *d*) could be used, with rather accurate results for some cases, and with conservatism for some cases, especially the one that has a relative slenderness above approximately 2.0. It will however somewhat underestimate for the cases in the small cluster at approximately $\lambda_{rel}=0.5$ and $\chi=0.75$. It will also quite heavily overestimate all the 21 cases that seems to align a bit lower than all the EC3 curves. This overestimation in the EC3, was expected, as this was also pointed out by Schillo, et al. [11].

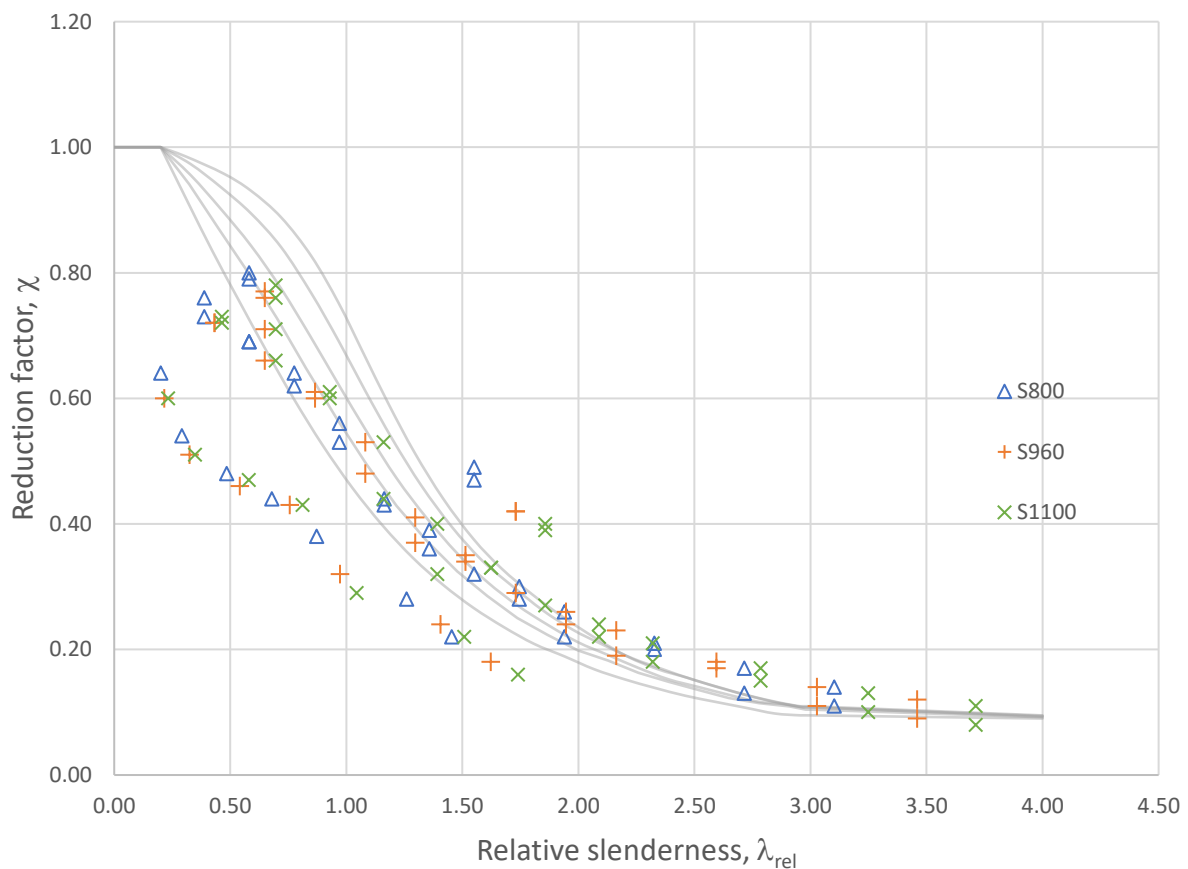


Figure 35: Reduction factor vs. relative slenderness for all test, with buckling curves from EC3.

These 21 cases, that has outlined a new curve, proves to be the seven last specimens (see for example Table 10), for all three steel grades. What proves to differentiate these, from all the other analysed sections, are that they are classified as cross section 4, for both web and flange. While all other cases are only classified as cross section 4 for one of them.

Since all cases analyse sections of class 4, all of them are prone to local buckling (according to the definition of cross section class). It can then be noted that also what seem like global buckling can be observed for the specimens with high slenderness. One such case is illustrated in Figure 36a for specimen S12F9W9 and was generally the case for S10F9W9 to S14F9W9, where the slenderness ranges from 90 to 160. This is somewhat in line with the limits for elastic buckling mentioned in section 2.3.2. This is also the reason for the convergence in the results for higher slenderness.

Elsewise, there is a good correlation between where the buckling was estimated to occur based on the slenderness (Table 5). For example specimen S1F5W8 (Figure 36b) buckles in the web, while in S5F10W10 (Figure 36c) the flange buckles and for S16F9W10 (Figure 36d) both flange and web buckles.

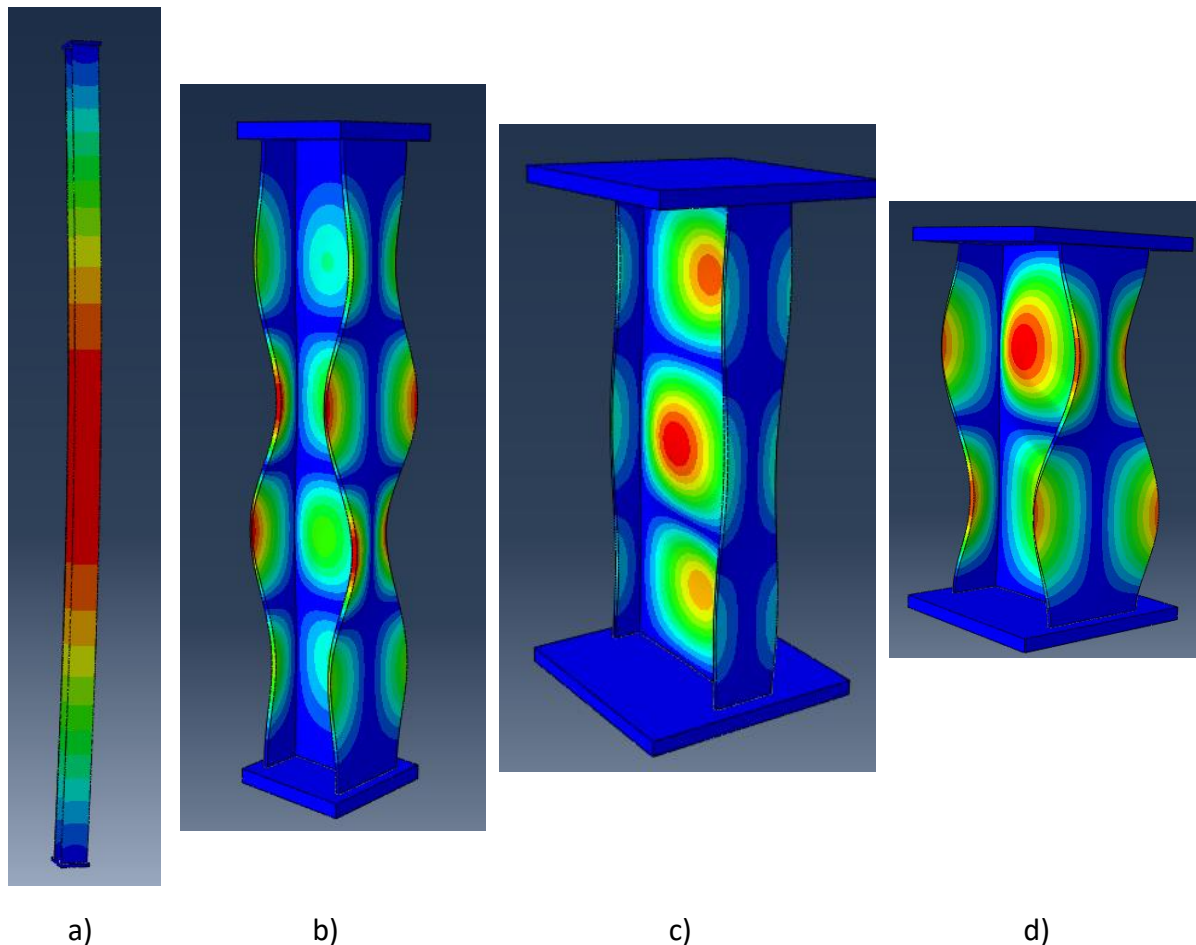


Figure 36: Buckling shapes of specimen S12F9W9 (a), S1F5W8 (b), S5F10W10 (c) and S16F9W10 (d).

4.1. Evaluation of the Model

Through the validation process the FE-model was validated against the tests on I-sections performed by Cao, et al. [18]. These tests were made of the same material as the tensile tests for the S800 material model that was used in their FE-model. It was further assumed that the same model would be applicable to other steel grades.

Due to potentially small variations in material properties between the different steel grades, they might behave somewhat differently with regards to buckling. Thus, the defined FE-model could potentially yield inaccurate results for the steel grades of S960 and S1100 since they are based on tensile tests performed in the work by others, as well as the FE-model not being verified against compressional tests on complete sections. The differences in buckling behaviour between these three materials are however assumed small, since they are all HSS with mainly small variations in ductility and strength. Thus, it is assumed that the same FE-model has yielded reliable results for the additional steel grades.

Another aspect that was not included in the performed analyses above, is the residual stress. The buckling curves given in EC3 are defined so that residual stress, imperfections etc. are taken into consideration [39]. It is pointed out by Schillo, et al. [11] that the effect of residual stresses on buckling capacity, is not directly related to increase in steel grade. For buckling of S800 welded I-section, Cao et.al [18] investigated the effect of residual stress, which proved to be rather small, in the range of 1.65-5.51% difference in critical load. Due to this, and to reduce the modelling time significantly, the residual stress was not included in the analyses of S800, S960 and S1100 I-sections in this study.

Safety factors and safety margins are not a topic that has been attained much attention for these analyses. It is assumed that safety factors regarding load and material are included in the calculation rules given in the Eurocodes, which is taken into consideration when defining new proposed buckling curves.

In the calculation of necessary reduction factor, the use of A_{eff} , was not taken into consideration. This is due to the goal of buckling curves purely for class 4 sections, thus removing the need for implementing A_{eff} .

4.2. Proposal for Buckling Curves

Based on what was observed in the results, two new buckling curves are advised to cover buckling of S800, S960 and S1100 welded I-sections. The first, named curve e , will cover the cases where only the web or flange are classified as cross section class 4. This curve seems necessary as the curve d in EC3 would result in optimistic capacities for low slenderness cases. Thus, the new curve e , will mostly be an adjustment of curve d from EC3. The second one, named f , covers the 21 cases that were relatively far off from the curves in EC3; the ones where both flange and web are cross section class 4.

In Figure 37, the two additional buckling curves are presented. The distribution in the results causes some difficulties when attempting to define new buckling curves that will yield accurate without causing unnecessary underestimation of the results for other cases.

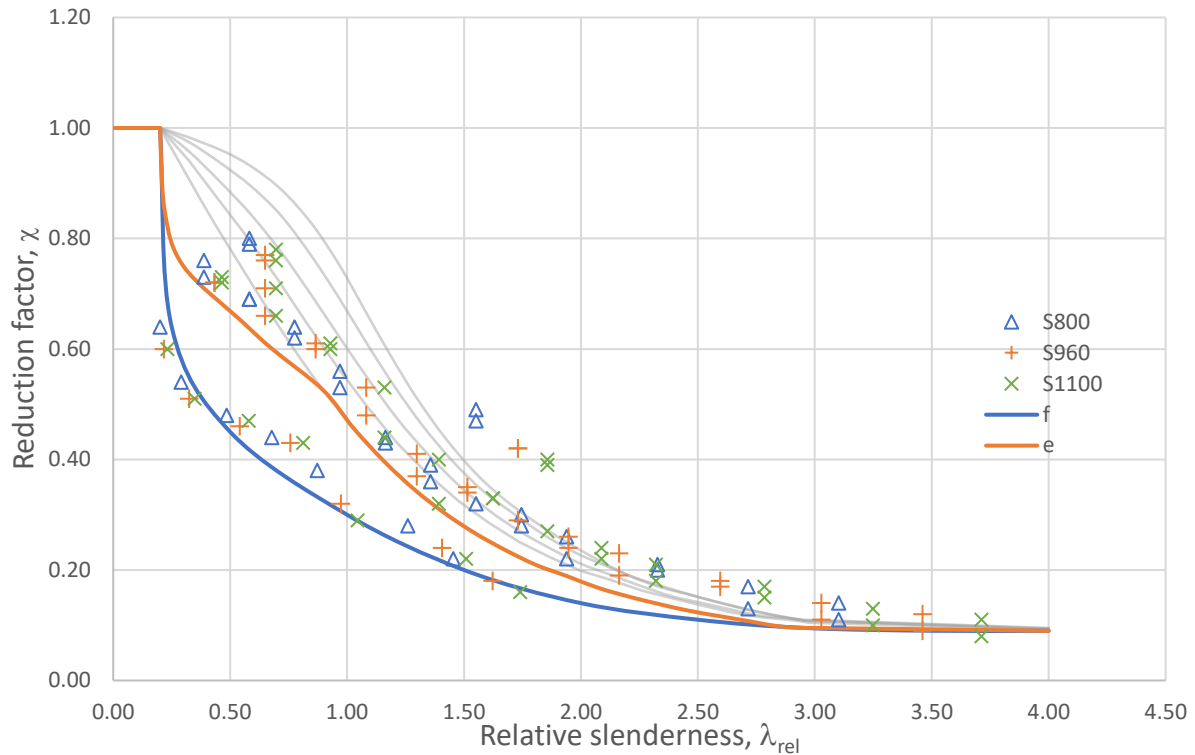


Figure 37: Suggestions for new buckling curves, curve e (orange) and curve f (blue).

Further, the proposed buckling curves for S800-S1100 are used to calculate the critical buckling load of the same sections and in the FE-analysis according to the method in EC3 (Eqn. 1), with approximate values for the reduction factor (χ) collected manually using the curves, as this is how it often is performed when designing according to EC3. The results are then compared to the results from the FE-analyses. Note that in the calculations, material factor is neglected, i.e. $\gamma_M=1.0$. This way, the accuracy of the curves is better illustrated.

The results from these calculations are summarized in

Table 11. As expected, there is a high variation in accuracy, due to the wide range of results as seen earlier. However, it is most important that the curves yield conservative results, which they in general do. There are some exceptions to this:

- S14F9W9: Overestimated by 1% for S960, and 13% for S1100. This one of the slenderest specimens tested, and the relative slenderness of the specimens is located at above 3.5 where all curves converge in the elastic-buckling-zone. The capacity is also rather low (estimated to 371 kN in the FEA), thus, a relatively small discrepancy of 50 kN appears as large in percentage-comparison.
- S15F9W10: Overestimated by 17% (S800), 19% (S960) and 16% (S1100). These large overestimations are caused due to the relative slenderness being close to the 0.2 plateau-limit, which is as determined in EC3. This indicates that for HSS, this limit should be somewhat reduced for HSS. It could also justify that the γ_M should be increased, to for example 1.1 as suggested by Schillo, et al. [11], but this would also increase the conservatism for the other cases with higher slenderness.
- S16F9W10: Small overestimations of 3 and 2 % for S800 and S960. These are low percentages and assumed to be covered sufficiently by other safety factors in the design process, for example the material factor.

Apart from these, all results are on the conservative side, too a varying degree, ranging from -50% to 0. The largest discrepancies occur for the cases that are located above all curves from EC3 (Figure 37), meaning those curves will also yield potentially high conservative results.

It could be argued that for more accurate results it would be beneficial to use multiple curves. However, part of the goal for this thesis is to keep the design process simple, and therefore it was investigated possibilities for additional buckling curves, rather than additional steps to the design process. Buckling is also a stability problem, that in structures might have drastic consequences. Taking this into account, it seems sensible to define few, but conservative buckling curves for HSS, which has been performed for I-sections of S800, S960 and S1100.

Table 11: Calculation of buckling capacity with suggested curves.

Curve	ID	S800			S960			S1100		
		χ	$N_{b,Rd}$	Discr ep.	χ	$N_{b,Rd}$	Discr ep.	χ	$N_{b,Rd}$	Discr ep.
e	S1F1W4	0.63	1397	-21 %	0.59	1570	-23 %	0.60	1830	-21 %
	S1F5W8	0.63	1503	-21 %	0.59	1689	-24 %	0.60	1968	-23 %
	S2F1W7	0.27	735	-45 %	0.22	719	-48 %	0.20	748	-49 %
	S2F5W8	0.27	644	-44 %	0.22	630	-48 %	0.20	656	-50 %
	S3F9W9	0.70	2140	-5 %	0.71	2605	-3 %	0.72	3027	-3 %
	S4F9W9	0.63	1926	-10 %	0.59	2165	-17 %	0.60	2523	-16 %
	S5F9W9	0.56	1712	-11 %	0.53	1945	-14 %	0.51	2144	-16 %
	S6F9W9	0.47	1437	-12 %	0.42	1541	-14 %	0.40	1682	-11 %
	S7F9W9	0.40	1223	-11 %	0.35	1284	-5 %	0.30	1261	-8 %
	S8F9W9	0.32	978	-11 %	0.28	1027	-18 %	0.24	1009	-28 %
	S10F9W9	0.20	612	-30 %	0.19	697	-24 %	0.16	673	-29 %
	S11F9W9	0.19	581	-17 %	0.16	587	-19 %	0.14	589	-22 %
	S12F9W9	0.14	428	-30 %	0.12	440	-30 %	0.11	462	-29 %
	S13F9W9	0.11	336	-20 %	0.10	367	-14 %	0.10	420	-5 %
	S14F9W9	0.10	306	-15 %	0.10	367	1 %	0.10	420	13 %
	S3F10W10	0.70	1905	-9 %	0.71	2319	-2 %	0.72	2694	-1 %
	S4F10W10	0.63	1715	-9 %	0.62	2025	-7 %	0.60	2245	-10 %
	S5F10W10	0.56	1524	-13 %	0.53	1731	-13 %	0.51	1909	-15 %
	S6F10W10	0.47	1279	-17 %	0.42	1372	-21 %	0.40	1497	-25 %
	S7F10W10	0.40	1089	-9 %	0.35	1143	-15 %	0.30	1123	-26 %
	S8F10W10	0.32	871	-18 %	0.28	914	-21 %	0.24	898	-29 %
	S9F10W10	0.27	735	-18 %	0.22	719	-25 %	0.20	748	-28 %
	S10F10W10	0.20	544	-34 %	0.19	621	-29 %	0.16	599	-36 %
	S11F10W10	0.19	517	-28 %	0.16	523	-31 %	0.14	524	-35 %
S12F10W10	0.14	381	-35 %	0.12	392	-35 %	0.11	412	-35 %	
S13F10W10	0.11	299	-35 %	0.10	327	-31 %	0.10	374	-24 %	
S14F10W10	0.10	272	-31 %	0.10	327	-18 %	0.10	374	-10 %	
f	S15F9W10	0.75	2881	17 %	0.72	3319	19 %	0.70	3698	16 %
	S16F9W10	0.56	2151	3 %	0.53	2443	2 %	0.51	2694	-1 %
	S17F9W10	0.46	1767	-5 %	0.43	1982	-8 %	0.42	2219	-11 %
	S18F9W10	0.38	1460	-14 %	0.37	1706	-14 %	0.35	1849	-20 %
	S19F9W10	0.33	1268	-14 %	0.30	1383	-7 %	0.29	1532	-2 %
	S21F9W10	0.25	960	-11 %	0.22	1014	-10 %	0.20	1056	-10 %
	S22F9W10	0.22	845	-1 %	0.18	830	-2 %	0.16	845	-1 %

5. Conclusion

Through the study presented above, the possibilities of defining buckling curves applicable to designing HSS-columns of class section 4. The validated FE-model for S800 I-sections was applied on and extensive investigation of buckling in S800, S960 and S1100. When comparing these results to the buckling curves given in EC3, it was clear that none of them was suitable to cover the local buckling of HSS, and therefore new buckling curves for these steel grades are advised.

Most of the results distributed somewhat scattered along the buckling curves in EC3. But a group of the results lined up below the curves in EC, thus there were indications of similar results as observed in previous studies; high overestimation of buckling capacity of HSS-sections. This group consisted of results from 21 specimens, 7 from each steel grade, and turned out to be the specimens that were classified as cross section class 4, for both the flange and the web.

Based on what was observed, two additional curves, which cover welded I-sections of S800, S960 and S1100 are proposed. Curve *e*, where only the web or flange are in cross section class 4, and curve *f* for the cases where both are cross section class 4.

When comparing the results from the FE-analysis, and the results using the proposed curves, these curves were determined based on the results yielding the lowest buckling capacity, resulting in potentially high conservatism for some of the tested specimens.

In conclusion, an adjusted version of the curve *d* in EC3 (curve *e*) and an additional buckling curve (curve *f*) has been advised for HSS I-sections in class 4. It should be used with caution around the plateau-limit of 0.2 relative slenderness. Apart from this it has proved to yield reliable and conservative results when used to design according EC3, without any additional steps.

5.1. Further Work

For further work several additional topics may be of interest to investigate, some suggestions are given below:

- As additional verification of the conclusions above, it would be beneficial to perform physical test on complete I-sections of steel grades S960 and S1100. Preferably one could perform tests on a few of the sections which were analysed. Or one can perform tests of other dimensions of I-sections and perform additional FE-analysis for these.
- Even though it was pointed out by in research presented, that the effect of residual stresses was small for S800 welded I-sections. It could be of interest to investigate that this also is the case for S960 and S1100.
- Above, I-sections are the only section type evaluated. A natural extension of this would be to investigate the local buckling behaviour of other sections as well, for example T-, H- and box-sections. Further it would then be interesting to investigate if some of the same behaviour is seen there with regards to the sections where both flange and web are class 4 sections.
- With development in steel production, the investigation of new steel alloys is of course relevant, but since there seems to be a great cover for HSS up to a very high yield strength, this would be mostly of interest if there where to come HSS with improved ductility or change in other material properties than strength.

Bibliography

- [1] B. N. Sandaker, M. Sandvik, and B. Vik, *Materialkunnskap*. Lillestrøm: Byggenæringens forlag, 2003.
- [2] UN IEA, "Global status report for buildings and construction (2020)," 2020. [Online]. Available: <https://globalabc.org/news/launched-2020-global-status-report-buildings-and-construction>
- [3] UN Environment Programme (UNEP). "Building sector emissions hit record high, but low-carbon pandemic recovery can help transform sector – UN report." <https://www.unep.org/news-and-stories/press-release/building-sector-emissions-hit-record-high-low-carbon-pandemic> (accessed 4. February, 2022).
- [4] C. Maraveas, Z. C. Fasoulakis, and K. D. Tsavdaridis, "Mechanical properties of high and very high steel at elevated temperatures and after cooling down," *Fire Science Reviews*, vol. 6, no. 1, pp. 1-13, 2017.
- [5] F. Schröter, "Trends of using high-strength steel for heavy steel structures," *Dillinger Hüttenwerke, Germany*, 2006.
- [6] J.-O. Sperle and L. Hallberg, "Environmental advantages of using high strength steel," in *The 2nd international conference on clean technologies in the steel industry*, 2011.
- [7] J.-O. Sperle, "Environmental advantages of using advanced high strength steel in steel constructions," in *Nordic Steel Construction Conference*, 2012.
- [8] P. K. Larsen, *Konstruksjonsteknikk: Laster og bæresystemer*. Bergen: Fagbokforlaget, 2008.
- [9] *Eurocode 3: Design of steel structures - Part 1-1: General rules and rules for buildings*, NS-EN 1993-1-1:2005+A1:2014+NA:2015, Standard Norge, 2015.
- [10] *ANSI/AISC 360-16: Specification for Structural Steel Buildings*, American Institute of Steel Construction, 2016.
- [11] N. Schillo *et al.*, *Rules on high strength steel (RUOSTE)*. 2016.
- [12] J. Wang, S. Afshan, N. Schillo, M. Theofanous, M. Feldmann, and L. Gardner, "Material properties and compressive local buckling response of high strength steel square and rectangular hollow sections," *Engineering Structures*, vol. 130, pp. 297-315, 2017/01/01/ 2017, doi: <https://doi.org/10.1016/j.engstruct.2016.10.023>.
- [13] S. Chen, H. Fang, J.-z. Liu, and T.-M. Chan, "Design for local buckling behaviour of welded high strength steel I-sections under bending," *Thin-Walled Structures*, vol. 172, p. 108792, 2022/03/01/ 2022, doi: <https://doi.org/10.1016/j.tws.2021.108792>.
- [14] W. Wang, X. Li, and H. Al-azzani, "Experimental study on local buckling of high-strength Q960 steel columns at elevated temperatures," *Journal of Constructional Steel Research*, vol. 183, p. 106716, 2021/08/01/ 2021, doi: <https://doi.org/10.1016/j.jcsr.2021.106716>.
- [15] S. Shuchang, Y. Qiang, G. Xin, and P. Yiliang, "Experimental and Numerical Investigation on Global Buckling of Q690 High Strength Steel Tubes under Axial Compression," in *2020 4th International Conference on Material Science and Technology, 22-23 Jan. 2020*, UK, 2020, vol. 774: IOP Publishing, in IOP Conf. Ser., Mater. Sci. Eng. (UK), p. 012081 (7 pp.), doi: 10.1088/1757-899X/774/1/012081. [Online]. Available: <http://dx.doi.org/10.1088/1757-899X/774/1/012081>
- [16] W. Wang and X. Qiu, "An analytical study for global buckling of circular tubes under axial and oblique compression," *International Journal of Mechanical Sciences*, vol. 126, pp. 120-129, 2017/06/01/ 2017, doi: <https://doi.org/10.1016/j.ijmecsci.2017.03.019>.
- [17] X. Cao *et al.*, "Local buckling of 800 MPa high strength steel welded T-section columns under axial compression," *Engineering Structures*, vol. 194, pp. 196-206, 2019, doi: 10.1016/j.engstruct.2019.05.060.

- [18] X. Cao *et al.*, "Experimental study on local buckling of 800 MPa HSS welded I-section columns under axial compression," *Thin-Walled Structures*, vol. 155, 2020, doi: 10.1016/j.tws.2020.106878.
- [19] X. Cao *et al.*, "Local overall interactive buckling behaviour of 800 MPa high-strength steel welded H-section members under axial compression," *Thin-Walled Structures*, vol. 164, 2021, doi: 10.1016/j.tws.2021.107793.
- [20] B. Li, C. Cheng, Z. Song, X. Cao, and Z. Kong, "Local buckling behaviour of high strength steel welded box-section columns under axial compression," *Thin-Walled Structures*, vol. 171, p. 108677, 2022/02/01/ 2022, doi: <https://doi.org/10.1016/j.tws.2021.108677>.
- [21] V. M. Richardsen, "A review on high strength steel and numerical modelling of buckling," 2021.
- [22] World Steel Association AISBL. "Defining Steels." <https://ahssinsights.org/metallurgy/defining-steels/> (accessed 05. February, 2022).
- [23] M. Amraei, A. Ahola, S. Afkhami, T. Björk, A. Heidarpour, and X.-L. Zhao, "Effects of heat input on the mechanical properties of butt-welded high and ultra-high strength steels," *Engineering Structures*, vol. 198, p. 109460, 2019/11/01/ 2019, doi: <https://doi.org/10.1016/j.engstruct.2019.109460>.
- [24] Norwegian Steel Association. "Stålsorter." <https://www.stalforbund.no/stalsorter/> (accessed 05. March 2022).
- [25] SteelConstruction.info. "Steel material properties." https://www.steelconstruction.info/Steel_material_properties (accessed 9. March, 2022).
- [26] Hobart Brothers LLC. "Tips for Welding High Strength Steel and Selecting Filler Metals." <https://www.hobartbrothers.com/2018/04/tips-for-welding-high-strength-steel-and-selecting-filler-metals/> (accessed 10. March, 2022).
- [27] Y. Liu, L. S. Zhang, L. P. Sun, and B. Li, "Numerical study on effects of buffer bulbous bow structure in collisions," in *Recent Advances in Structural Integrity Analysis - Proceedings of the International Congress (APCF/SIF-2014)*, L. Ye Ed. Oxford: Woodhead Publishing, 2014, pp. 168-172.
- [28] O. Lohne. "Store norske leksikon: Duktilitet." <https://snl.no/duktilitet> (accessed 11. May, 2022).
- [29] P. Hradil and A. Talja, "Ductility limits of high strength steels," *Online at FIMECC Research Portal and VTT webpage*, 2016.
- [30] N. Christensen and A. Almar-Næss. "Stål." Store norske leksikon. <http://snl.no/st%C3%A5l> (accessed 31. March, 2022).
- [31] M. C. Theyssier, "3 - Manufacturing of advanced high-strength steels (AHSS)," in *Welding and Joining of Advanced High Strength Steels (AHSS)*, M. Shome and M. Tumuluru Eds.: Woodhead Publishing, 2015, pp. 29-53.
- [32] J. Kömi, P. Karjalainen, and D. Porter, "Direct-quenched structural steels," in *Encyclopedia of iron, steel, and their alloys*: CRC Press, 2016, pp. 1109-1125.
- [33] H. E. Boyer, P. Archambault, F. Moreaux, and N. I. Kobasko, "Techniques of Quenching," in *Theory and Technology of Quenching: A Handbook*, B. Liščić, H. M. Tensi, and W. Luty Eds. Berlin, Heidelberg: Springer Berlin Heidelberg, 1992, pp. 341-389.
- [34] N. Ryum. "Seigherding." Store norske leksikon. <https://snl.no/seigherding> (accessed 02. February, 2022).
- [35] Norsk Stål. "Norsk Stål." <https://www.norskstaal.no> (accessed 5. March, 2022).
- [36] *Hot rolled products of structural steels - Part 6: Technical delivery conditions for flat products of high yield strength structural steels in the quenched and tempered condition*, NS-EN 10025-6:2019, Standard Norge, 2019.
- [37] A. Hasanbeigi, "Steel Climate Impact," 2022.

- [38] R. Stroetmann, "High strength steel for improvement of sustainability," in *Proceedings of the 6th European Conference on Steel and Composite Structures, Proceedings*, 2011, vol. 100, p. 31.
- [39] P. K. Larsen, *Dimensjonering av stålkonstruksjoner*. Bergen: Fagbokforlaget, 2015.
- [40] *Eurocode 3: Design of steel structures - Part 1-12: Additional rules for the extension of EN 1993 up to steel grades S 700*, NS-EN 1993-1-12:2007+NA:2009, Standard Norge, 2007.
- [41] C. Topkaya and S. Sahin, "A comparative study of AISC-360 and EC3 strength limit states," *International Journal of Steel Structures*, vol. 11, pp. 13-27, 03/01 2011, doi: 10.1007/S13296-011-1002-x.
- [42] A. M. Khaled, N. S. Mahmoud, and F. A. Salem, "Comparison Between Different Steel Codes," *Al-Azhar University Civil Engineering Research Magazine (CERM)*, 2019.
- [43] N. Subramanian, "4.8 Local Buckling of Plates," in *Steel Structures - Design and Practice*: Oxford University Press.
- [44] R. D. Cook, D. S. Malkus, M. E. Plesha, and R. J. Witt, *Concepts and applications of finite element analysis*, 4th ed. United States: John Wiley & sons, INC., 2001.
- [45] T. B. Quimby. "A Beginner's Guide to the Steel Construction Manual, 13th ed.: Chapter 6 - Buckling Concepts." <https://www.bgstructuralengineering.com/BGSCM13/BGSCM006/index.htm> (accessed 21. April, 2022).
- [46] L. Euler, "Sur la force des colonnes," *Memoires de l'academie des sciences de Berlin*, pp. 252-282, 1759.
- [47] N. Subramanian, "5.4 Elastic Buckling of Slender Compression Members," in *Steel Structures - Design and Practice*: Oxford University Press.
- [48] A. Aghayere and J. Vigil, "5.2 Euler Critical Buckling Load," in *Structural Steel Design (3rd Edition)*: Mercury Learning and Information.
- [49] D. Iles, "Determining the buckling resistance of steel and composite bridge structures," *Berkshire: The Steel Construction Institute*, 2012.
- [50] "MECCANICA: KNEKING." Universitetet i Tromsø. <http://meccanica.uit.no/fasthet/knekking.htm> (accessed 25. April, 2022).
- [51] H. Ban, G. Shi, Y. Shi, and M. A. Bradford, "Experimental investigation of the overall buckling behaviour of 960MPa high strength steel columns," *Journal of Constructional Steel Research*, vol. 88, pp. 256-266, 2013/09/01/ 2013, doi: <https://doi.org/10.1016/j.jcsr.2013.05.015>.
- [52] B. Somodi and B. Kövesdi, "Flexural buckling resistance of cold-formed HSS hollow section members," *Journal of Constructional Steel Research*, vol. 128, pp. 179-192, 2017/01/01/ 2017, doi: <https://doi.org/10.1016/j.jcsr.2016.08.014>.
- [53] A. Su, Y. Sun, Y. Liang, and O. Zhao, "Experimental and numerical studies of S960 ultra-high strength steel welded I-sections under combined compression and minor-axis bending," *Engineering Structures*, vol. 243, p. 112675, 2021/09/15/ 2021, doi: <https://doi.org/10.1016/j.engstruct.2021.112675>.
- [54] F. Wang, Y. Liang, and O. Zhao, "Experimental and numerical studies of pin-ended press-braked S960 ultra-high strength steel channel section columns," *Engineering Structures*, vol. 215, p. 110629, 2020/07/15/ 2020, doi: <https://doi.org/10.1016/j.engstruct.2020.110629>.
- [55] S. P. Timoshenko and J. M. Gere, *Theory of Elastic Stability*. New York, 1961.
- [56] SIMULIA. "Getting Started with Abaqus/CAE: 8.2 The solution of nonlinear problems." <http://130.149.89.49:2080/v2016/books/gsa/default.htm> (accessed 4. April, 2022).
- [57] SIMULIA. "Abaqus Theory Guide: 2.2.1 Nonlinear solution methods in Abaqus/Standard." <http://130.149.89.49:2080/v2016/books/stm/default.htm> (accessed 2. March, 2022).
- [58] Ondrej. "CSI Knowledge Base: Nonlinear buckling." <https://wiki.csiamerica.com/display/kb/Nonlinear+buckling> (accessed 27. March, 2022).

- [59] Ondrej. "CSI Knowledge Base: Eigenvalue vs. Nonlinear buckling analysis." <https://wiki.csiamerica.com/display/kb/Eigenvalue+vs.+Nonlinear+buckling+analysis> (accessed 27. March, 2022).
- [60] SIMULIA. "ABAQUS Analysis User's Manual: 6.2.3 Eigenvalue buckling prediction." <http://130.149.89.49:2080/v2016/books/usb/default.htm> (accessed 2. April, 2022).
- [61] SIMULIA. "ABAQUS Analysis User's Manual: 6.2.4 Unstable collapse and postbuckling analysis." <http://130.149.89.49:2080/v2016/books/usb/default.htm> (accessed 2. March, 2022).
- [62] SIMULIA. "ABAQUS Theory Manual: 2.3.2 Modified Riks algorithm." <http://130.149.89.49:2080/v2016/books/stm/default.htm> (accessed 2. March, 2022).
- [63] N. Vasiros, "Nonlinear analysis of structures," *The Arc-Length method*. Harvard, 2015.
- [64] E. Riks, "An incremental approach to the solution of snapping and buckling problems," *International Journal of Solids and Structures*, vol. 15, no. 7, pp. 529-551, 1979/01/01/ 1979, doi: [https://doi.org/10.1016/0020-7683\(79\)90081-7](https://doi.org/10.1016/0020-7683(79)90081-7).
- [65] SIMULIA. "Getting Started with ABAQUS/Explicit: 5.2 Plasticity in ductile metals." <https://abaqus-docs.mit.edu/2017/English/SIMACAEGSARefMap/simagsa-c-matdefining.htm> (accessed 25. April, 2022).
- [66] W. Ramberg and W. R. Osgood, "Description of stress-strain curves by three parameters," National Advisory Committee for Aeronautics, 1943.
- [67] P. S. Patwardhan, R. A. Nalavde, and D. Kujawski, "An Estimation of Ramberg-Osgood Constants for Materials with and without Luder's Strain Using Yield and Ultimate Strengths," *Procedia Structural Integrity*, vol. 17, pp. 750-757, 2019/01/01/ 2019, doi: <https://doi.org/10.1016/j.prostr.2019.08.100>.
- [68] W. Sas, A. Głuchowski, and A. Szymański, "Impact of the stabilization of compacted cohesive soil – sandy clay on yield criterion improvement," *Annals of Warsaw University of Life Sciences - SGGW Land Reclamation*, vol. 46, pp. 139-151, 05/01 2014, doi: 10.2478/ssgw-2014-0012.
- [69] H. Bhadeshia and R. Honeycombe, "2.3 Interstitial Solid Solution Strengthening," in *Steels - Microstructure and Properties (4th Edition)*: Elsevier, pp. 26-28.
- [70] SIMULIA. "ABAQUS Theory Manual: 4.3.1 Metal plasticity models." <https://classes.engineering.wustl.edu/2009/spring/mase5513/abaqus/docs/v6.6/books/stm/default.htm?startat=ch04s03ath103.html> (accessed 5. May, 2022).
- [71] SIMULIA. "Abaqus Theory Manual: 4.3.5 Models for metals subjected to cyclic loading." <https://classes.engineering.wustl.edu/2009/spring/mase5513/abaqus/docs/v6.6/books/stm/default.htm?startat=ch04s03ath107.html> (accessed 5. May, 2022).
- [72] SIMULIA. "Abaqus Theory Guide: Johnson-Cook plasticity." <https://abaqus-docs.mit.edu/2017/English/SIMACAEMATRefMap/simamat-c-johnsoncook.htm> (accessed 5. May, 2022).
- [73] SIMULIA. "Abaqus Theory Guide: Models for metals subjected to cyclic loading." <https://abaqus-docs.mit.edu/2017/English/SIMACAEMATRefMap/simamat-c-hardening.htm> (accessed 5. May, 2022).
- [74] SIMULIA. "Abaqus Analysis User's Guide: 3.2.28 Translating ANSYS input files to Abaqus input files." <http://130.149.89.49:2080/v6.13/books/usb/default.htm?startat=pt01ch03s02abx28.html> (accessed 27. April, 2022).
- [75] Y. Kwon and G. Hancock, "Post-buckling analysis of thin-walled channel sections undergoing local and distortional buckling," *Computers & structures*, vol. 49, no. 3, pp. 507-516, 1993.
- [76] J.-L. Ma, T.-M. Chan, and B. Young, "Material properties and residual stresses of cold-formed high strength steel hollow sections," *Journal of Constructional Steel Research*, vol. 109, pp. 152-165, 2015/06/01/ 2015, doi: <https://doi.org/10.1016/j.jcsr.2015.02.006>.

Appendices

- Appendix A - Results: Validation of FE-model
- Appendix B - Results: S800, S960 and S1100 I-sections

APPENDIX A

Validation of FE-model

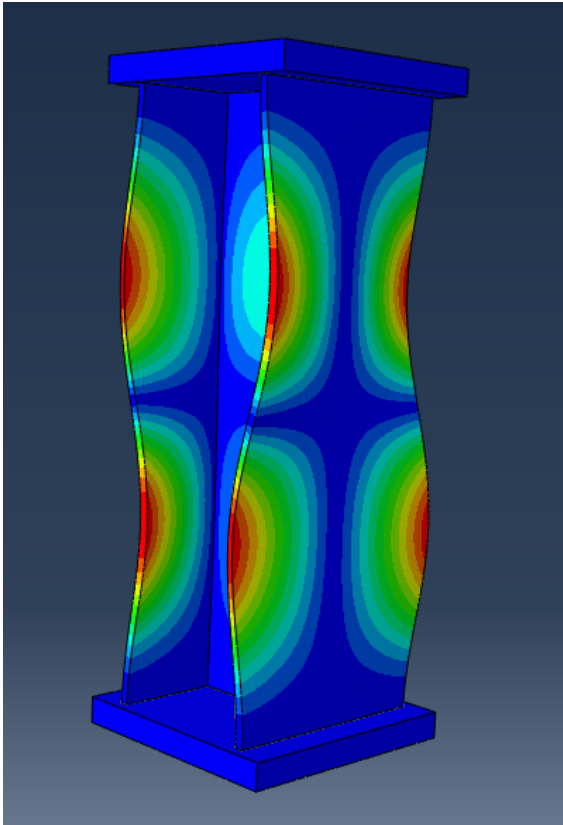
In this appendix, results from the validation process of the FE-model are presented. The most important results from the analysis are reported: eigenvalue from the first eigenmode, max LPF value which gives the critical load (N_{cr}). This result is then compared to the results in the reference articles. A screen shot of the deformed FE-model (scaled) is also attached to illustrate the buckling shape.

H-A1

Eigenvalue nr. 1 = 3507 (kN)
LPF_{max} =0.713
N_{cr} = 2500 kN

Discrepancy, test: 5.0 %
Discrepancy, FEA: -0.1%

Buckling shape:



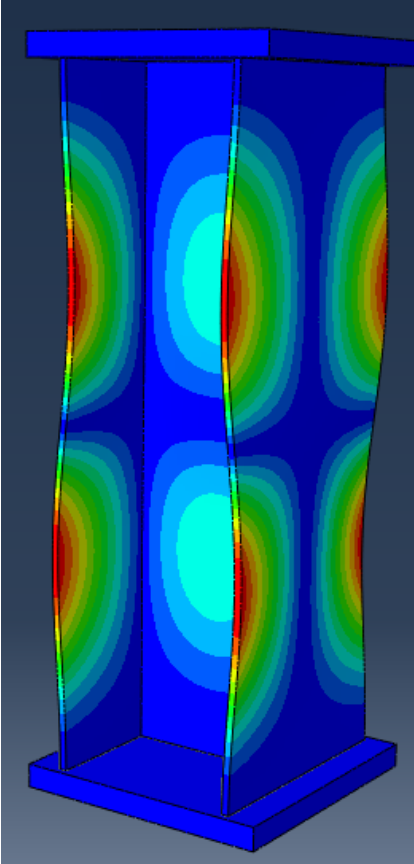
H-A2

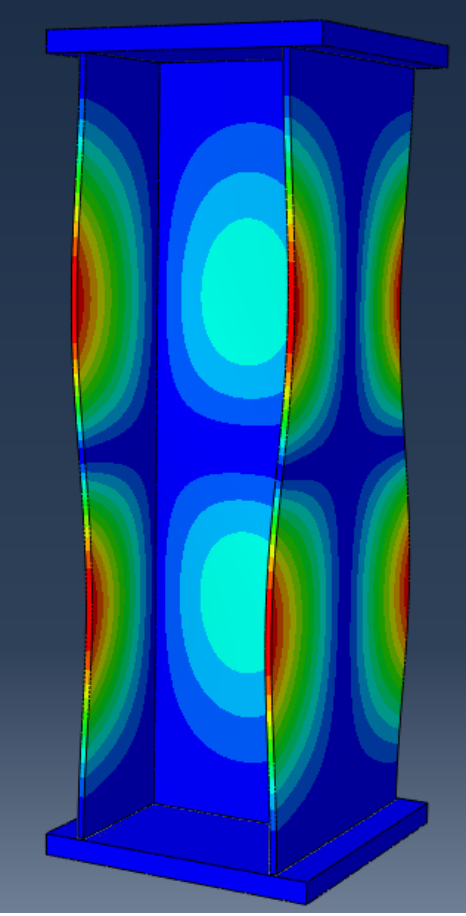
Eigenvalue nr. 1 = 2703 (kN)
LPF_{max} = 0.952

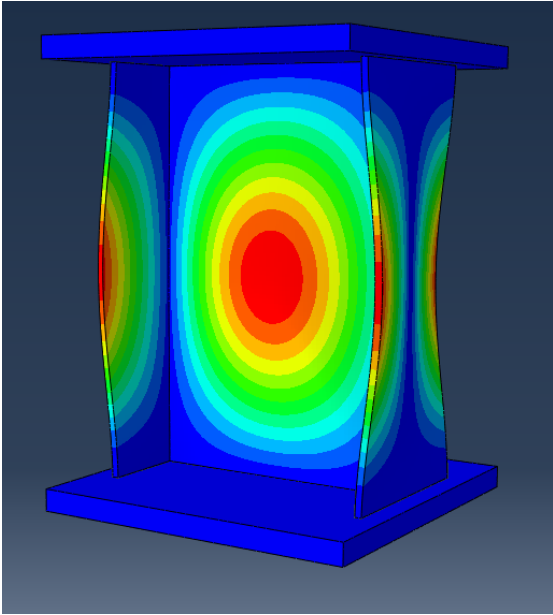
N_{cr} = 2574 kN

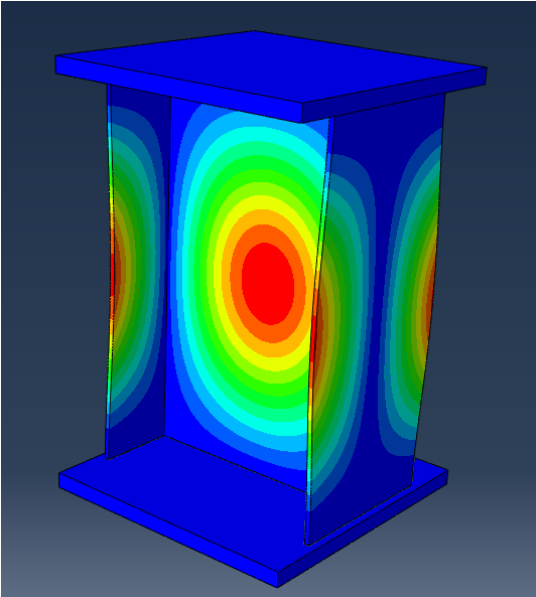
Discrepancy, test: 0.6%
Discrepancy, FEA: -1.8%

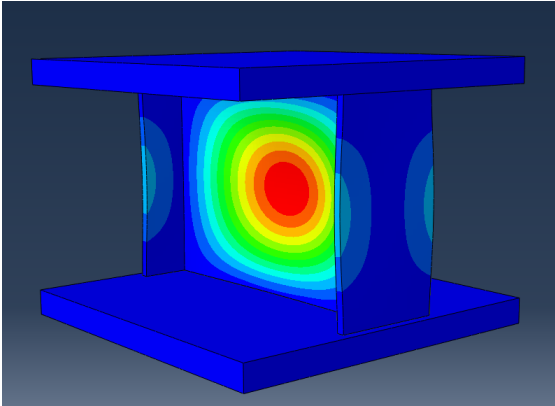
Buckling shape:

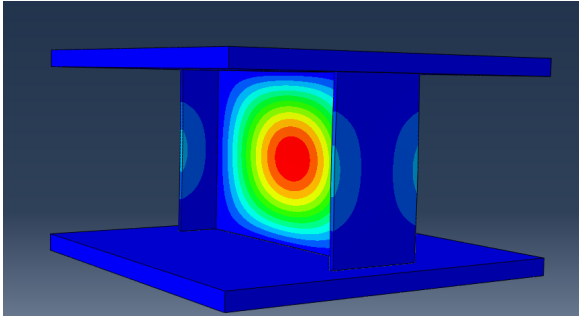


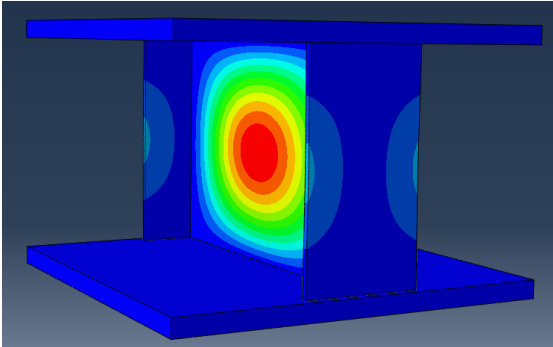
H-A3	
Eigenvalue nr. 1 = 2240 (kN) LPF _{max} = 1.296 N _{cr} = 2903 kN	
Discrepancy, test: 0.7% Discrepancy, FEA: 3.3%	
Buckling shape:	

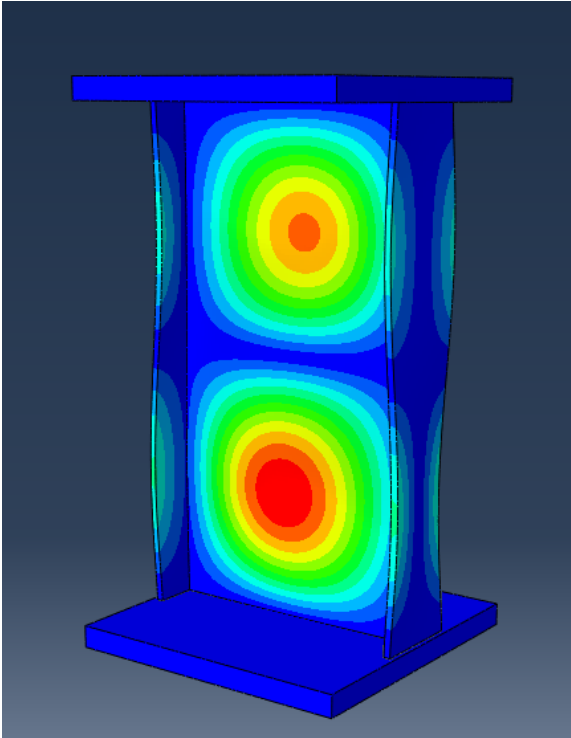
H-B1
Eigenvalue nr. 1 =2860 (kN) LPF _{max} = 0.857 N _{cr} = 2450 kN
Discrepancy, test: -1.6% Discrepancy, FEA: 3.0%
Buckling shape: 

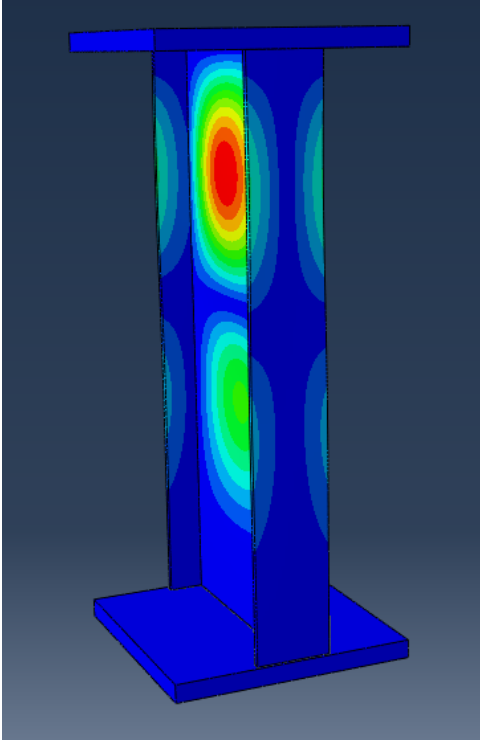
H-B2	
Eigenvalue nr. 1 =2384 (kN) LPF _{max} = 1.120 N _{cr} = 2670 kN	
Discrepancy, test: -0.7% Discrepancy, FEA: 4.0%	
Buckling shape:	

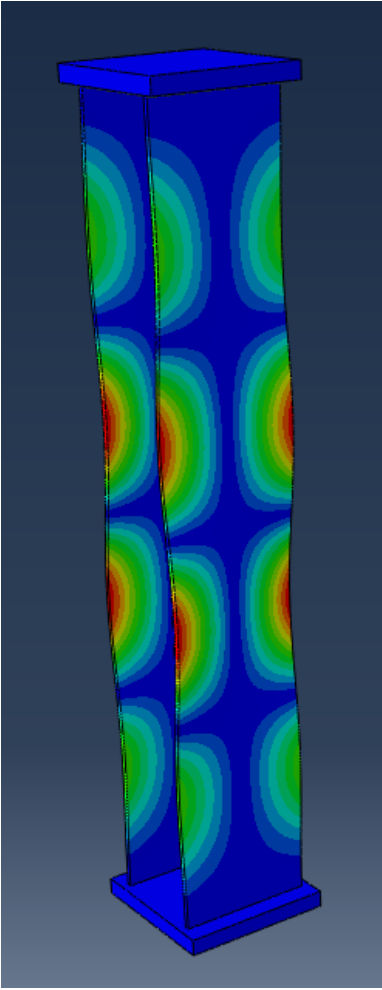
H-C1	
Eigenvalue nr. 1 = 2187 (kN) LPF _{max} = 1.104 N _{cr} = 2415 kN	
Discrepancy, test: 1.0% Discrepancy, FEA: -0.6%	
Buckling shape:	

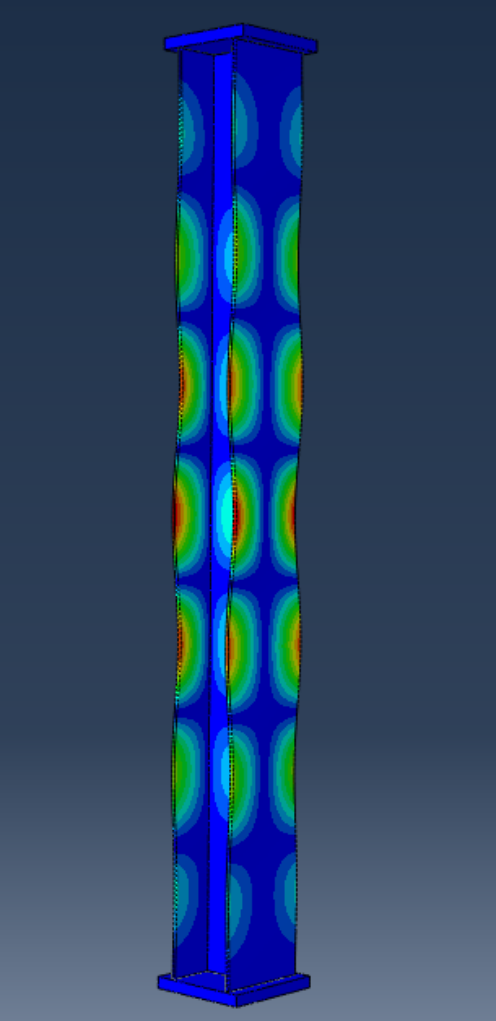
H-C2	
Eigenvalue nr. 1 = 1703 (kN) LPF _{max} = 1.490 N _{cr} = 2537 kN	
Discrepancy, test: 3.1% Discrepancy, FEA: -0.9%	
Buckling shape:	

H-C3	
Eigenvalue nr. 1 = 1390 (kN) LPF _{max} = 1.997	
N _{cr} = 2776 kN	
Discrepancy, test: 28.3%	
Discrepancy, FEA: 3.9%	
Buckling shape:	

H-D1
Eigenvalue nr. 1 = 2045 (kN) LPF _{max} = 0.940 N _{cr} = 1921 kN
Discrepancy, test: -0.3% Discrepancy, FEA: 1.8%
Buckling shape: 

H-D2
Eigenvalue nr. 1 = 2219 (kN) LPF _{max} = 0.820 N _{cr} = 1819kN
Discrepancy, test: 4.4% Discrepancy, FEA: 3.5%
Buckling shape: 

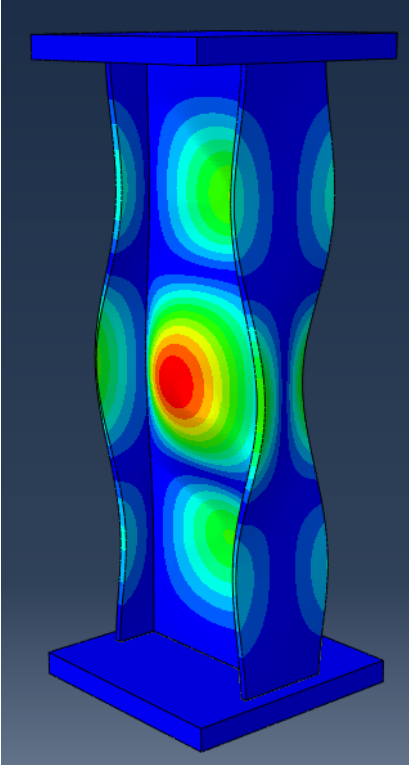
H-D3
Eigenvalue nr. 1 = 2975 (kN) LPF _{max} = 0.858 N _{cr} = 2553 kN
Discrepancy, test: 6.2% Discrepancy, FEA: -0.4%
Buckling shape: 

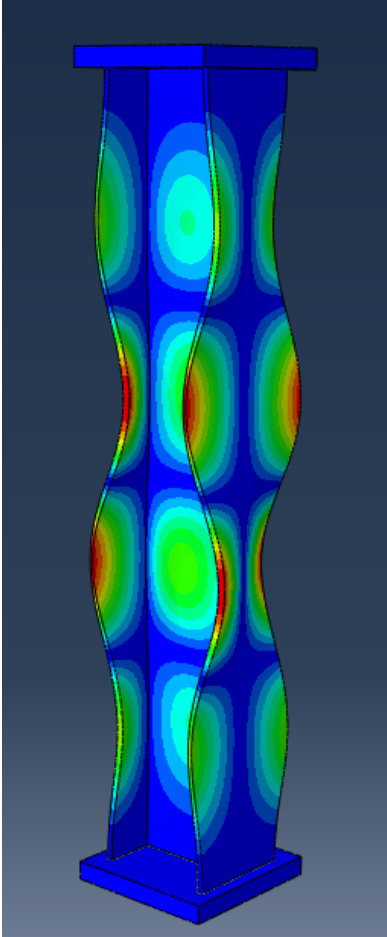
H-D4	
Eigenvalue nr. 1 = 3006 (kN) LPF _{max} = 0.822 N _{cr} = 2470 kN	
Discrepancy test: 2.6% Discrepancy FEA: -3.2%	
Buckling shape:	

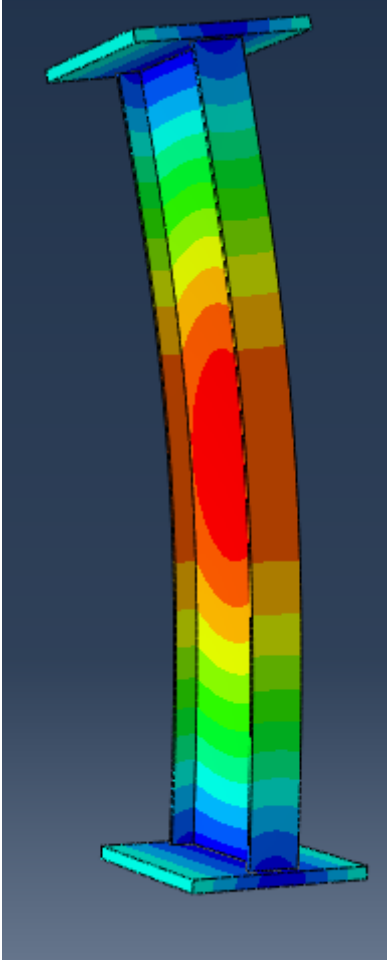
APPENDIX B

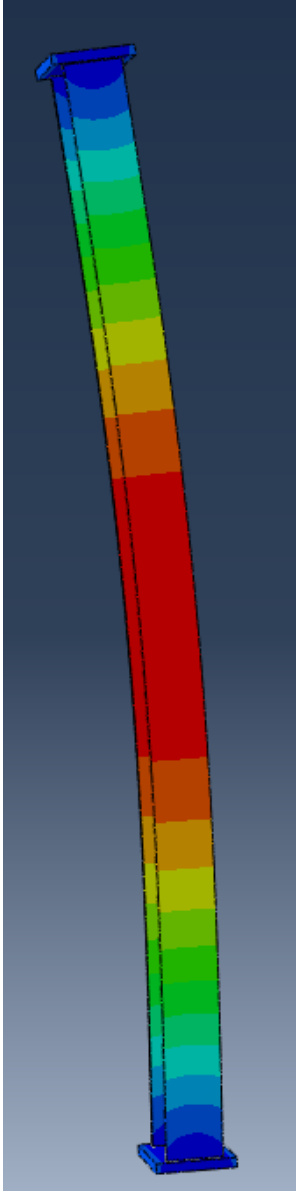
Results from the parametric study of S800, S960 and S1100 welded I-sections.

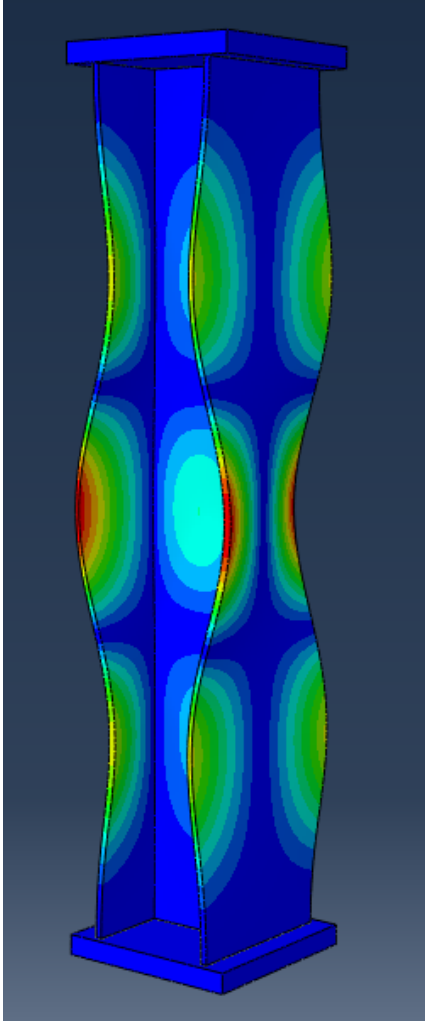
In this appendix, results from the parametric study on local buckling of steel sections using FE-modelling is presented. The most important results from the analysis are reported, eigenvalue from the first eigenmode and max LPF value, which together gives the critical load (N_{cr}). A screen shot of the deformed FE-model (scaled) is also attached to illustrate the buckling shape, which was identical for the three different steel grades.

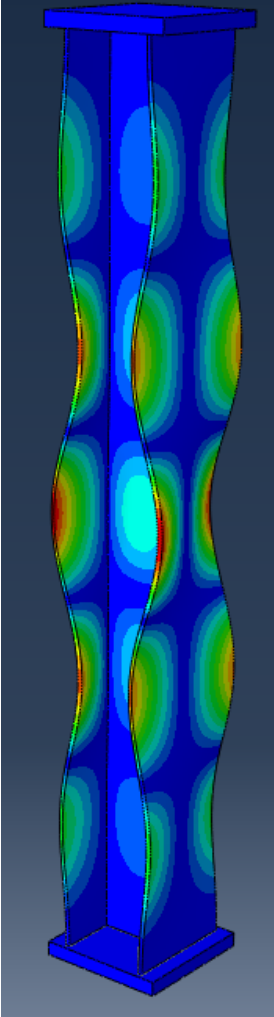
S1F1W4		
S800	S960	S1100
Eigenvalue nr. 1 = 3317 (kN) LPF _{max} = 0.530	Eigenvalue nr. 1 = 3199(kN) LPF _{max} = 0.634	Eigenvalue nr. 1 = 3199(kN) LPF _{max} = 0.726
N _{cr} = 1758 kN	N _{cr} = 2028 kN	N _{cr} = 2322 kN
Buckling shape: <div style="text-align: center; margin-top: 10px;">  </div>		

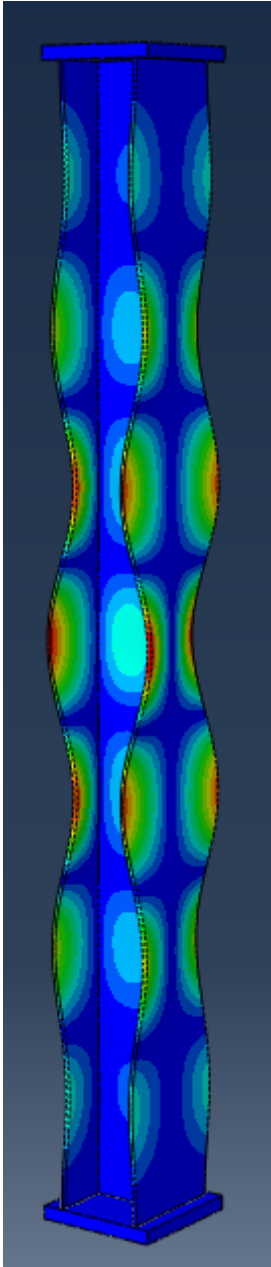
S1F5W8		
S800	S960	S1100
Eigenvalue nr. 1 = 3770 (kN) LPF _{max} = 0.507	Eigenvalue nr. 1 = 3640 (kN) LPF _{max} = 0.612	Eigenvalue nr. 1 = 3640 (kN) LPF _{max} = 0.706
N _{cr} = 1911 kN	N _{cr} = 2228 kN	N _{cr} = 2569kN
Buckling shape: <div style="text-align: center; margin-top: 10px;">  </div>		

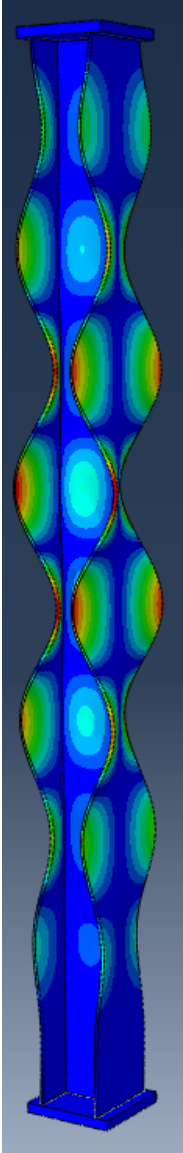
S2F1W7		
S800	S960	S1100
Eigenvalue nr. 1 = 1813 (kN) LPF _{max} = 0.740	Eigenvalue nr. 1 = 1750 (kN) LPF _{max} = 0.790	Eigenvalue nr. 1 = 1750 (kN) LPF _{max} = 0.836
N _{cr} = 1342 kN	N _{cr} = 1383 kN	N _{cr} = 1462 kN
Buckling shape:		
		

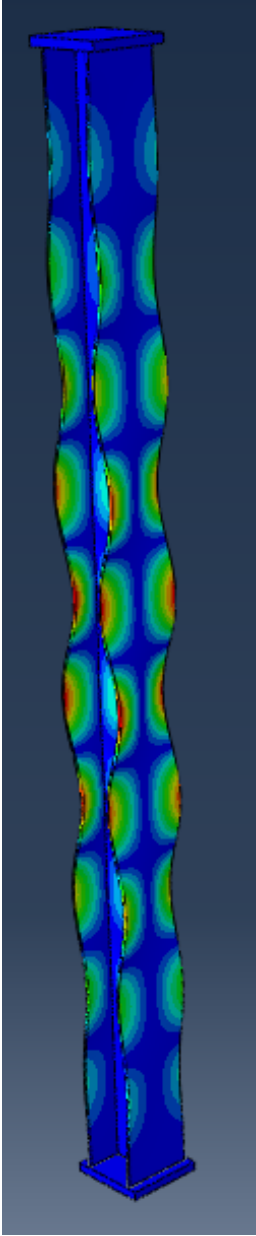
S2F5W8		
S800	S960	S1100
Eigenvalue nr. 1 = 1926 (kN) LPF _{max} = 0.594	Eigenvalue nr. 1 = 1860 (kN) LPF _{max} = 0.657	Eigenvalue nr. 1 = 1857 (kN) LPF _{max} = 0.711
N _{cr} = 1144 kN	N _{cr} = 1221 kN	N _{cr} = 1320 kN
Buckling shape: <div style="text-align: center; margin-top: 10px;">  </div>		

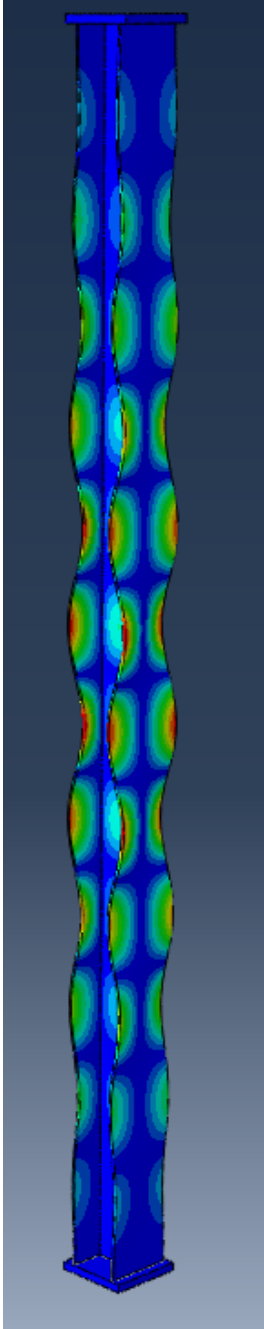
S3F9W9		
S800	S960	S1100
Eigenvalue nr. 1 = 2759(kN) LPF _{max} = 0.820	Eigenvalue nr. 1 = 2660 (kN) LPF _{max} = 1.005	Eigenvalue nr. 1 = 2660 (kN) LPF _{max} = 1.169
N _{cr} = 2262 kN	N _{cr} = 2673 kN	N _{cr} = 3108 kN
Buckling shape:		
		

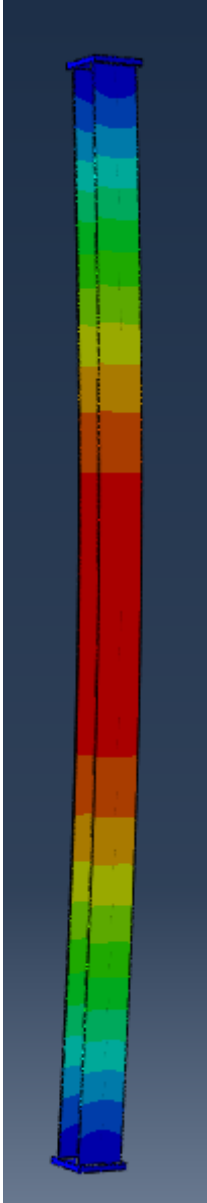
S4F9W9		
S800	S960	S1100
Eigenvalue nr. 1 = 2687 (kN) LPF _{max} = 0.795	Eigenvalue nr. 1 = 2590 (kN) LPF _{max} = 1.010	Eigenvalue nr. 1 = 2590 (kN) LPF _{max} = 1.160
N _{cr} = 2136 kN	N _{cr} = 2616 kN	N _{cr} = 3004 kN
Buckling shape: <div style="text-align: center; margin-top: 10px;">  </div>		


S5F9W9		
S800	S960	S1100
Eigenvalue nr. 1 = 2660 (kN) LPF _{max} = 0.720	Eigenvalue nr. 1 = 2570 (kN) LPF _{max} = 0.882	Eigenvalue nr. 1 = 2568 (kN) LPF _{max} = 0.999
N _{cr} = 1915 kN	N _{cr} = 2267kN	N _{cr} = 2565kN
Buckling shape:		
		

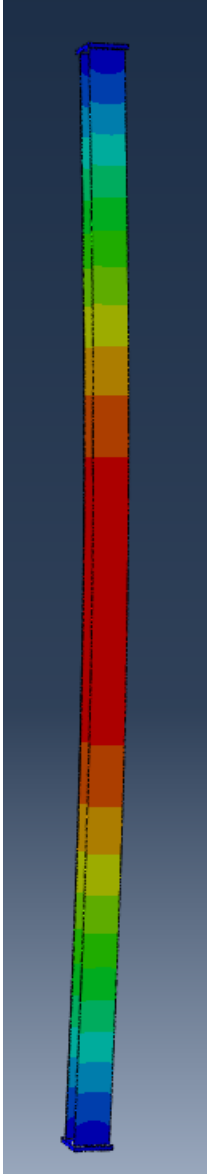
S6F9W9		
S800	S960	S1100
Eigenvalue nr. 1 = 2648 (kN) LPF _{max} = 0.618	Eigenvalue nr. 1 =2560 (kN) LPF _{max} = 0.696	Eigenvalue nr. 1 = 2555 (kN) LPF _{max} = 0.738
N _{cr} = 1638 kN	N _{cr} = 1782 kN	N _{cr} = 1886kN
Buckling shape: <div style="text-align: center; margin-top: 20px;">  </div>		


S7F9W9		
S800	S960	S1100
Eigenvalue nr. 1 = 2644 (kN) LPF _{max} = 0.518	Eigenvalue nr. 1 = 2550 (kN) LPF _{max} = 0.533	Eigenvalue nr. 1 = 2550 (kN) LPF _{max} = 0.535
N _{cr} = 1368 kN	N _{cr} = 1358 kN	N _{cr} = 1364 kN
Buckling shape: <div style="text-align: center; margin-top: 10px;">  </div>		


S8F9W9		
S800	S960	S1100
Eigenvalue nr. 1 = 2640 (kN) LPF _{max} = 0.418	Eigenvalue nr. 1 = 2550 (kN) LPF _{max} = 0.493	Eigenvalue nr. 1 = 2547 (kN) LPF _{max} = 0.547
N _{cr} = 1104 kN	N _{cr} = 1258 kN	N _{cr} = 1392 kN
Buckling shape: <div style="text-align: center; margin-top: 10px;">  </div>		

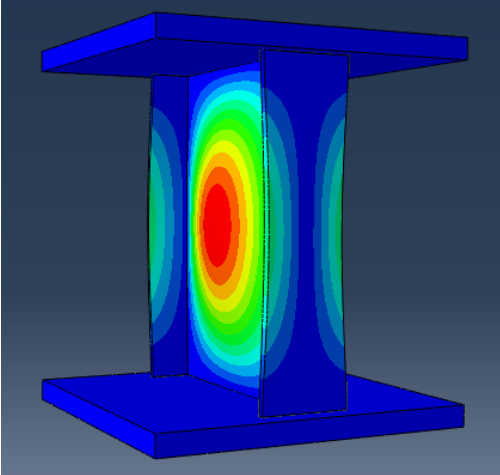
S10F9W9		
S800	S960	S1100
Eigenvalue nr. 1 = 1990 (kN) LPF _{max} = 0.439	Eigenvalue nr. 1 = 1920(kN) LPF _{max} = 0.475	Eigenvalue nr. 1 = 1919 (kN) LPF _{max} = 0.497
N _{cr} = 873 kN	N _{cr} = 912 kN	N _{cr} = 953 kN
Buckling shape: <div style="text-align: center; margin-top: 20px;">  </div>		

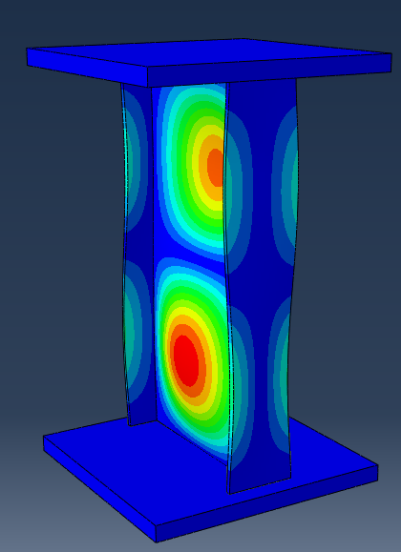
S11F9W9		
S800	S960	S1100
Eigenvalue nr. 1 = 1617 (kN) LPF _{max} = 0.434	Eigenvalue nr. 1 = 1560(kN) LPF _{max} = 0.462	Eigenvalue nr. 1 = 1560 (kN) LPF _{max} = 0.485
N _{cr} = 702 kN	N _{cr} = 721 kN	N _{cr} = 757 kN
Buckling shape: <div style="text-align: center; margin-top: 20px;">  </div>		

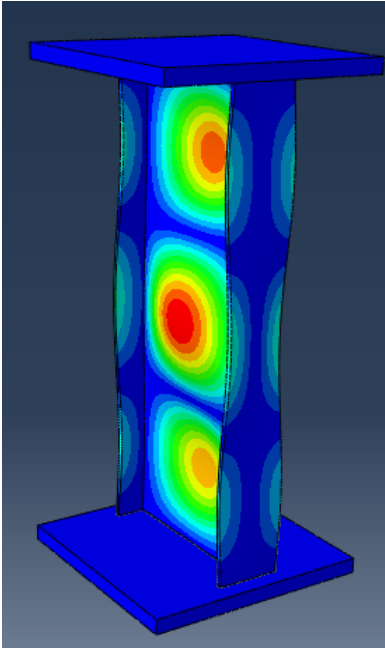
S12F9W9		
S800	S960	S1100
Eigenvalue nr. 1 = 1130 (kN) LPF _{max} = 0.544	Eigenvalue nr. 1 = 1090(kN) LPF _{max} = 0.576	Eigenvalue nr. 1 = 1090 (kN) LPF _{max} = 0.598
N _{cr} = 615 kN	N _{cr} = 628 kN	N _{cr} = 652kN
Buckling shape: <div style="text-align: center; margin-top: 20px;">  </div>		

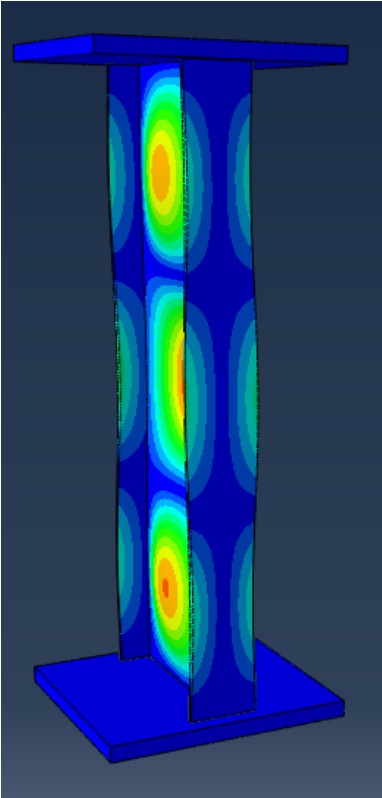
S13F9W9		
S800	S960	S1100
Eigenvalue nr. 1 = 834 (kN) LPF _{max} = 0.504	Eigenvalue nr. 1 =804 (kN) LPF _{max} = 0.531	Eigenvalue nr. 1 = 804 (kN) LPF _{max} = 0.548
N _{cr} = 420 kN	N _{cr} = 427kN	N _{cr} = 441 kN
Buckling shape: <div style="text-align: center; margin-top: 20px;">  </div>		

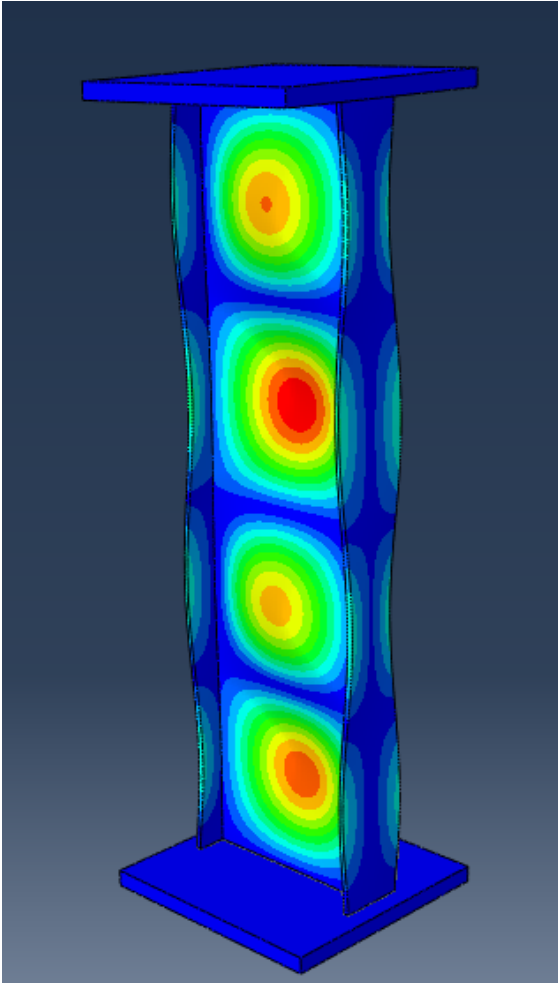
S14F9W9		
S800	S960	S1100
Eigenvalue nr. 1 = 640 (kN) LPF _{max} = 0.563	Eigenvalue nr. 1 = 617(kN) LPF _{max} = 0.587	Eigenvalue nr. 1 = 617 (kN) LPF _{max} = 0.605
N _{cr} = 349 kN	N _{cr} = 362 kN	N _{cr} = 373 kN
Buckling shape: <div style="text-align: center; margin-top: 20px;">  </div>		

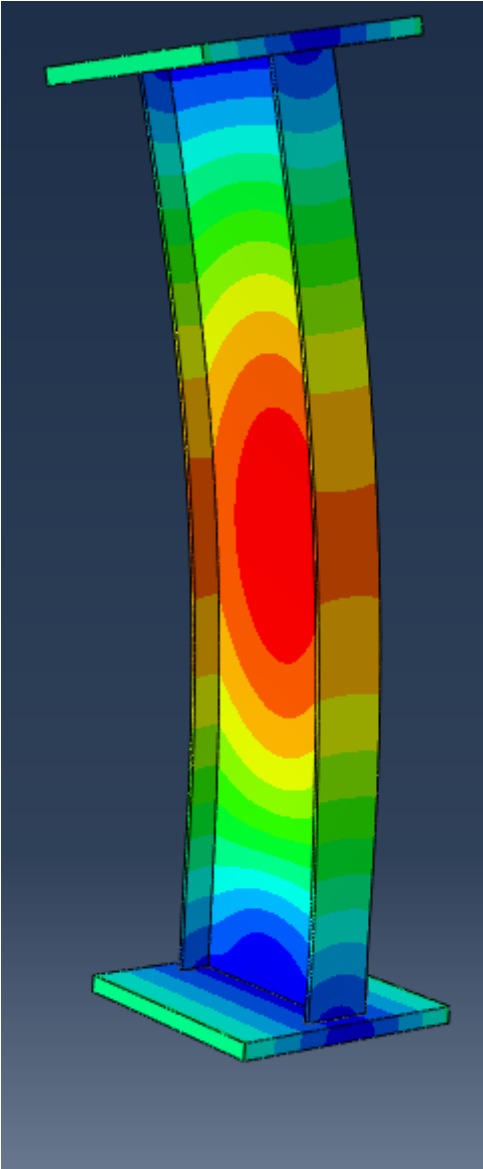
S3F10W10		
S800	S960	S1100
Eigenvalue nr. 1 = 1900 (kN) LPF _{max} = 1.048	Eigenvalue nr. 1 = 1920 (kN) LPF _{max} = 1.234	Eigenvalue nr. 1 = 1920 (kN) LPF _{max} = 1.417
N _{cr} = 2086 kN	N _{cr} = 2369 kN	N _{cr} = 2721 kN
Buckling shape: <div style="text-align: center; margin-top: 10px;">  </div>		

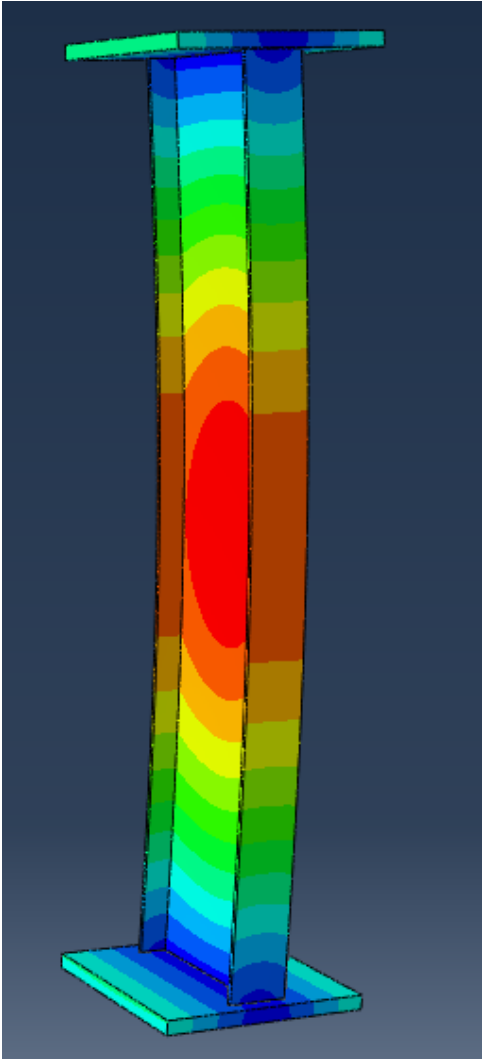
S4F10W10		
S800	S960	S1100
Eigenvalue nr. 1 = 1880 (kN) LPF _{max} = 1.000	Eigenvalue nr. 1 = 1816(kN) LPF _{max} = 1.200	Eigenvalue nr. 1 = 1816(kN) LPF _{max} = 1.369
N _{cr} = 1800 kN	N _{cr} = 2179 kN	N _{cr} = 2721 kN
Buckling shape:		
		

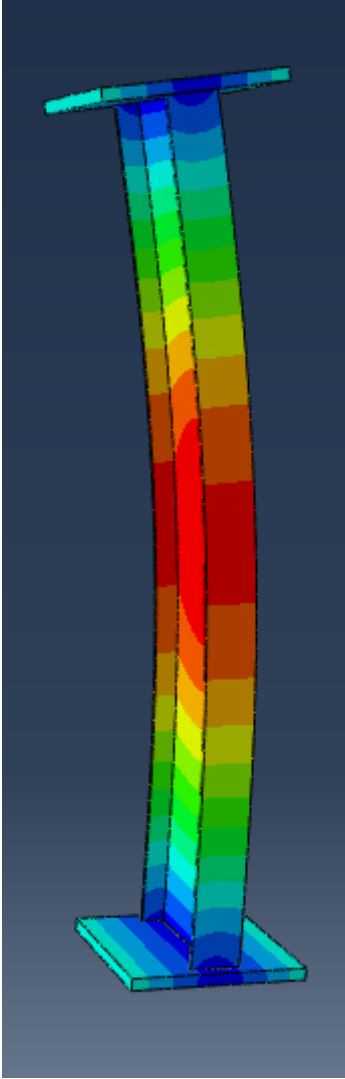
S5F10W10		
S800	S960	S1100
Eigenvalue nr. 1 = 1907 (kN) LPF _{max} = 0.922	Eigenvalue nr. 1 = 1840 (kN) LPF _{max} = 1.081	Eigenvalue nr. 1 = 1840 (kN) LPF _{max} = 1.226
N _{cr} = 1757 kN	N _{cr} = 1989 kN	N _{cr} = 2255 kN
Buckling shape:		
		

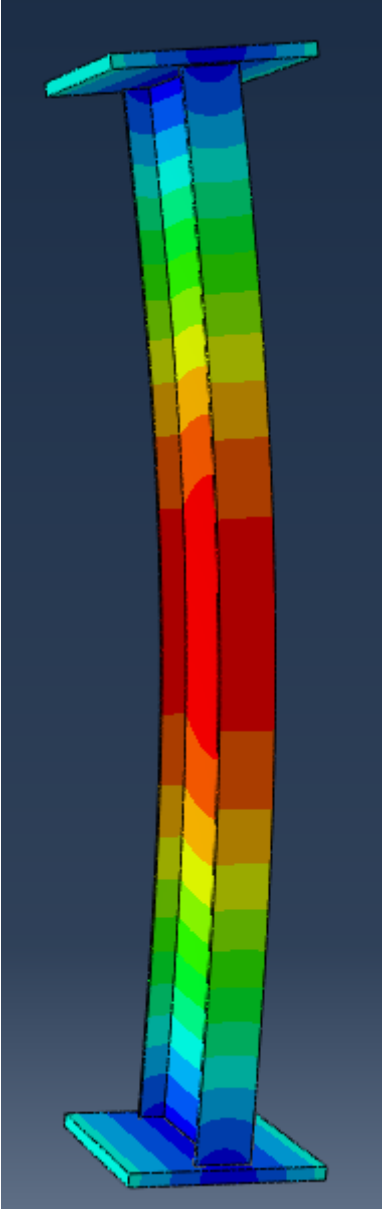
S6F10W10		
S800	S960	S1100
Eigenvalue nr. 1 = 1880 (kN) LPF _{max} = 0.818	Eigenvalue nr. 1 = 1815 (kN) LPF _{max} = 0.957	Eigenvalue nr. 1 = 1815 (kN) LPF _{max} = 1.096
N _{cr} = 1537 kN	N _{cr} = 1737 kN	N _{cr} = 1989 kN
Buckling shape: <div style="text-align: center; margin-top: 10px;">  </div>		


S7F10W10		
S800	S960	S1100
Eigenvalue nr. 1 = 1876 (kN) LPF _{max} = 0.637	Eigenvalue nr. 1 =1810 (kN) LPF _{max} = 0.742	Eigenvalue nr. 1 = 1810 (kN) LPF _{max} = 0.835
N _{cr} = 1195 kN	N _{cr} = 1343kN	N _{cr} = 1512 kN
Buckling shape:		
		


S8F10W10		
S800	S960	S1100
Eigenvalue nr. 1 = 1884 (kN) LPF _{max} = 0.567	Eigenvalue nr. 1 = 1820 (kN) LPF _{max} = 0.637	Eigenvalue nr. 1 = 1817 (kN) LPF _{max} = 0.835
N _{cr} = 1068 kN	N _{cr} = 1159 kN	N _{cr} = 1266 kN
Buckling shape:		
		

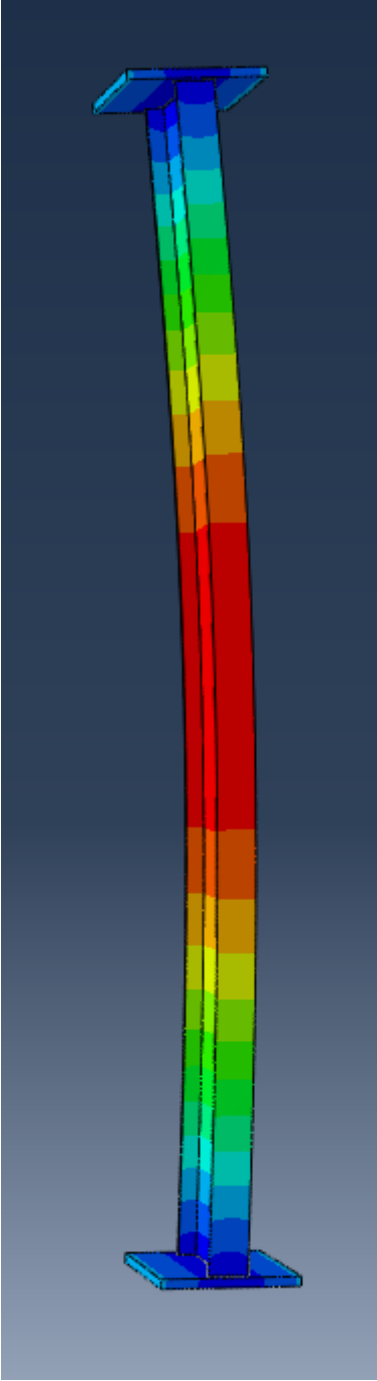
S9F10W10		
S800	S960	S1100
Eigenvalue nr. 1 = 1813 (kN) LPF _{max} = 0.493	Eigenvalue nr. 1 = (kN) LPF _{max} = 0.548	Eigenvalue nr. 1 = 1750 (kN) LPF _{max} = 0.592
N _{cr} = 894 kN	N _{cr} = 959 kN	N _{cr} = 1035 kN
Buckling shape: <div style="text-align: center; margin-top: 10px;">  </div>		

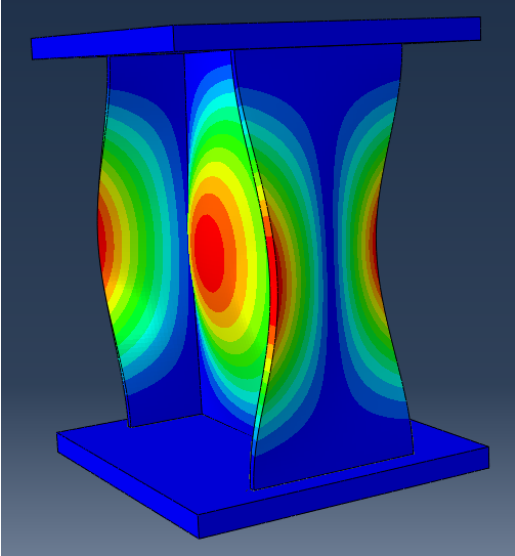
S10F10W10		
S800	S960	S1100
Eigenvalue nr. 1 = 1553 (kN) LPF _{max} = 0.534	Eigenvalue nr. 1 = 1498 (kN) LPF _{max} = 0.585	Eigenvalue nr. 1 = 1498 (kN) LPF _{max} = 0.624
N _{cr} = 829 kN	N _{cr} = 876 kN	N _{cr} = 934 kN
Buckling shape: <div style="text-align: center; margin-top: 20px;">  </div>		

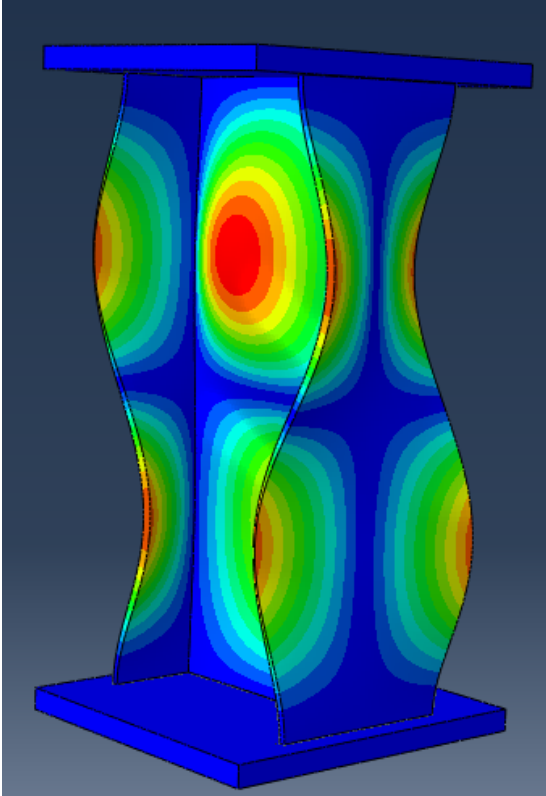
S11F10W10		
S800	S960	S1100
Eigenvalue nr. 1 = 1310 (kN) LPF _{max} = 0.551	Eigenvalue nr. 1 = 1265(kN) LPF _{max} = 0.595	Eigenvalue nr. 1 = 1260 (kN) LPF _{max} = 0.639
N _{cr} = 722 kN	N _{cr} = 753 kN	N _{cr} = 805 kN
Buckling shape:		
		

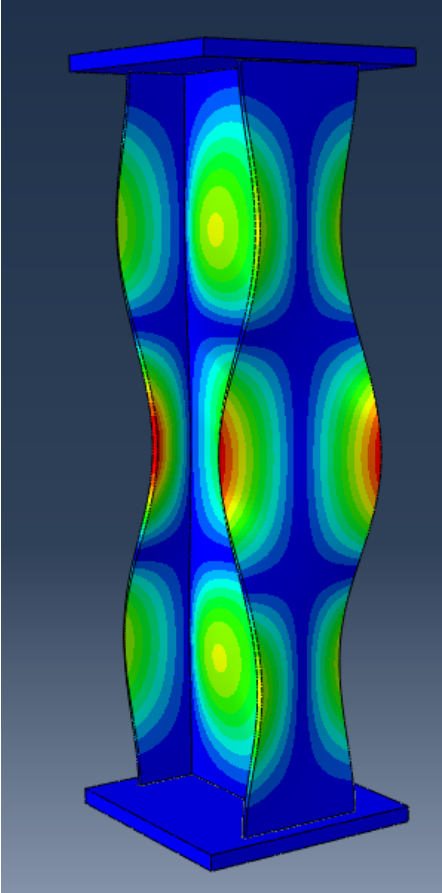
S12F10W10		
S800	S960	S1100
Eigenvalue nr. 1 = 951 (kN) LPF _{max} = 0.618	Eigenvalue nr. 1 = 917 (kN) LPF _{max} = 0.696	Eigenvalue nr. 1 = 917 (kN) LPF _{max} = 0.732
N _{cr} = 587 kN	N _{cr} = 638 kN	N _{cr} = 805 kN
Buckling shape: <div style="text-align: center; margin-top: 20px;">  </div>		

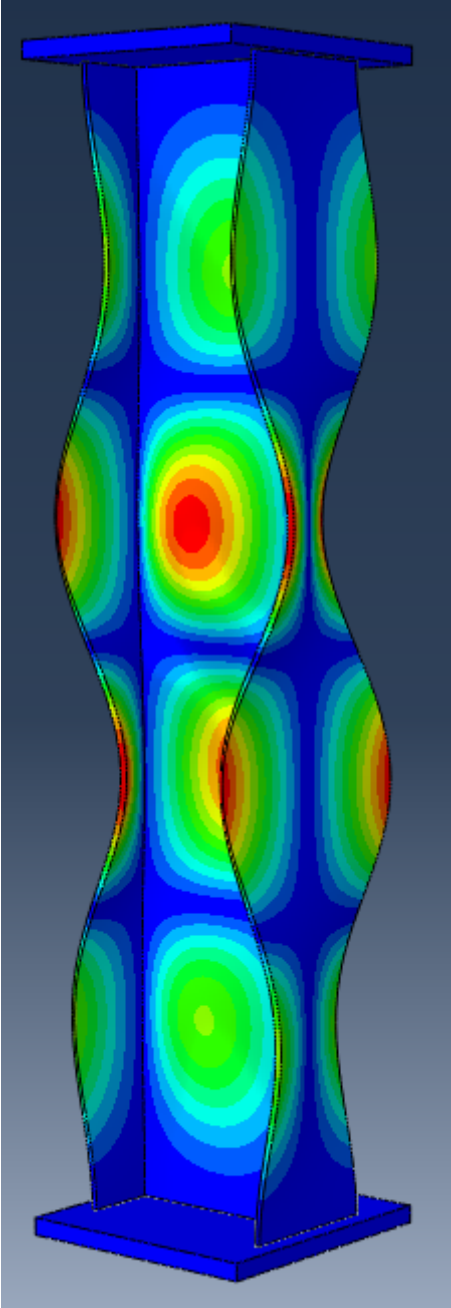
S13F10W10		
S800	S960	S1100
Eigenvalue nr. 1 = 714 (kN) LPF _{max} = 0.649	Eigenvalue nr. 1 = 688 (kN) LPF _{max} = 0.688	Eigenvalue nr. 1 = 688 (kN) LPF _{max} = 0.719
N _{cr} = 463 kN	N _{cr} = 473 kN	N _{cr} = 495kN
Buckling shape: <div style="text-align: center; margin-top: 20px;">  </div>		

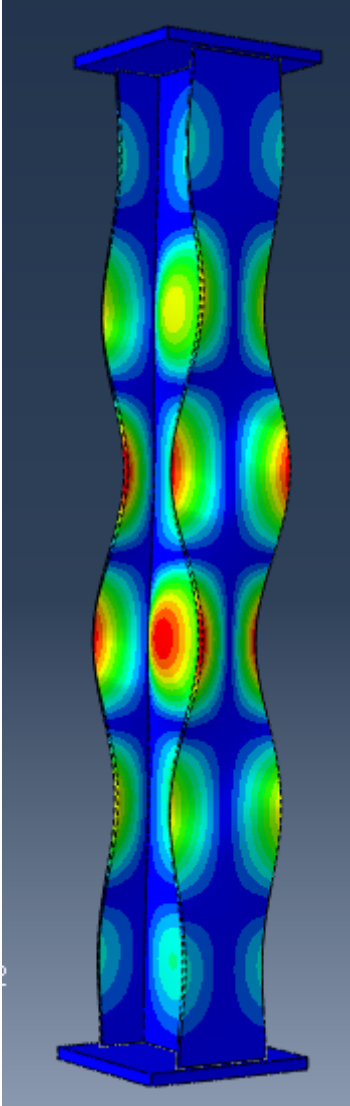
S14F10W10		
S800	S960	S1100
Eigenvalue nr. 1 = 550 (kN) LPF _{max} = 0.715	Eigenvalue nr. 1 = 530 (kN) LPF _{max} = 0.754	Eigenvalue nr. 1 = 534 (kN) LPF _{max} = 0.778
N _{cr} = 393 kN	N _{cr} = 399kN	N _{cr} = 416 kN
Buckling shape: <div style="text-align: center; margin-top: 20px;">  </div>		

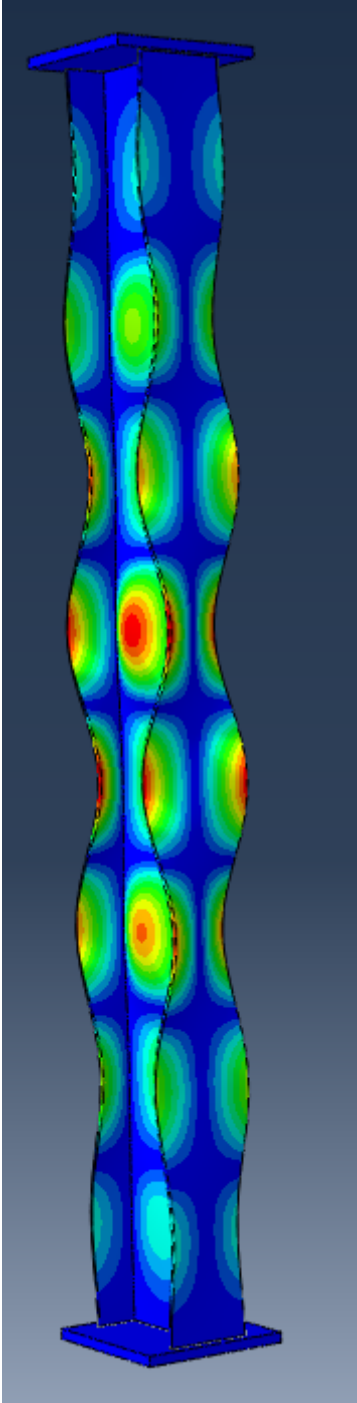
S15F9W10		
S800	S960	S1100
Eigenvalue nr. 1 = 2690 (kN) LPF _{max} = 0.918	Eigenvalue nr. 1 = 2598 (kN) LPF _{max} = 1.070	Eigenvalue nr. 1 = 2598 (kN) LPF _{max} = 1.229
N _{cr} = 2469 kN	N _{cr} = 2780 kN	N _{cr} = 3192kN
Buckling shape:		
		

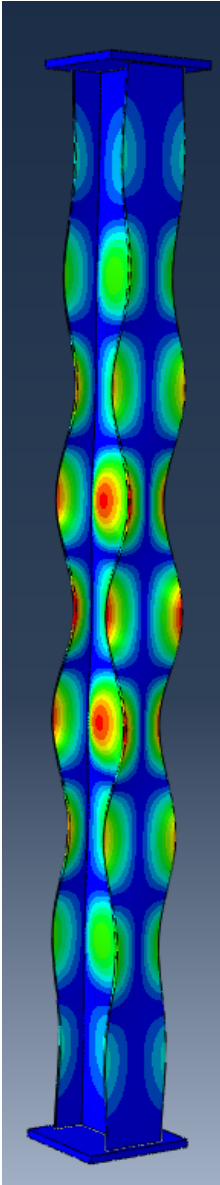
S16F9W10		
S800	S960	S1100
Eigenvalue nr. 1 = 2480 (kN) LPF _{max} = 0.839	Eigenvalue nr. 1 = 2390(kN) LPF _{max} = 1.057	Eigenvalue nr. 1 = 2393 (kN) LPF _{max} = 1.206
N _{cr} = 2081 kN	N _{cr} = 2525 kN	N _{cr} = 2886 kN
Buckling shape:		
		

S17F9W10		
S800	S960	S1100
Eigenvalue nr. 1 = 2357 (kN) LPF _{max} = 0.792	Eigenvalue nr. 1 = 2390kN) LPF _{max} = 0.952	Eigenvalue nr. 1 = 2270 (kN) LPF _{max} = 1.096
N _{cr} = 1867 kN	N _{cr} = 2161 kN	N _{cr} = 2488 kN
Buckling shape: <div style="text-align: center; margin-top: 10px;">  </div>		

S18F9W10		
S800	S960	S1100
Eigenvalue nr. 1 = 2316 (kN) LPF _{max} = 0.731	Eigenvalue nr. 1 = 2234 (kN) LPF _{max} = 0.889	Eigenvalue nr. 1 = 2234 (kN) LPF _{max} = 1.031
N _{cr} = 1694 kN	N _{cr} = 1986 kN	N _{cr} = 2302 kN
Buckling shape:		
		

S19F9W10		
S800	S960	S1100
Eigenvalue nr. 1 = 2300(kN) LPF _{max} = 0.640	Eigenvalue nr. 1 = 2215 (kN) LPF _{max} = 0.674	Eigenvalue nr. 1 = 2215 (kN) LPF _{max} = 0.702
N _{cr} = 1472 kN	N _{cr} = 1492 kN	N _{cr} = 1556 kN
Buckling shape:		
		

S21F9W10		
S800	S960	S1100
Eigenvalue nr. 1 = 2280 (kN) LPF _{max} = 0.472	Eigenvalue nr. 1 = 2200 (kN) LPF _{max} = 0.514	Eigenvalue nr. 1 = 2195 (kN) LPF _{max} = 0.534
N _{cr} = 1076 kN	N _{cr} = 1130 kN	N _{cr} = 1171 kN
Buckling shape:		
		

S22F9W10		
S800	S960	S1100
Eigenvalue nr. 1 = 2270 (kN) LPF _{max} = 0.375	Eigenvalue nr. 1 = 2200 (kN) LPF _{max} = 0.385	Eigenvalue nr. 1 = 2192 (kN) LPF _{max} = 0.390
N _{cr} = 851 kN	N _{cr} = 846 kN	N _{cr} = 855kN
Buckling shape: <div style="text-align: center; margin-top: 20px;">  </div>		